Dose calculation formalisms and consensus dosimetry parameters for intravascular brachytherapy dosimetry: Recommendations of the AAPM Therapy Physics Committee Task Group No. 149

Sou-Tung Chiu-Tsao[a)]
Quality Mediphys LLC, 17 Jade Lane, Denville, New Jersey 07834

Dennis R. Schaart
Delft University of Technology, IRI Mekelweg 15, 2629 JB Delft, The Netherlands

Christopher G. Soares
National Institute of Standards and Technology, 100 Bureau Drive, Stop 8460, Gaithersburg, Maryland 20899-8460

Ravinder Nath
Yale University School of Medicine, WW-229, 333 Cedar Street, New Haven, Connecticut 06510

(Received 16 March 2007; revised 19 June 2007; accepted for publication 2 July 2007; published 15 October 2007)

Since the publication of AAPM Task Group 60 report in 1999, a considerable amount of dosimetry data for the three coronary brachytherapy systems in use in the United States has been reported. A subgroup, Task Group 149, of the AAPM working group on Special Brachytherapy Modalities (Bruce Thomadsen, Chair) was charged to develop recommendations for dose calculation formalisms and the related consensus dosimetry parameters. The recommendations of this group are presented here. For the Cordis ^{192}Ir and Novoste ^{90}Sr/^{90}Y systems, the original TG-43 formalism in spherical coordinates should be used along with the consensus values of the dose rate constant, geometry function, radial dose function, and anisotropy function for the single seeds. Contributions from the single seeds should be added linearly for the calculation of dose distributions from a source train. For the Guidant ^{32}P wire system, the modified TG-43 formalism in cylindrical coordinates along with the recommended data for the 20 and 27 mm wires should be used. Data tables for the 6, 10, 14, 18, and 22 seed trains of the Cordis system, 30, 40, and 60 mm seed trains of the Novoste system, and the 20 and 27 mm wires of the Guidant system are presented along with our rationale and methodology for selecting the consensus data. Briefly, all available datasets were compared with each other and the consensus dataset was either an average of available data or the one obtained from the most densely populated study; in most cases this was a Monte Carlo calculation. © *2007 American Association of Physicists in Medicine*. [DOI: 10.1118/1.2767184]

Key words: brachytherapy, dosimetry, restenosis, intravascular brachytherapy

TABLE OF CONTENTS

I. INTRODUCTION

Restenosis at the site of percutaneous interventions remains a major limitation in the management of coronary and peripheral vessel diseases. The incidence of restenosis after angioplasty of a *de novo* coronary artery obstruction varies from 10% to 40% and is related to a number of risk factors. The pathophysiology involves several mechanisms (elastic recoil, negative remodeling, and neointimal hyperplasia) in response to the injury caused by the angioplasty. Over the last two decades numerous drugs and devices have been tried in an attempt to reduce restenosis. Although numerous treatment modalities have been tested in randomized controlled trials, only intravascular brachytherapy (IVBT) and recently the implantation of drug-eluting stents have been shown to significantly decrease the likelihood of restenosis. Stents provide mechanical scaffolding, which prevents recoil and remodeling. However, the implantation of stents also initiates the neointimal hyperplasia leading to the phenomenon of in-stent restenosis. To alleviate this process, drug-eluting stents release an antiproliferative drug that helps in the prevention of neointimal hyperplasia, and IVBT employs ionizing radiation for the same purpose. However, in the United States, drug-eluting stents (DES) are approved only for treating *de novo* lesions, while IVBT is approved only for treating in-stent restenosis. Hence the clinical applications of these two modes of treatment may be complementary.[1,2] Although drug-eluting stents have proven to be successful in reducing restenosis and the need for revascularization compared to bare-metal stents in several recent trials,[3–5] restenosis still occurs in drug-eluting stent patients, especially those with more complex lesions and other medical conditions such as diabetes. A recent study from Washington Hospital Center[6] has demonstrated the safety and efficacy of intravascular brachytherapy for the treatment of patients with in-stent restenosis after implantation of drug-eluting stents.

The use of ionizing radiation in the management of proliferative disorders such as malignancies has been well known for over a century. In addition, ionizing radiation has also been used extensively in nonmalignant proliferative disorders such as keloid formation, heterotopic ossification, and pterygium. Thus, the use of IVBT in the management of restenosis in blood vessel diseases has a sound scientific basis, and its efficacy in humans has been established in randomized clinical trials.

Randomized, controlled clinical trials have shown that brachytherapy using beta[7,8] or gamma emitters[9,10] is highly effective in decreasing the incidence of recurrent in-stent restenosis as measured angiographically and by intravascular ultrasound. Brachytherapy also decreases the incidence of major adverse cardiac events (primarily the need for further revascularization), compared with placebo. Based on these studies, three brachytherapy systems (two beta and one gamma) have been approved by the Food and Drug Administration (FDA) for the treatment of in-stent restenosis. These systems have been used in more than 30 000 patients. For patients with in-stent restenosis, IVBT after recanalization has become a proven modality for treatment.

The three FDA approved IVBT systems, which were utilized for most of the clinical trials in the United States, are the Checkmate system from Cordis Corporation, the Beta-Cath system from Novoste Corporation, and the Galileo system from Guidant Corporation. In this article certain commercially available products are referred to by name. These references are for information purposes only and do not imply that these products are the best or only available for the purpose, and do not imply endorsement by the National Institute of Standards and Technology. All of these are afterloading systems by means of which sealed radioactive brachytherapy sources are manually or automatically advanced into a delivery catheter previously positioned inside the patient. The sources in these three systems are based on the radionuclides ^{192}Ir, ^{90}Sr/^{90}Y, and ^{32}P, respectively.

For completeness, it is mentioned that a variety of other radionuclides have seen limited clinical testing or have been considered interesting, but do not appear to be likely candidates for immediate commercial development. At present, no trials are being conducted using these isotopes. These radionuclides include ^{48}V, ^{62}Cu, ^{68}Ge/^{68}Ga, ^{90}Y, ^{99m}Tc, ^{103}Pd, ^{106}Ru/^{106}Rh, ^{109}Cd, ^{114m}In/^{114}In, ^{125}I, ^{133}Xe, ^{144}Ce/^{144}Pr, ^{145}Sm, ^{153}Gd, ^{153}Sm, ^{166}Ho, ^{169}Yb, ^{181}W, ^{186}Re, ^{188}Re, ^{188}W/^{188}Re, and ^{198}Au; in this article, we do not pay any further attention to these other radionuclides.

It is also to be mentioned that in the early days of IVBT there was great interest in permanently implanted radioactive stents. Other IVBT delivery systems used in clinical trials included catheters with radioactive membranes, radioactive liquid-filled balloons, and radioactive gas-filled balloons. However, clinical results for these systems have yielded, at best, ambiguous and inconsistent results. Miniature x-ray tubes have also been considered, but technological difficulties have so far prevented these devices from becoming used routinely. Thus, we chose not to describe these systems for this report.

IVBT benefits from a team approach that brings together the expertise of the interventional cardiologist, radiation oncologist and medical physicist. Each of these professionals plays an important role in the optimization of the safety and efficacy of this procedure. In 1999, the AAPM Task Group 60 report described many of the tasks performed by the medical physicist and recommended dosimetry procedures in order to standardize them. The AAPM TG-60 report[11] is now about 8 years old and several new developments have occurred in this field. In this article, we present an update to the TG-60 report. The update has been written to address specific topics where the AAPM needs to make new recommendations. Our focus is to recommend a standard dose calculation formalism and provide the consensus dosimetry parameters for each of the commonly used IVBT systems.

Even though the application of intravascular brachytherapy is decreasing, patients are still being treated[12,13] by IVBT and reference data for the sources used in the three major IVBT systems are still needed for future evaluations of the large body of clinical trial experience that has already been accumulated. These data are essential for a uniform treatment of retrospective dosimetry for possible future epi-

demiological studies of the treated population. In addition, they will be useful if such sources are used in any possible future applications.

The dosimetry protocols used so far in the IVBT clinical trials have been very simple. The manufacturer of the device specified the dose rate profile as a function of distance along the perpendicular bisector of the source/train, and this dose rate profile was used to calculate the dwell time for delivering the prescription dose at the prescription point. If it is desired to calculate the dose at other points, then it is necessary to use a formalism, which allows the user to calculate the dose rate at an arbitrary point in space. In this report, we address the calculation formalisms for dose distributions. The recommendations presented here by this Task Group abide by the AAPM recommendation that consensus recommendations be obtained from the results of (at least) two independent investigations.

II. BACKGROUND

II.A. Approved IVBT systems

A brief description of the three FDA-approved IVBT systems based on ^{192}Ir, ^{90}Sr/^{90}Y, and ^{32}P and their associated clinical applications is given below. The sources used in these systems are described in more detail in Sec. II B.

II.A.1. ^{192}Ir

^{192}Ir is the only gamma emitter that has been clinically used in IVBT thus far. This radionuclide is used in the Checkmate system from Cordis Corporation. The sources, consisting of a number of ^{192}Ir seeds inside a nylon ribbon, are manufactured by Best Medical International. Treatment times for IVBT are typically 15 to 40 min. The delivery device consists of a cylindrical lead storage "pig." The sources are manually advanced by the radiation oncologist into a specially designed noncentering intraarterial catheter.

Dose prescription has been designed via one of two protocols. In the SCRIPPS (Scripps Coronary Radiation to Inhibit Proliferation Post Stenting)[14] and GAMMA-I[9] trials dose prescription was based on multiple cut intravascular ultrasound (IVUS) measurements of vessel diameter to determine minimal and maximal distances to the external elastic lamina. Dose was prescribed as 8 Gy at the maximum luminal distance, limited by the constraint of 30 Gy maximum dose to the nearest luminal distance. Alternatively, in the WRIST (Washington Radiation for In-Stent Restenosis Trial)[15] and GAMMA-II trials dose was prescribed at some fixed point from the source ribbon. The prescription dose for the WRIST trial was 15 Gy at 2 mm for vessel sizes 2.4 to 4.0 mm and 15 Gy at 2.4 mm for vessel sizes 4.0 to 5.0 mm. The prescription dose for the GAMMA-II trial was 14 Gy at 2 mm for vessel sizes 2.7 to 4.0 mm.

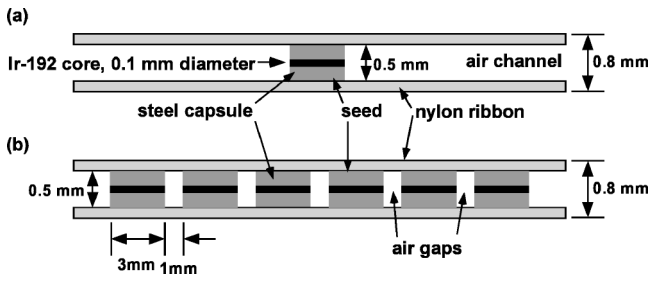

FIG. 1. Schematic showing (a) a single ^{192}Ir seed, and (b) 6-seed ^{192}Ir train in nylon ribbon. The solid black area indicates the radioactive Pt/Ir core at the center of each seed. The gray area around the black shows the stainless steel encapsulation around the core.

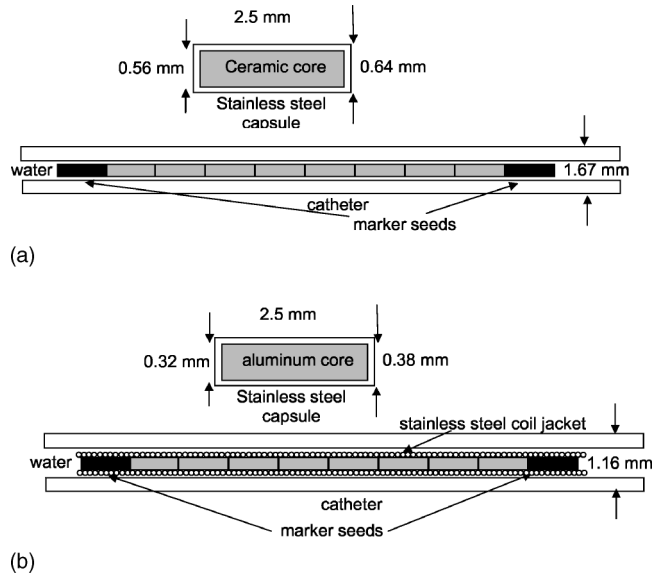

FIG. 2. Schematic showing (a) 5 F single seed of ^{90}Sr/^{90}Y and an 8-seed train with gold markers on the ends, and (b) 3.5 F single seed of ^{90}Sr/^{90}Y and an 8-seed train with Pt/Ir markers at the ends in a stainless steel wire jacket.

II.A.2. ^{90}Sr/^{90}Y

The source in the first approved beta particle IVBT device, the Beta-Cath system, is ^{90}Sr/^{90}Y. The Beta-Cath system, developed and tested by Novoste Corporation, has been used in the START (Stents and Radiation Therapy)[16] trials, BERT (Beta Energy Restenosis Trial),[17] and BRIE (Beta Radiation In Europe)[18] trials. The Novoste source consists of a string ("train") of ^{90}Sr/^{90}Y seeds. The seeds are stored in a hand-held delivery device and are advanced by a closed-loop hydraulic system, which uses sterile saline to advance (and then retract) the seeds into and out of a noncentered catheter. Two source sizes have been used: The older 5 F (1.65 mm diameter) and a newer 3.5 F (1.16 mm) system. Dose is prescribed at a fixed distance, 2 mm, from the center of the source. For vessels 2.7–3.3 mm in diameter, the prescription dose is 18.4 Gy, and for vessel diameters 3.3–4.0 mm, the prescription dose is 23.0 Gy. These dose values are based on revised data from NIST on the actual doses prescribed in the trial.

II.A.3. ^{32}P

The second important beta emitter used in IVBT is ^{32}P. The Galileo system from Guidant Corporation consists of a

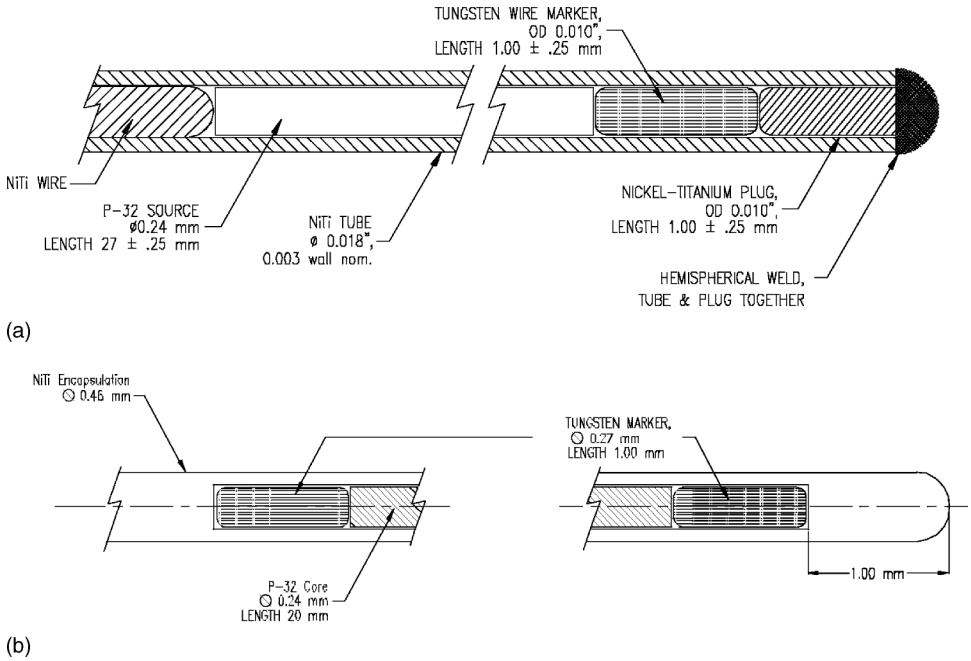

FIG. 3. (a) Schematic of the 20 mm Guidant ^{32}P wire source. Reproduced from Mourtada *et al.* 2003 (Ref. 29) with permission from author. (b) Schematic of the 27 mm Guidant ^{32}P wire source. Reproduced from Mourtada *et al.* 2000 (Ref. 30) with permission from author.

computer-controlled afterloader, similar to a conventional HDR unit, equipped with a ^{32}P wire source. Several types of perfusion centering catheters have been made available for this system. The Galileo system has been tested in the INHIBIT (Intimal Hyperplasia Inhibition with Beta In-stent Trial)[19] and PREVENT (Proliferation REduction with Vascular ENergy Trial)[8] trials. In these trials, dose was prescribed at a fixed depth, 1 mm, into the vessel wall, and the prescription dose was 20 Gy. The vessel diameter was determined from the angioplasty balloon diameter and from fluoroscopy. Vessel diameters of 2.4–3.7 mm can be treated using balloons of 2.5, 3.0, and 3.5 mm diameter. The Galileo system is the only one approved for source pullback, i.e., stepping the source to treat longer lesions.

II.B. Description of sources

II.B.1. ^{192}Ir seed train sources

The ^{192}Ir seed train assembly in a nylon ribbon has been used in tumor brachytherapy for decades.[20] The ^{192}Ir radionuclide is an emitter of a complex scheme of gamma rays, x rays, beta particles, conversion electrons and Auger electrons.[21–23] It emits approximately 2.1 gammas per decay ranging in energy primarily between 296 and 612 keV, with an average energy of 370 keV. The half life is 74 days. In the Cordis Checkmate system, model 81-01 ^{192}Ir seeds (3 mm length) from Best Medical (Springfield, VA) are assembled in a hollow nylon ribbon, with a 1 mm gap between neighboring seeds (see Fig. 1).[24] Each seed is 0.5 mm in outer diameter. The inner Pt/Ir core (0.1 mm in diameter) is encapsulated by stainless steel of 0.2 mm thickness radially. Seed activities are typically 33 mCi per seed. The seed ends are not encapsulated, allowing the emission of beta particles and internal conversion electrons through the 1 mm air gaps. The ^{192}Ir ribbon systems approved by the FDA include three different lengths, namely, 23 mm (6 seeds), 39 mm (10 seeds), and 55 mm (14 seeds). For longer lesions, seed trains of up to 23 seeds have also been used in the Long WRIST clinical trial,[25] but they are not approved by the FDA for market release.

II.B.2. ^{90}Sr/^{90}Y seed train sources

^{90}Sr is a pure beta emitter with a 28.8 year halflife,[26] and 546 keV maximum beta energy. The daughter isotope ^{90}Y is also a pure beta emitter with a 64 h halflife, maximum beta energy of 2.28 MeV and an average beta energy of 0.935 MeV. It is primarily the ^{90}Y beta particles that are used for therapy, although ^{90}Y is in secular equilibrium with the parent ^{90}Sr, and both radiations are emitted. The original 5 F Novoste Beta-Cath system was first used in clinical trials in 1997 and consists of trains of individual 2.5 mm long ^{90}Sr/^{90}Y seed sources with no separation between the seeds. The seed activities are typically 3.5 mCi per seed. Depending upon the lesion length being treated, trains of 30 mm (12 seeds), 40 mm (16 seeds), or 60 mm (24 seeds) were used. Figure 2(a) shows the single seed construction, as well as a train of seeds. The individual seeds consist of a 2.5 mm long by 0.56 mm diameter ceramic cylindrical core encapsulated in a stainless steel cylindrical capsule with 0.04 mm walls and 0.05 mm ends.[27] The seed trains were brought into the patient hydraulically in a 5 F (1.67 mm) diameter eccentric three-lumen treatment catheter, with gold marker seeds at either end of the seed train.

In 2000, a second source design was introduced, with a narrower diameter, delivered in a 3.5 F diameter catheter. In this design, the nominal 2.5 mm long core material is now a sintered aluminum powder in which the ^{90}Sr/^{90}Y is bound, with a 0.32 mm diameter. The core is encapsulated in a stainless steel capsule with 0.03 mm thick sides and ends. The individual seeds in the train are held together by a jacket made from a stainless steel coil having 0.445 mm diameter

and including Pt/Ir alloy markers at each end.[28] The train is brought into the patient in a three-lumen eccentric catheter with a 1.16 mm diameter. Both the individual seed and the seed train in a catheter are shown in Fig. 2(b).

II.B.3. ^{32}P wire sources

^{32}P is a pure beta emitter with a 14.3 day halflife, a maximum beta energy of 1.71 MeV, and an average beta energy of 0.695 MeV. The 20 and 27 mm ^{32}P wire sources manufactured by Guidant Corporation are shown in Figs. 3(a) and 3(b), respectively. Both sources are composed of a flexible, polymer core containing the ^{32}P radionuclide, which is encapsulated in superelastic NiTi tubing. The 20 mm source design[29] is the successor of the 27 mm design[30] and is essentially the same, except for the nominal length of the radioactive core and the addition of a second x-ray marker at the proximal side of the core. The 20 mm source can be used in automated stepping mode for the irradiation of longer lesions. For this source, the manufacturing tolerance in the active source length as represented by the distance between the proximal and distal 50% isodose lines was +0.9 to −0.5 mm. More details can be found in the aforementioned references.

II.C. Determination of dose distributions in IVBT

The introduction of intravascular brachytherapy has created new challenges in the field of brachytherapy dosimetry, because of the necessity to know accurately the dose distribution with submillimeter resolution at very small distances from the source. A brief overview of the various methods used for determining the dose distribution about intravascular sources is given below.

II.C.1. Monte Carlo calculations

An important advantage of Monte Carlo simulations is that the dose distribution can be calculated with high spatial resolution. A variety of well-validated general-purpose Monte Carlo codes are currently available for brachytherapy dosimetry and sufficient computing power for dose calculations on brachytherapy sources is widely available. It is therefore not surprising that many authors have used this technique for the calculation of dose distributions about IVBT sources. However, it is not trivial to obtain correct results using Monte Carlo calculations, as can be seen, for example, from the discussions given in Sec. V. General-purpose codes that have been used for the studies included in the present comparison are CYLTRAN, part of the ITS 3.0 package;[31] EGS4;[32] EGSnrc;[33] MCNP4B;[34] MCNP4C;[35] MCNPX;[36] PENELOPE;[37] and GEANT4[38] In a few studies, special codes have been developed by the authors for IVBT dosimetry.[39,40]

II.C.2. Experimental measurements

Near-field dosimetry of brachytherapy sources is complicated by the very high dose gradients associated with small sources at short distances in water or water-equivalent materials. To avoid dosimeter volume averaging effects, very high resolution (less than 0.5 mm) is required. For ^{192}Ir sources at 1 cm or greater distances, 1 mm × 1 mm × 1 mm thermoluminescence dosimeters (TLDs) sufficiently minimize volume averaging effects and are the most commonly used systems for dosimetry at these distances.[39] However, at the distances of interest in intravascular brachytherapy, recourse must be made to detectors that offer higher spatial resolution. Detectors that offer submillimeter resolution include radiochromic film,[41] small-volume scintillators,[42] and ultrathin TLDs.[43] In addition, very-small-volume extrapolation ionization chambers serve as primary dosimetry standards for beta particle brachytherapy sources in the United States,[44] Germany,[44] and the Netherlands.[45]

Radiochromic film offers the necessary spatial resolution (better than 0.1 mm in all dimensions), near water equivalence for photons above 100 keV and for beta particles, and the required sensitivity for these relatively high dose and dose rate field measurements. Most of the experimental results compared in Sec. IV for intravascular brachytherapy sources were obtained with this method. There are several good reviews on the use of radiochromic film available in the literature.[46–48] Precautions required in the use of radiochromic film include proper consideration of the measurement depth in nonaqueous media (see Sec. III D), time and temperature dependence of the measured optical density, and energy dependence of the response to photons with energies below 100 keV.[49,50]

II.D. Review of dose calculation formalisms

II.D.1. Spherical coordinates

The dose calculation formalism of the AAPM TG-43 is expressed in polar coordinates although it actually uses a spherical coordinate system since there is no assumed dependence on the azimuthal angle. This formalism has become the standard for the dosimetry of interstitial brachytherapy gamma sources for cancer treatment.[51]

The general, two-dimensional (2D) dose-rate equation from the 2004 update of the TG-43 protocol[52] is given by

$$\dot{D}(r,\theta) = S_K \Lambda \frac{G_L(r,\theta)}{G_L(r_0,\theta_0)} g_L(r) F(r,\theta), \tag{1}$$

where r denotes the distance from the center of the active source to the point of interest $P(r,\theta)$, r_0 denotes the reference distance, which is specified to be 1 cm in this protocol for gamma-particle emitting sources, and θ denotes the polar angle specifying the point-of-interest relative to the source longitudinal axis (see Fig. 4). The reference angle, θ_0, lies in the source transverse plane, and is specified to be 90° or $\pi/2$ rad. S_K is the air kerma strength of the source. It has units of μGy h^{-1} m^2 or U.

The dose rate constant, Λ, equals the ratio of absorbed dose rate at the reference position, $P(r_0,\theta_0)$ in a water equivalent phantom, and S_K. Λ has units of cGy h^{-1} U^{-1}, which reduces to cm^{-2}:

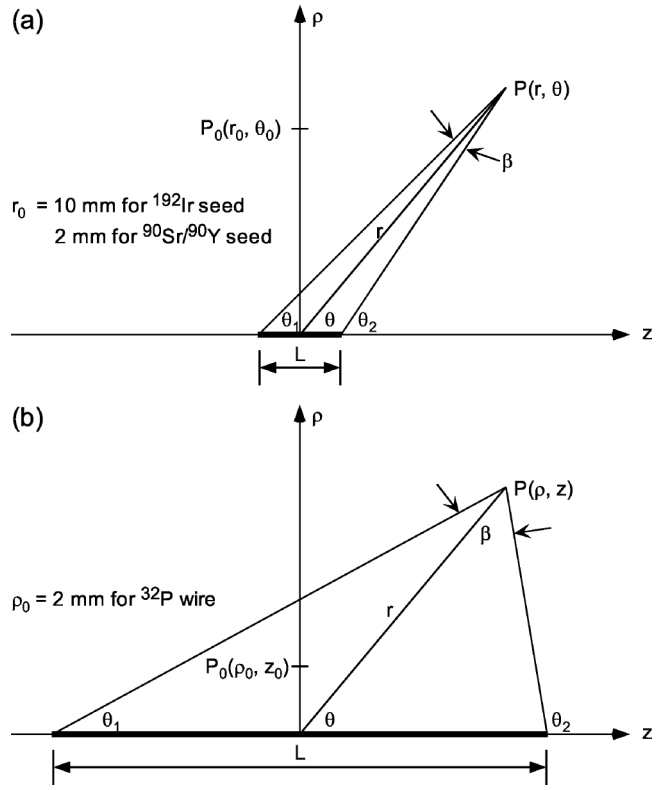

FIG. 4. Diagrams showing the source and the point of interest $P(r,\theta)$, (a) for short sources, ^{192}Ir and ^{90}Sr/^{90}Y seeds and (b) long ^{32}P wire sources. In the TG-43 dose calculation formalisms, the point P is defined by means of the polar coordinates r and θ, while the angle β is used to calculate the geometry function of a line source with finite length L. The coordinates ρ and z are used in the new formalism for beta line sources.

$$\Lambda = \frac{\dot{D}(r_0,\theta_0)}{S_K}. \tag{2}$$

The dose-rate constant depends on both the radionuclide and the source model and is influenced by both the source internal design and the experimental methodology used by the primary standard to realize S_K.

$G_L(r,\theta)$ is the geometry function (cm^{-2}) that describes the dose distribution in the absence of scattering and attenuation within the source itself and any surrounding materials. The geometry function in its most general form is given by

$$G_L(r,\theta) = \frac{\int_V [\vartheta(\mathbf{r}')\mathrm{d}V'/|\mathbf{r}'-\mathbf{r}|^2]}{\int_V \vartheta(\mathbf{r}')\mathrm{d}V'}, \tag{3}$$

where $\vartheta(\mathbf{r}')$ represents the density of radioactive material within volume element dV' at the point $\mathbf{r}'$ within the source, and V denotes integration over the source radioactive core.

In IVBT it is appropriate to use the line-source model, which gives rise to the following geometry function:

$$G_L(r,\theta) = \begin{cases} \dfrac{\beta}{Lr\sin\theta}, & \text{if } \theta \neq 0^\circ, \\ (r^2 - L^2/4)^{-1}, & \text{if } \theta = 0^\circ, \end{cases} \tag{4}$$

where β is the angle, in radians, subtended by the tips of the hypothetical line source with respect to the calculation point, $P(r,\theta)$, and L is the active source length (see Fig. 4).

The radial dose function, $g_L(r)$, accounts for dose fall-off on the transverse plane due to photon scattering and attenuation, i.e., excluding the fall-off accounted for by the geometry function. $g_L(r)$ is defined by Eq. (5) and is equal to unity at $r_0 = 1$ cm:

$$g_L(r) = \frac{\dot{D}(r,\theta_0)}{\dot{D}(r_0,\theta_0)}\frac{G_L(r_0,\theta_0)}{G_L(r,\theta_0)} \tag{5}$$

$F(r,\theta)$ is the 2D anisotropy function that accounts for angular dependence of photon absorption and scatter in the encapsulation and the medium is defined as

$$F(r,\theta) = \frac{\dot{D}(r,\theta)}{\dot{D}(r,\theta_0)}\frac{G_L(r,\theta_0)}{G_L(r,\theta)}. \tag{6}$$

Other than inclusion of the subscript "L," this definition is identical to the original TG-43 definition.

For beta-particle emitting seed sources, the same formalism has been proposed, with the difference that the product of air kerma strength and dose rate constant in Eq. (1) is replaced by the reference absorbed dose rate $\dot{D}_w$ (2 mm) at the reference radial distance, r_0, of 2 mm from the center of the source in water.[11]

II.D.2. Cylindrical coordinates

It has been shown by Schaart *et al.*[53] that the TG-43 formalism, which was originally developed for point-like sources, does not work well for long intravascular line sources, and in principle fails completely for beta particle line sources with a length L larger than twice the range R of the beta particles ($L > 2R$). The cause of this failure lies in the fact that the radial dose function $g_L(r)$ is a function of the (polar) distance r to the center of the source. If the source emits beta radiation with a range R, and if we neglect bremsstrahlung for simplicity, $g_L(r)$ becomes zero for $r > R$. Therefore, if the source length exceeds $2R$, there are points (notably at values of θ near 0° and 180°) that are located at distances $r > R$ from the source center but where the absorbed dose rate remains finite. At such points, the anisotropy function $F(r,\theta)$ would become infinite.

In reality, $F(r,\theta)$ remains finite because of the presence of bremsstrahlung, but it nevertheless increases to very large values. The resulting large and rapid variations make a table of $F(r,\theta)$ difficult to interpolate accurately. This finding has later been confirmed by others.[54–56] Since it is in fact one of the main purposes of the TG-43 formalism to minimize dose calculation errors due to interpolation, Schaart *et al.* proposed an adaptation of the formalism that appears to work well for intravascular line sources and also preserves the es-

sential advantages of the TG-43 approach. The new formalism is conceptually similar to the TG-43 formalism. However, the parameters of the new formalism are redefined to avoid the singularity problem described above. Furthermore, the new formalism is defined in cylindrical coordinates, (ρ,z,ϕ), which better match the source-target geometry. This has the advantage that an evenly spaced matrix of data points within the region of interest is easily obtained using equidistant intervals along the axes. The origin of the cylindrical coordinate system is located at the source center, while the z axis coincides with the long symmetry axis of the source, as indicated in Fig. 4. Under the assumption that the source is cylindrically symmetric, it suffices to use only the coordinates (ρ,z), where ρ is used to denote the cylindrical radial distance in order to avoid confusion with the polar or spherical distance r used in the TG-43 formalism.

In the cylindrical coordinate formalism, the dose rate distribution about a beta particle line source in water is expressed as follows:

$$\dot{D}(\rho,z)=\dot{D}(\rho_0,z_0)[G(\rho,z)/G(\rho_0,z_0)]g(\rho)F(\rho,z). \tag{7}$$

Here, $\dot{D}(\rho_0,z_0)$ denotes the source strength that is defined as the reference absorbed dose rate (absorbed dose rate in water at the reference point), i.e., at $\rho_0=2$ mm and $z_0=0$. Similar to the TG-43 formalism in spherical coordinates, a geometry function is used to suppress the influence of the inverse square law on the other parameters. The general definition of the geometry function has been given in Sec. II D. Since the absorbed dose rate along a long, uniform beta particle line source is very uniform and almost independent of source length except near the ends of the source, it is appropriate to use the geometry function for an infinite line source, as originally proposed by Schaart *et al.* In this approximation, the geometry function reduces to[53]

$$G(\rho,z)=G(\rho)=\frac{1}{\rho}. \tag{8}$$

This geometry function is recommended for all beta line sources to which the formalism is applied.

The transverse dose function $g(\rho)$, which is normalized to unity at the reference point, is defined as follows:

$$g(\rho)=\frac{G(\rho_0,z_0)}{G(\rho,z_0)}\frac{\dot{D}(\rho,z_0)}{\dot{D}(\rho_0,z_0)}. \tag{9}$$

The transverse dose function plays a similar role as the radial dose function, in that it characterizes the dose rate distribution along the transverse bisector of the source. However, the transverse dose function is a function of the cylindrical radial distance ρ instead of the spherical distance r. Therefore, if the above geometry function is used, $g(\rho)$ approximately characterizes the entire dose distribution about a uniform beta line source, except in the dose fall-off regions near the ends of the source.

The nonuniformity function $F(\rho,z)$, which is normalized to unity on the transverse axis, is defined as

$$F(\rho,z)=\frac{G(\rho,z_0)}{G(\rho,z)}\frac{\dot{D}(\rho,z)}{\dot{D}(\rho,z_0)}. \tag{10}$$

Substitution of the above geometry function [Eq. (8)] shows that the first factor on the right-hand side of this equation is equal to unity, so the nonuniformity function completely describes the axial variation of the dose rate in terms of the ratio of the dose rate at a point and the dose rate on the central transverse axis at the same radial distance. Thus, this function accounts for the dose fall-off near the source ends, but also for any dose rate nonuniformity that may result from variations in, e.g., the activity distribution or the encapsulation thickness along the length of the source.

It is to be noted that, in the meantime, other authors have also proposed line source formalisms based on cylindrical coordinates. Patel *et al.*,[54] for example, proposed a formalism comprised of a transverse dose function equal to the radial depth-dose distribution normalized at the reference point, and a modulation function, equal to $F(\rho,z)$ as defined above. Instead of the geometry function $G(\rho,z)$, however, these authors proposed a so-called distribution factor consisting of a modified Fermi–Dirac function, which can be seen as a fit to the typical variation of the dose distribution of a beta particle line source in the longitudinal direction. The potential advantage of this approach is that the modulation function remains close to unity if the distribution factor can be fit well to the dose distribution of the source under consideration. This was successfully demonstrated for a ^{90}Y beta particle line source. The dose distribution about other source designs may be very different, however. In some cases, it may therefore appear difficult to fit the distribution factor to the dose distribution, resulting in a rapidly varying modulation function that is difficult to interpolate. A second disadvantage of this method is that the distribution factor does not account for the influence of the inverse square law in the transverse direction. For this reason, the transverse dose function falls off just as steeply as the radial depth-dose distribution itself.

In a second paper, the same group compared the TG-43 formalism with the line source formalism proposed by Schaart *et al.* for a ^{192}Ir line source composed of a 30 mm long Ir wire encapsulated in a thin-walled Ni/Ti tube.[56] The TG-43 geometry function for a finite line source with a length $L=30$ mm was used in both cases.[11] Interestingly, the beta particles emitted by ^{192}Ir appeared to contribute significantly to the dose rate at radial distances up to about 1.5 mm. As a result, the anisotropy function showed rapid variations at these radial distances. In contrast, the nonuniformity function remained close to unity throughout the entire region of clinical interest. Because of this and the fact that the use of cylindrical coordinates requires a smaller matrix of $F(\rho,z)$ values to accurately describe the dose distribution, we conclude that the cylindrical formalism is more suitable for intravascular line sources. Note that although there is no space between the seeds in either of the Novoste source train systems, the single seed TG-43/60 formalism described in Sec. II D 1 is preferred for these sources since this approach al-

lows greater flexibility in radiation field calculations by allowing the consideration of curved sources (see Sec. III C).

Wang and Li[55] used a formalism that is similar to the one proposed by Schaart *et al.* except that a central region of axial dose uniformity is presupposed. As a result, the formalism exhibits discontinuities in both $G(\rho,z)$ and $F(\rho,z)$ at the z values between which the dose distribution is presupposed to be uniform. This formalism was successfully demonstrated using a Monte Carlo calculated dose distribution of a uniform 27 mm long Guidant ^{32}P beta particle line source. A limitation of this formalism, however, is that it is inherently unsuitable for sources that lack the presupposed region of longitudinal uniformity. For the same reason, it is impossible to use this formalism for the representation of, e.g., film measurements on real sources, which in general are not perfectly uniform.

The geometry function given in Eq. (8) has a very simple form. This function has been selected based on the arguments given below. It has recently been suggested that a more precise representation of the geometry function (sometimes called particle streaming function) could be obtained via a Monte Carlo evaluation of Eq. (3), especially if the radioactivity distribution inside the source has a complex geometry.[57,58] In reaction to these and other papers, however, several arguments have been given to select only a few, simple, analytical geometry functions for use in brachytherapy treatment planning.[59–61]

First, it should be recognized that possible differences between Eq. (3) and the selected, approximate geometry function do *not* introduce errors in the dose calculation as long as the geometry function applied in dose calculations are the same as the one used by the authors who prepared the TG-43/60 data set.

Second, the role of the geometry function is to suppress the influence of the inverse-square law on the other dose calculation parameters. As a result, these other parameters become less rapidly varying functions. This is essential for accurate interpolation between tabulated data points and may even permit extrapolation to points outside the tabulated data range. However, this approach works only if the geometry function can be recalculated *exactly* at any point in space. Hence, the geometry function should be an analytical function: Providing this rapidly varying function in the form of, for example, a table of Monte Carlo results would reintroduce interpolation errors that the geometry function is in fact supposed to eliminate.

Third, it is important that a limited set of geometry functions be used in clinical practice. This minimizes the chance of errors resulting from the use of the wrong geometry function, and makes it more likely that all of the geometry functions used are indeed available in all commercial treatment planning systems.

III. METHOD OF OBTAINING CONSENSUS DATA

III.A. Single seed source data

When authors provided measured or calculated data for individual seed sources, the comparisons of results were relatively straightforward. In general, the comparisons were performed in three steps. First the dose rate constants for single seed sources were compared. For ^{192}Ir sources the dose rate constant was expressed in terms of dose rate per unit air kerma strength at the reference distance of 1 cm from the source center in water. For ^{90}Sr/^{90}Y seeds the quantity compared was dose rate per unit contained activity at the reference distance of 2 mm from the seed center in water. For expressing contained activity of ^{90}Sr/^{90}Y seeds, the convention of using only the parent activity was followed. The second step was the comparison of relative depth-dose profiles or, equivalently, radial dose functions for single seed sources. The latter comparison was much more sensitive to small variations due to the removal of the strong distance dependence through application of the geometry function. Finally, anisotropy function data were compared graphically for fixed radial distances as a function of angle.

In comparing dose rate constants and selecting the consensus value, there were several considerations. One can argue that the value from a single reference should be selected as being representative of the collection of values available in the literature. Alternatively, one can argue that an averaged value of experimental and calculated values should be used. In this work, both approaches have been followed (see Sec. IV), depending on the source type.

In comparing radial dose functions and anisotropy functions of single seeds, only one set of functions has been chosen for each system rather than averaging data from many authors. The chosen functions were usually from Monte Carlo calculations that spanned the required range of radial distances and angles and had sufficiently fine spacing to make the interpolation between points accurate. Analytical functions were fit to the chosen radial dose function data when they were not available in the literature. The degree to which the data agreed with available experimental measurements was considered in the selection of the Monte Carlo study for recommended values.

An important aspect of the comparison was also a consideration of how well the radial dose and anisotropy functions for single sources predicted the dose profiles measured and calculated for ribbon and train sources. This is discussed further in Sec. IV.

III.B. Line source data

For the special case of ^{32}P wire sources, generally results are only available for the entire wire length. As discussed in Sec. II D 2, the TG-43 formalism is not appropriate for these sources and a cylindrical formalism is used instead. In this formalism the quantities for comparison are the reference absorbed dose rate per unit contained activity per unit active source length, the transverse dose function, and the nonuniformity function. Similar arguments with respect to the choice of consensus values for these parameters can be made in exact analogy to the TG-43 parameters discussed in the previous section. Details for the choices made are given in Sec. IV.

III.C. Train source data

For the case of ^{192}Ir ribbons and ^{90}Sr/^{90}Y seed trains, measured data are generally available only for trains of sources rather than individual sources. Calculations, on the other hand, are usually available for both trains and single sources. As mentioned above, one of the crucial methods of comparison of various available values of the TG-43 parameters is to use the principle of superposition of dose distributions for a single source to predict the dose profile for a train source. The predicted profiles are then compared to measured and calculated profiles. Generally these comparisons were confined to relative depth-dose profiles and to axial distributions at radial distances of 1 or 2 mm, as well as distributions perpendicular to the source axis at a depth of 2 mm. In the axial distribution comparisons, the decision was made to normalize the dose profiles to an average value over the central $\frac{2}{3}$ of the physical source length, rather than at a point at the source center. This was done to reduce the influence of local variations in the profiles (e.g., due to source nonuniformity or measurement uncertainties) on the comparison. This convention was used throughout the comparisons presented in this work. The same convention has been used in the away-and-along tables presented in Sec. IV. Note that for the purposes of performing the averaging over the central $\frac{2}{3}$ of the physical source length, a maximum distance between points of 0.1 mm shall be used. Since most measurements of nonuniformity are performed with radiochromic film, this is well within the capabilities of this dosimeter.

For the special case of the 2.5 mm long ^{32}P wire segments calculated by Mourtada *et al.*[62] the superposition principle was also used to construct wire source dose distributions for comparison with measurements and calculations. These segments are short enough to be usable under the TG-43 formalism and thus represent a method for modeling curved sources, which is impossible to do under the cylindrical formalism. As the Mourtada data are the only available data, they are recommended as the consensus values for 2.5 mm long ^{32}P wire segment superposition calculations.

III.D. Media scaling

Dose measurements on therapeutic beta particle sources are often performed in solid phantoms made from low-Z materials such as A-150 plastic, WT1, polystyrene, or poly(methyl methacrylate) (PMMA). The depth-dose distribution in such a solid phantom is generally different from that in water, therefore requiring a correction. Monte Carlo calculations, in which the phantom medium is replaced by water, can be used for such corrections. Another possibility is to correct through scaling.

In the late 1960s, Cross proposed that the depth-dose distributions of plane and point beta particle sources in different low-Z media are very similar and can be related to one another via a scaling factor on distance.[63] Since then, this so-called scaling method has been used for a variety of applications, and the results in low-Z media appear to be accurate to within 2% to 3% for the types of sources just mentioned.[64] Recently, the applicability of the scaling method has been extended to line sources with zero or finite diameter by Schaart.[65]

For a point source, the dose distribution in one low-Z medium can be calculated from that in another low-Z medium as follows:[63,64]

$$D_2(r) = \eta^3 \frac{\xi_2^2}{\xi_1^2} D_1\left(\eta \frac{\xi_2}{\xi_1} r\right), \tag{11}$$

where r is the distance to the source in units of length, η is the scaling factor, or relative attenuation, of medium 2 relative to medium 1, and ξ_1 and ξ_2 are the densities of medium 1 and 2, respectively.

For a cylindrical source having a length larger than twice the beta particle range, the depth-dose distributions in different media are related by[65]

$$\rho D_2(\rho) = \eta\left[\rho_s + \eta\frac{\xi_2}{\xi_1}(\rho - \rho_s)\right] D_1\left[\rho_s + \eta\frac{\xi_2}{\xi_1}(\rho - \rho_s)\right], \tag{12}$$

where ρ is the radial distance to the longitudinal source axis and ρ_s is the outer radius of the source. For $\rho_s = 0$, this equation reduces to

$$D_2(\rho) = \eta^2 \frac{\xi_2}{\xi_1} D_1\left(\eta \frac{\xi_2}{\xi_1} \rho\right). \tag{13}$$

We have applied media scaling in some cases where the original publication contained dosimetric data for media other than water. In such cases this is clearly indicated.

IV. DATA COMPARISON AND RECOMMENDATIONS

IV.A. Source strength of catheter-based IVBT sources

For a given source type, the two most important quantities in the determination of the dose delivered to the target are the brachytherapy source strength and the amount of time the source is left in the target (i.e., the irradiation time) assuming all other parameters are known (i.e., source position in reference to the target, etc.). The source strength of each delivered source is provided by the vendor to the user. It is the responsibility of the medical physicist to verify the accuracy of the source strength before its first clinical use.

Two different definitions of brachytherapy source strength are in use. For photon sources the AAPM TG-32,[66] TG-43,[51,52] and TG-60,[11] recommend that source strength be specified in terms of the air kerma strength, S_K. For beta sources from catheter based systems, the AAPM TG-60 report recommends that source strength be specified in terms of absorbed dose rate to water at 2 mm radial distance, $\dot{D}_w(2\text{ mm})$. In this report, we make the following recommendations for the specification of source strength of IVBT sources.

IV.A.1. Gamma emitting ^{192}Ir sources

Iridium-192 sources used for intravascular brachytherapy are calibrated in an identical manner to those used in conventional brachytherapy.[51] Individual seeds are calibrated at NIST with primary standards in terms of air kerma strength. For ^{192}Ir sources the primary standard is a re-entrant chamber, which was originally calibrated against a NIST primary standard free air ionization chamber.[67] Such calibrated sources are distributed to manufacturers and secondary laboratories for calibration of secondary standards, which are typically well-type ionization chambers.

We recommend that no changes in the calibration of source strength of gamma emitting ^{192}Ir sources be made. Air kerma strength standards and the procedures for the transfer of primary standards to the ADCLs and the user are well understood and extensively described in the literature.

Briefly, air kerma strength, S_K, is the air kerma rate, $\dot{K}_\delta(d)$ *in vacuo* and due to photons of energy greater than δ, at distance d, multiplied by the square of this distance, d^2:

$$S_K = \dot{K}_\delta(d) d^2. \tag{14}$$

The quantity d is the distance from the source center to the point of $\dot{K}_\delta(d)$ specification (usually but not necessarily associated with the point of measurement) which should be located on the transverse bisector of the source (the plane normal to the longitudinal axis of the source, which bisects the radioactivity distribution). The distance d can be any distance that is large relative to the maximum linear dimension of the radioactivity distribution so that S_K is independent of d. $\dot{K}_\delta(d)$ is usually inferred from air kerma rate measurements performed in a free-air geometry at distances typically of the order of 1 m.[49] The qualification *in vacuo* means that the measurements should be corrected for photon attenuation and scattering in air and any other medium interposed between the source and detector, as well as photon scattering from any nearby objects including walls, floors, and ceilings. Of course, air kerma rate may also be calculated to subvert some of the limitations imposed on practical measurements. The energy cutoff, δ, is intended to exclude low-energy or contaminant photons (e.g., characteristic x rays originating in the outer layers of steel or titanium source cladding) that increase $\dot{K}_\delta(d)$ without contributing significantly to dose at distances greater than 0.1 cm in tissue.

IV.A.2. Beta emitting ^{32}P and ^{90}Sr/^{90}Y sources

Currently, beta-emitting catheter based systems are calibrated at primary and secondary laboratories in terms of reference absorbed dose rate (absorbed dose rate to water at a reference distance of 2 mm in water) measured in water equivalent plastic using an extrapolation ionization chamber equipped with a 1 mm diameter collecting electrode.[30,41] This approach for the primary standard for beta emitting IVBT sources has the advantage of yielding the quantity of interest in an absolute sense. Similarly to ^{192}Ir sources, calibrated sources are distributed to manufacturers and secondary laboratories for calibration of secondary standards, which are typically well-type ionization chambers.

It should be noted that $\dot{D}_w$(2 mm) is often supplemented with values of contained activity, as this is the quantity used by some vendors and users in the determination of source strength in the clinic. Knowing the contained activity and the details of the source design, one can infer $\dot{D}_w$(2 mm) by using the results of Monte Carlo simulations. The manufacturers of both the ^{90}Sr/^{90}Y and ^{32}P systems do provide contained activity as well as $\dot{D}_w$(2 mm) in their source specifications. For the former, only the parent activity is specified. Manufacturer measurements of contained activity are performed using well ionization chambers with activity calibrations traceable to primary standards. It should be noted that manufacturer statements of contained activity and reference absorbed dose rate are not independent but are based on a single determination with a system calibrated either in terms of one quantity or the other, with the complementary quantity inferred using a reference (usually Monte Carlo based) relationship between contained activity and reference absorbed dose rate. We recommend that the primary standard based upon an in-medium measurement of dose using an

TABLE I. Dose rate constant, Λ (at 10 mm), and dose rate per unit air kerma strength at 2 mm along the transverse axis of an ^{192}Ir seed, both in units of cGy h^{-1} U^{-1}.

Author	Λ (cGy h^{-1} U^{-1}) at 10 mm	Dose Rate (cGy h^{-1} U^{-1}) at 2 mm
Patel *et al.* (Ref. 72)	1.108	23.82
Williamson (Ref. 39)	1.11	
Nath *et al.* (TG-43) (Ref. 51)	1.12	
Wang and Sloboda (Ref. 68)	1.115	
Anctil *et al.* (Ref. 69)	1.1	
Wang and Li (Ref. 27)	1.109	23.76
Chen and Nath (Ref. 70)	1.124	
Papagiannis *et al.* (Ref. 40)	1.104	24.04
Ye *et al.* (Ref. 71)	1.129	24.9

TABLE II. Coefficients, a_i, for the reference radial dose function for ^{192}Ir, ^{90}Sr/^{90}Y single seed sources [Eq. (15)] and for the transverse dose function for ^{32}P wire sources [Eq. (16)]. The fit for ^{192}Ir is valid for 0.5 mm$\leq r \leq$90 mm, that for ^{90}Sr/^{90}Y for 0.5 mm$\leq r \leq$9.9 mm. The fit for ^{32}P is valid for 0.5 mm$\leq \rho \leq$6.5 mm.

Coefficient	^{192}Ir	^{90}Sr/^{90}Y	^{32}P
a_0	9.89054×10^{-1}	1.42392×10^{0}	6.51289×10^{-1}
a_1	8.81319×10^{-4}	-1.20120×10^{0}	5.92999×10^{-2}
a_2	3.51778×10^{-5}	1.82809×10^{0}	-2.55906×10^{-1}
a_3	-1.46637×10^{-6}	-1.46740×10^{0}	4.03760×10^{-2}
a_4	9.24370×10^{-9}	6.75438×10^{-1}	-4.32949×10^{-3}
a_5		-1.95682×10^{-1}	
a_6		3.67827×10^{-2}	
a_7		-4.46911×10^{-3}	
a_8		3.38232×10^{-4}	
a_9		-1.44859×10^{-5}	
a_{10}		2.68025×10^{-7}	

TABLE III. List of values of the radial dose function, $g_L(r)$, for ^{192}Ir and ^{90}Sr/^{90}Y single seed sources using effective lengths of 3 and 2.5 mm, respectively. Values of $g(\rho)$ for ^{32}P wire sources (20 and 27 mm long) are also listed in the rightmost column. These values were generated with Eqs. (15) and (16) and the coefficients given in Table II for the respective radionuclides. Note that both r and ρ are expressed in millimeters. The fit for ^{192}Ir is valid for $0.5\ \text{mm} \leq r \leq 90\ \text{mm}$, that for ^{90}Sr/^{90}Y for $0.5\ \text{mm} \leq r \leq 9.9\ \text{mm}$. The fit for ^{32}P is valid for $0.5\ \text{mm} \leq \rho \leq 6.5\ \text{mm}$.

r or ρ (mm)	^{192}Ir $g_L(r)$	^{90}Sr/^{90}Y $g_L(r)$	^{32}P $g(\rho)$
0.5	0.990	1.134×10^{0}	1.862×10^{0}
1.0	0.990	1.096×10^{0}	1.634×10^{0}
1.5	0.990	1.067×10^{0}	1.322×10^{0}
2.0	0.991	1.001×10^{0}	1.000×10^{0}
2.5	0.991	9.088×10^{-1}	7.131×10^{-1}
3.0	0.992	8.034×10^{-1}	4.797×10^{-1}
3.5	0.993	6.919×10^{-1}	3.028×10^{-1}
4.0	0.993	5.780×10^{-1}	1.772×10^{-1}
4.5	0.994	4.660×10^{-1}	9.441×10^{-2}
5.0	0.994	3.621×10^{-1}	4.465×10^{-2}
5.5	0.995	2.718×10^{-1}	1.817×10^{-2}
6.0	0.995	1.978×10^{-1}	6.125×10^{-3}
6.5	0.996	1.389×10^{-1}	1.636×10^{-3}
7.0	0.996	9.223×10^{-2}	
7.5	0.997	5.587×10^{-2}	
8.0	0.998	3.025×10^{-2}	
8.5	0.999	1.617×10^{-2}	
9.0	0.999	9.814×10^{-3}	
10.0	1.000		
20.0	1.010		
30.0	1.015		
40.0	1.010		
50.0	0.996		
60.0	0.972		
70.0	0.942		
80.0	0.913		
90.0	0.891		

extrapolation chamber should continue to be used as the primary quantity for specification of beta particle sources for IVBT.

It is anticipated that well-type ionization chambers will continue to be the principal instrument used to transfer calibrations of sources between laboratories. For this purpose it is extremely important that the inserts used to position the sources within the chamber volume be standardized since the chamber calibration coefficient will be different for each source design and chamber insert type.

It should also be noted that, strictly speaking, the well chamber will measure a quantity that is related to source contained activity. Use of the well-chamber reading to infer reference absorbed dose rate cannot be done without knowledge that the activity is distributed uniformly in the source (which may, e.g., be verified via film measurements). This is particularly important for beta-particle line sources since the reference absorbed dose rate is influenced only by the central section of the source with a length of the same order of magnitude as the beta particle range.[41] Nonuniform sources thus have a different relationship between contained activity and reference absorbed dose rate than uniform sources. The latter case is usually assumed in modeling calculations made to yield this relationship.

Also necessary is the frequent use of reference sources to check the long-term stability of the response of the well chamber. The latter sources need not be calibrated since only the relative readings are necessary for this purpose. Sources with a long halflife such as ^{137}Cs or ^{90}Sr/^{90}Y are recommended for this purpose. Preferably they would be usable in the same insert as that used for the brachytherapy source calibrations so that insert integrity could be monitored as well.

In principle, any radiation sensitive detector in a calibrated reproducible geometry could be used to transfer calibrations between laboratories. For beta sources, the best detectors would be similar to the extrapolation chamber described above for the direct measurement of reference absorbed dose rate; the only difference being that calibration of the detector in a radiation field of known absorbed dose rate would be necessary. As with well-ionization chambers, the detector in its measurement geometry (phantom, holder, etc.) would be calibrated using a brachytherapy source with known reference absorbed dose rate. The system would require calibration for each type of source to be measured.

IV.B. Recommended dose calculation formalism

We recommend that the general, 2D dose-rate equation from the 2004 TG-43 protocol given in Eq. (1) be retained for photon and beta particle emitting seed sources. In this formalism we recommend using the line-source model given in Eq. (4). (The point source approximation is not considered appropriate for the close distances involved in intravascular brachytherapy source dosimetry.) Also, we recommend the use of linear superposition for the summation of doses from individual sources in a train. For the calculation of the dose distribution about the 20 and 27 mm Guidant ^{32}P line sources, we recommend the cylindrical formalism discussed in Sec. II D.

IV.C. Recommended dosimetry parameters

IV.C.1. ^{192}Ir seed train sources

IV.C.1.a. Source length.

The recommended value for the active source length L is 3.0 mm. This value has been used for the calculation of all data presented below.

IV.C.1.b. Dose rate constant.

Published values[27,39,40,51,68–72] of the dose rate constant [absorbed dose rate in water at 10 mm (1 cm) per unit air kerma strength (U)] were compared and are shown in Table I. For the sake of simplicity and consistency we recommend the TG-43 recommended value, 1.12 cGy U^{-1} h^{-1} of Nath *et al.*[51] for the Best model 81-01 ^{192}Ir seed as the reference value for this parameter. All published values are within 2% of this reference value.

Also shown in Table I are the four reported values for the dose rate at 2 mm in water per unit air kerma strength. These values are also in fair agreement with one another (the difference between the largest and smallest value $<5\%$).

IV.C.1.c. Radial dose function.

Four sets of published values for the radial dose function, $g_L(r)$, for a single ^{192}Ir seed source, are shown in Fig. 5.

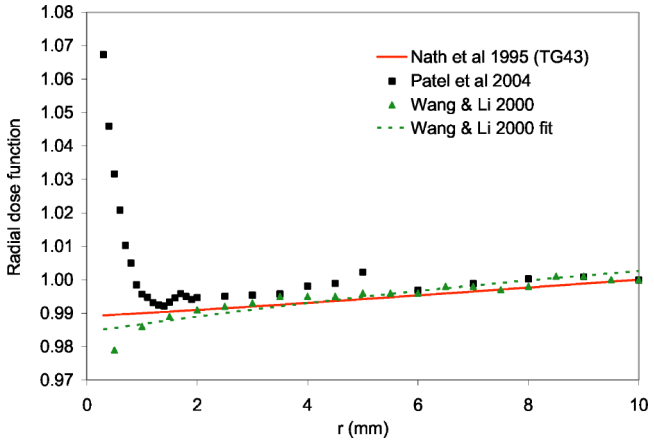

FIG. 5. Comparison of published radial dose functions for a single ^{192}Ir seed. The recommended data set is shown in red.

They all agree with one another to within about 2% at distances larger than 1 mm and within 4% between 0.5 and 1 mm. However, for shorter distances, the values by Patel *et al.*[72] rise steeply as the distance decreases. This is due to the inclusion of the contribution of the beta particles emitted by ^{192}Ir. Although we consider this study more correct at shorter distances, we again recommend the TG-43 values for the sake of simplicity and because these beta particles are absorbed in the nylon ribbon and do not contribute a significant dose to the tissues.[73] The recommended reference values are obtained from the TG-43 polynomial fit calculated down to 0.5 mm from the seed center (the closest distance from any tissue, even in an eccentric catheter and ribbon). This function is also shown in Fig. 5 and is given by

$$g_L(r) = \sum_{i=0}^{n} a_i r^i, \tag{15}$$

where n is the order of the polynomial used for the fit. The parameters of the fit are given in Table II. Note that r is expressed in millimeters. The range of application of this function is from 0.5 to 90 mm.

IV.C.1.d. 2D anisotropy function.

A sample of the published values[27,51,69,72,74–76] for the 2D anisotropy function, $F(r,\theta)$ for a single ^{192}Ir seed source is shown in Fig. 6. The recommended reference values for $r < 10$ mm are those given by Patel *et al.*[72] The values for $r \geqslant 10$ mm are from the TG-43 recommendation.[51] This choice was made based on the fact that this Monte Carlo study was the most densely populated and also considered the beta particles and electrons emitted by the seed source. As shown in Fig. 6 the chosen set agrees well with those of other authors, except at short distances and small angles where the beta particle contribution influences the function. These values are shown in Table IV. For reference purposes, the values of the product of r^2 and the geometry function, $G_L(r,\theta)$, for a source with a 3 mm active length are displayed in Table V(a). The main reason for using the TG-43 data for distances $r \geqslant 1$ cm is that the dose contributions at these distances are relatively unimportant for IVBT. In order to keep only one data set for ^{192}Ir (Best) seeds used in conventional brachytherapy for distances of 1 cm and greater, the existing TG-43 values are recommended. However, these values may change when new recommendations from the high energy source working group become available in the future.

IV.C.1.e. Comparison of dose distributions.

The dose distributions for a single seed, and a 39 mm (10 seed) train, calculated using the reference parameters, are tabulated in Tables VI and VII, respectively. Dose rates at 2 mm, averaged over the central $\frac{2}{3}$ of the train length are shown in Table VIII for commonly used train lengths. For comparison with published measurements and calculations,[27,72,75,77,78] relative depth-dose profiles and axial dose profiles for 23 mm (6 seed trains) are shown in Figs. 7 and 8, respectively. Because the transverse dose profiles at the train center (located at an interseed gap) and at the seed center are very different, these are shown separately in Figs. 7(a) and 7(b)

IV.C.2. ^{90}Sr/^{90}Y seed train sources

IV.C.2.a. Source length.

The recommended value for the active source length L is 2.5 mm. This value has been used for the calculation of all data presented below.

IV.C.2.b. Reference absorbed dose rate per unit activity.

Published values[27,28,79] of the absorbed dose rate in water at 2 mm per unit contained activity were compared and are shown in Table IX. The average of the published values shown, 1.10 Gy min^{-1} mCi^{-1}, was chosen as the reference value for both 5 F and 3.5 F seeds. As shown in Table IX, all published values are within 2% of this reference value. The differences between the values published for the 5 F and 3.5 F sources were not considered to be significant. In some cases, as specified in the table, authors used the combined activities of the parent ^{90}Sr and daughter ^{90}Y for the activity specification. In these cases, it was necessary to multiply the published value by a factor of 2 to account for this.

Table X shows published values[27,28,71,80–82] of the absorbed dose rate (Gy min^{-1}) in water at 2 mm per unit contained activity (mCi) for train sources of various lengths. Where train values were not given explicitly in the references, they were calculated from the value for a single seed (see Table IX) and the radial dose function and anisotropy function published in the same reference. The scatter in the published values for train sources is considerably greater than for a single seed, mainly due to the inclusion of some measured ("exp") data in the comparisons. The recommended reference values for the dose rate per unit contained activity are 0.154, 0.113, and 0.0746 Gy min^{-1} mCi^{-1} for seed trains of lengths, 30, 40, and 60 mm, respectively. As in Table IX, it was sometimes necessary to multiply published values by a factor of 2 to account for the activity specification used.

IV.C.2.c. Radial dose function.

Published values[27,28,41] for the radial dose function for a single ^{90}Sr/^{90}Y seed source are shown in Fig. 9. The recom-

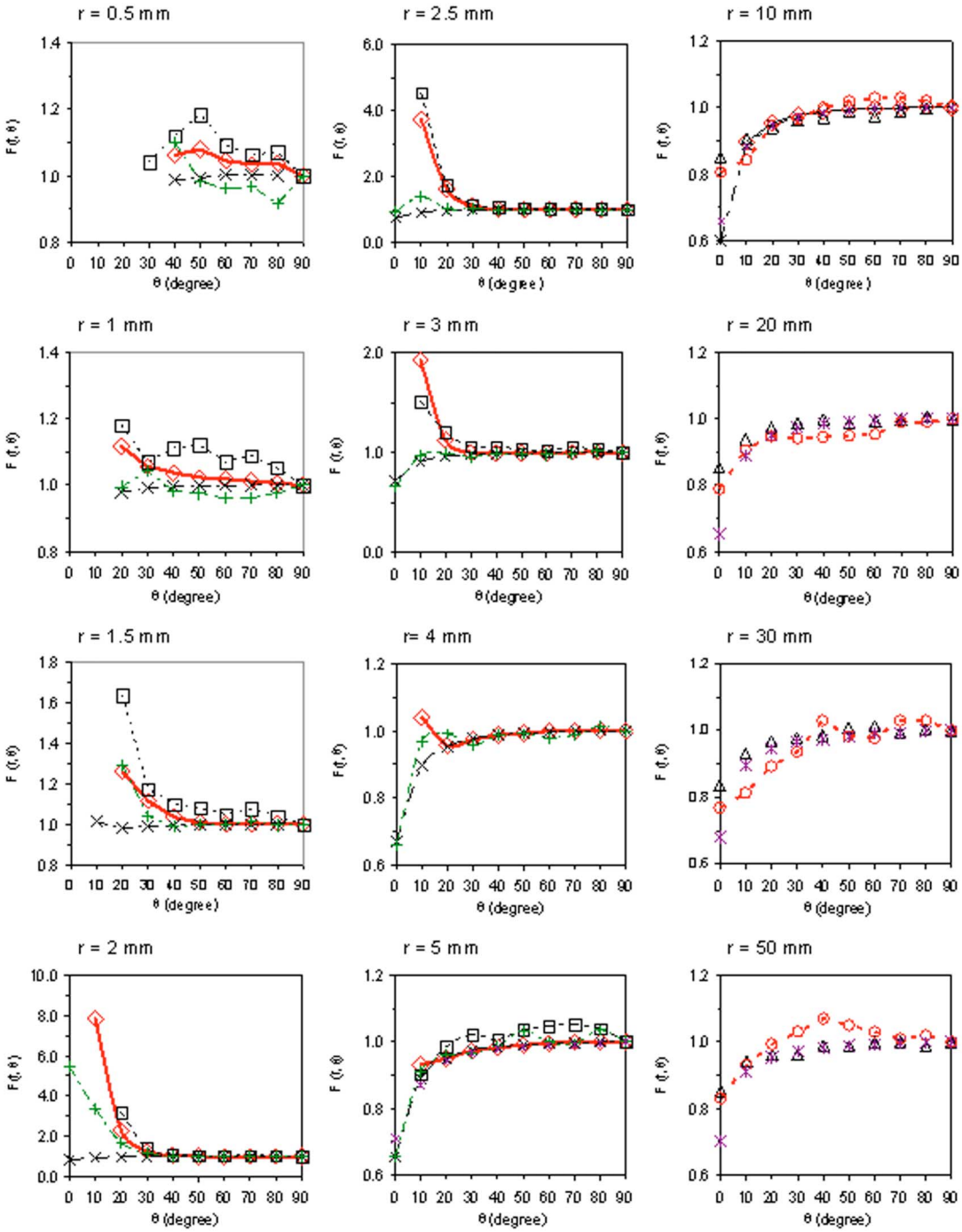

FIG. 6. Comparison of published 2D anisotropy functions, $F(r,\theta)$, for a single ^{192}Ir seed. The data reported by Patel *et al.* (Ref. 72), Wang and Li (Ref. 27), Soares (Ref. 75), Yang and Chan (Ref. 74), Anctil *et al.* (Ref. 69), Capote *et al.* (Ref. 76), and Nath *et al.* (Ref. 51) are shown by the symbol types diamond, cross, square, plus sign, triangle, star, and circle, respectively. Recommended data are shown in red.

mended reference values are a fit of the Wang and Li (2002)[28] data for the 5 F source. This function is also shown plotted in Fig. 9 and is given by Eq. (15). The parameters of the fit are given in Table II. Note that r is expressed in millimeters. The range of application of this function is from 0.5 to 9.9 mm. The recommended values of the radial dose function are also tabulated in Table III.

IV.C.2.d. 2D anisotropy function.

A sample of the published values[27,28,41] for the 2D anisotropy function, $F(r,\theta)$, for a single ^{90}Sr/^{90}Y seed source is shown in Fig. 10. The recommended reference values are those given by Wang and Li (2002)[28] for the 5 F source. These data are shown in Table XI. For reference purposes, the values of the geometry function multiplied by the distance squared for a 2.5 mm seed are listed in Table V(b).

IV.C.2.e. Comparison of dose distributions.

TABLE IV. Recommended values of the anisotropy function, $F(r,\theta)$, for a single ^{192}Ir seed.

r (mm)	θ (degrees) 0	10	20	30	40	50	60	70	80	90
0.5	—	—	—	—	1.063	1.079	1.045	1.034	1.038	1.000
0.6	—	—	—	1.032	1.078	1.040	1.037	1.018	1.027	1.000
0.7	—	—	—	1.077	1.073	1.043	1.025	1.024	1.020	1.000
0.8	—	—	—	1.070	1.036	1.032	1.008	1.019	1.013	1.000
0.9	—	—	1.085	1.072	1.053	1.022	1.019	1.017	1.011	1.000
1.0	—	—	1.117	1.057	1.037	1.023	1.018	1.012	1.005	1.000
1.1	—	—	1.098	1.061	1.025	1.021	1.013	1.007	1.002	1.000
1.2	—	—	1.076	1.047	1.028	1.014	1.007	1.005	1.002	1.000
1.3	—	—	1.099	1.058	1.023	1.010	1.007	1.004	1.003	1.000
1.4	—	—	1.151	1.059	1.030	1.012	1.004	1.004	1.005	1.000
1.5	—	—	1.259	1.115	1.034	1.008	1.001	1.002	1.004	1.000
1.6	—	—	1.703	1.144	1.033	1.007	0.999	1.000	1.002	1.000
1.7	—	5.661	1.914	1.216	1.039	1.005	1.001	0.999	1.001	1.000
1.8	—	7.870	2.146	1.243	1.044	1.006	1.003	1.002	1.003	1.000
1.9	—	8.235	2.348	1.277	1.048	1.009	1.004	1.003	1.003	1.000
2.0	—	7.834	2.293	1.261	1.049	1.008	1.001	1.003	1.003	1.000
2.5	—	3.738	1.621	1.123	1.015	0.997	0.998	1.004	1.003	1.000
3.0	—	1.923	1.126	1.002	0.994	0.995	0.999	1.002	1.004	1.000
3.5	—	1.266	0.981	0.978	0.989	0.996	0.998	1.001	1.003	1.000
4.0	—	1.041	0.957	0.975	0.987	0.993	1.000	1.000	1.003	1.000
4.5	—	0.971	0.955	0.974	0.988	0.993	0.997	1.001	1.005	1.000
5.0	—	0.930	0.950	0.973	0.982	0.990	0.996	0.999	1.000	1.000
6.0	—	0.909	0.954	0.976	0.987	0.996	1.001	1.000	1.003	1.000
7.0	—	0.904	0.957	0.977	0.990	0.992	0.997	0.999	1.001	1.000
8.0	—	0.904	0.955	0.976	0.988	0.992	0.997	0.998	1.001	1.000
9.0	—	0.898	0.953	0.976	0.985	0.992	0.996	0.999	1.001	1.000
10	0.806	0.843	0.947	0.966	1.000	1.020	1.030	1.030	1.020	1.000
20	0.788	0.906	0.947	0.941	0.945	0.949	0.953	0.989	0.991	1.000
30	0.769	0.813	0.893	0.936	1.030	0.984	0.977	1.030	1.030	1.000
40	0.868	0.949	1.010	0.996	1.020	1.030	1.040	1.010	1.010	1.000
50	0.831	0.931	0.994	1.030	1.070	1.050	1.030	1.010	1.020	1.000
60	0.819	0.899	0.920	0.928	0.973	0.959	0.954	0.996	0.997	1.000
70	0.844	0.944	0.985	0.969	0.962	0.967	1.010	1.020	0.979	1.000
80	0.824	0.932	0.926	0.958	0.970	0.982	0.970	0.983	0.994	1.000
90	0.889	0.962	0.990	0.968	0.996	0.992	1.010	1.020	0.987	1.000

TABLE V. Geometry function $G_L(r,\theta)$ multiplied by r^2 for a seed source with (a) 3.0 mm (for ^{192}Ir) and (b) 2.5 mm (for ^{90}Sr/^{90}Y) active lengths.

(a)

r (mm)	θ (degrees) 0	10	20	30	40	50	60	70	80	90
0.5		2.891	1.409	0.928	0.698	0.570	0.494	0.448	0.424	0.416
1.0		5.273	2.392	1.510	1.113	0.900	0.777	0.705	0.667	0.655
1.5		4.523	2.296	1.571	1.222	1.025	0.907	0.836	0.798	0.785
2.0		2.062	1.685	1.390	1.187	1.050	0.959	0.901	0.868	0.858
2.5		1.511	1.389	1.255	1.139	1.047	0.980	0.935	0.909	0.901
3.0		1.310	1.251	1.176	1.102	1.039	0.990	0.955	0.934	0.927
4.0		1.155	1.131	1.097	1.060	1.026	0.996	0.975	0.961	0.957
5.0		1.094	1.081	1.062	1.039	1.018	0.998	0.984	0.975	0.972
7.0		1.046	1.040	1.031	1.020	1.009	1.000	0.992	0.987	0.985
10	1.023	1.022	1.019	1.015	1.010	1.005	1.000	0.996	0.993	0.993
20	1.006	1.005	1.005	1.004	1.003	1.001	1.000	0.999	0.998	0.998
30	1.003	1.002	1.002	1.002	1.001	1.001	1.000	1.000	0.999	0.999
40	1.001	1.001	1.001	1.001	1.001	1.000	1.000	1.000	1.000	1.000
50	1.001	1.001	1.001	1.001	1.000	1.000	1.000	1.000	1.000	1.000

(b)

r (mm)	θ (degrees) 0	10	20	30	40	50	60	70	80	90
0.5		3.430	1.653	1.079	0.807	0.656	0.566	0.513	0.485	0.476
1.0		5.723	2.518	1.595	1.187	0.969	0.843	0.769	0.729	0.717
1.5	3.273	2.620	1.892	1.463	1.207	1.046	0.944	0.880	0.845	0.834
2.0	1.641	1.576	1.431	1.277	1.147	1.049	0.977	0.930	0.903	0.894
2.5	1.333	1.310	1.251	1.176	1.102	1.039	0.990	0.955	0.934	0.927
3.0	1.210	1.198	1.165	1.121	1.074	1.030	0.995	0.969	0.953	0.947
4.0	1.108	1.103	1.088	1.067	1.043	1.019	0.998	0.982	0.973	0.969
5.0	1.067	1.064	1.055	1.042	1.028	1.013	0.999	0.989	0.982	0.980
7.0	1.033	1.032	1.028	1.021	1.014	1.007	1.000	0.994	0.991	0.990
10	1.016	1.015	1.013	1.010	1.007	1.003	1.000	0.997	0.995	0.995
20	1.004	1.004	1.003	1.003	1.002	1.001	1.000	0.999	0.999	0.999
30	1.002	1.002	1.001	1.001	1.001	1.000	1.000	1.000	0.999	0.999
40	1.001	1.001	1.001	1.001	1.000	1.000	1.000	1.000	1.000	1.000
50	1.001	1.001	1.001	1.000	1.000	1.000	1.000	1.000	1.000	1.000

The away-and-along table of recommended dose rates normalized to unity at the reference point for a single ^{90}Sr/^{90}Y seed source is displayed in Table XII. The dose distribution for a 40 mm (16 seed) train calculated using the reference parameters is tabulated in Table XIII. For comparison with published measurements and calculations,[27,28,41,80–84] relative depth-dose profiles for 30 mm (12 seed trains) and axial dose profiles for 40 mm (16 seed trains) are shown plotted in Figs. 11 and 12, respectively.

IV.C.3. ^{32}P *wire sources*

IV.C.3.a. Reference absorbed dose rate per unit activity. Published values[29,30,62,85–89] of the reference absorbed dose rate per unit contained activity for the 20 and 27 mm Guidant ^{32}P sources are shown in Table XIV (measurement results) and Table XV (simulation results). Also shown in these tables are the corresponding values of the reference absorbed dose rate per unit contained activity per unit active source length. This value is expected to be the same for both types of sources as may be explained as follows.

The reference absorbed dose rate may be assumed to be entirely due to beta particles, as the bremsstrahlung contribution at the reference point ($\rho_0 z_0$) is negligibly small. Therefore, only the parts of the source located within distances less than the beta particle range from the reference point can be assumed to contribute to the reference absorbed dose rate. Since the range of ^{32}P beta particles in water equals ~8 mm, this means for both the 20 and 27 mm sources that only the central section of the source, with a length of ~16 mm, contributes to the reference absorbed dose rate. Since the 20 and 27 mm source geometries are essentially the same except for the active source length, see Sec. II B 3, it then follows that the reference absorbed dose rate per unit activity is the same for both sources if the activity per unit source length is the same. More generally it can be said that the reference absorbed dose rate per unit activity per unit length is expected to be independent of source length for any ^{32}P line source with an active source length larger than twice the range of the beta particles.

For this reason, it was decided to calculate the recommended absorbed dose rate per unit activity for both the 20 and 27 mm sources from a single recommended value of the absorbed dose rate per unit activity per unit length. This value was derived as follows. First, we calculated the average of all published experimental values (0.622 cGy s^{-1} mCi cm) and the average of all published

TABLE VI. Away-and-along table for dose rates from a single ^{192}Ir seed normalized to unity at 2 mm along the transverse axis of the seed. Absolute absorbed dose rates in cGy h^{-1} for a seed of unit air kerma strength (1 U) can be obtained by multiplication with 24.12.

Along Axis	Away from Axis, ρ (mm)																										
z (mm)	0.5	0.6	0.7	0.8	0.9	1.0	1.1	1.2	1.3	1.4	1.5	1.6	1.7	1.8	1.9	2.0	2.5	3.0	3.5	4.0	4.5	5.0	6.0	7.0	8.0	9.0	10.0
0.0	8.052	6.327	5.114	4.242	3.572	3.057	2.651	2.317	2.044	1.815	1.625	1.463	1.323	1.200	1.092	1.000	0.672	0.481	0.360	0.280	0.223	0.183	0.127	0.094	0.072	0.057	0.047
1.0	7.021	5.464	4.378	3.589	3.037	2.599	2.242	1.970	1.746	1.554	1.401	1.267	1.152	1.051	0.962	0.887	0.613	0.446	0.340	0.267	0.215	0.176	0.124	0.092	0.071	0.057	0.046
1.2	6.368	4.964	4.009	3.320	2.820	2.402	2.082	1.838	1.623	1.455	1.314	1.187	1.080	0.990	0.909	0.840	0.587	0.432	0.331	0.261	0.211	0.173	0.123	0.092	0.071	0.056	0.046
1.4	6.038	4.774	3.864	3.190	2.653	2.243	1.934	1.691	1.496	1.344	1.213	1.103	1.006	0.927	0.855	0.789	0.560	0.416	0.320	0.255	0.207	0.171	0.121	0.091	0.070	0.056	0.046
1.6	8.371	5.778	4.177	3.214	2.595	2.127	1.812	1.570	1.381	1.241	1.112	1.013	0.925	0.855	0.789	0.734	0.528	0.399	0.310	0.247	0.202	0.168	0.119	0.090	0.070	0.056	0.046
1.8	10.05	6.396	4.396	3.250	2.499	1.985	1.661	1.425	1.252	1.108	1.015	0.923	0.845	0.783	0.727	0.680	0.497	0.379	0.298	0.239	0.197	0.163	0.118	0.088	0.069	0.055	0.045
2.0	8.377	5.574	3.900	2.876	2.197	1.777	1.454	1.236	1.097	0.990	0.898	0.825	0.764	0.710	0.667	0.624	0.467	0.360	0.286	0.232	0.190	0.160	0.116	0.087	0.068	0.055	0.045
2.2	5.749	4.039	2.976	2.306	1.801	1.503	1.241	1.087	0.963	0.864	0.794	0.735	0.686	0.641	0.604	0.569	0.436	0.342	0.273	0.223	0.185	0.155	0.113	0.086	0.067	0.054	0.045
2.4	3.698	2.831	2.181	1.745	1.459	1.210	1.040	0.908	0.823	0.757	0.695	0.651	0.613	0.579	0.547	0.518	0.405	0.322	0.261	0.215	0.178	0.151	0.111	0.085	0.067	0.054	0.044
3.0	1.272	1.026	0.852	0.729	0.669	0.614	0.576	0.541	0.516	0.495	0.472	0.453	0.435	0.419	0.403	0.389	0.322	0.268	0.224	0.188	0.160	0.138	0.103	0.080	0.064	0.052	0.043
4.0	0.418	0.347	0.331	0.310	0.306	0.298	0.291	0.285	0.282	0.276	0.273	0.267	0.263	0.257	0.252	0.247	0.219	0.193	0.169	0.148	0.130	0.115	0.090	0.072	0.058	0.048	0.040
5.0	0.206	0.189	0.185	0.183	0.185	0.181	0.178	0.179	0.176	0.175	0.173	0.172	0.171	0.169	0.167	0.165	0.153	0.140	0.127	0.116	0.104	0.095	0.077	0.063	0.053	0.044	0.038
6.0	0.131	0.119	0.124	0.120	0.122	0.121	0.122	0.121	0.120	0.120	0.120	0.119	0.118	0.118	0.116	0.116	0.111	0.105	0.098	0.091	0.084	0.077	0.065	0.055	0.047	0.040	0.034
7.0	0.096	0.085	0.086	0.086	0.086	0.087	0.086	0.087	0.087	0.087	0.087	0.087	0.087	0.087	0.086	0.086	0.084	0.080	0.076	0.072	0.068	0.063	0.055	0.048	0.041	0.036	0.031
8.0	0.063	0.062	0.066	0.063	0.065	0.065	0.065	0.065	0.065	0.066	0.066	0.066	0.066	0.066	0.066	0.066	0.064	0.063	0.061	0.058	0.055	0.053	0.047	0.041	0.037	0.032	0.029
9.0	0.052	0.051	0.049	0.049	0.049	0.051	0.051	0.051	0.051	0.051	0.051	0.052	0.052	0.052	0.052	0.052	0.051	0.050	0.049	0.048	0.046	0.044	0.040	0.036	0.032	0.029	0.026
10.0	0.039	0.040	0.040	0.040	0.040	0.040	0.041	0.041	0.041	0.041	0.041	0.041	0.041	0.042	0.042	0.042	0.042	0.041	0.041	0.040	0.038	0.037	0.034	0.031	0.028	0.026	0.023

TABLE VII. Away-and-along table for dose rates from an ^{192}Ir 10 seed train normalized to an average value of 1 over the central $\frac{2}{3}$ active source length of the seed train at ρ=2 mm. Absolute absorbed dose rates in cGy h^{-1} for a source containing 10 seeds of unit air kerma strength (1 U in each seed) can be obtained by multiplying with 39.97.

Along axis z (mm)	Away from axis, ρ (mm)																		
	0.5	0.6	0.7	0.8	0.9	1.0	1.5	2.0	2.5	3.0	3.5	4.0	4.5	5.0	6.0	7.0	8.0	9.0	10.0
0.0	12.864	8.573	5.169	3.764	3.065	2.504	1.342	0.988	0.789	0.653	0.554	0.477	0.418	0.370	0.298	0.247	0.209	0.179	0.155
0.5	5.853	5.388	4.253	3.339	2.630	2.292	1.344	0.994	0.792	0.654	0.553	0.477	0.418	0.370	0.298	0.247	0.209	0.179	0.155
1.0	5.189	4.181	3.463	2.937	2.542	2.225	1.387	1.015	0.800	0.657	0.554	0.477	0.418	0.370	0.298	0.247	0.208	0.179	0.155
1.5	5.274	4.259	3.546	3.043	2.639	2.318	1.433	1.034	0.807	0.659	0.555	0.478	0.418	0.370	0.298	0.247	0.208	0.178	0.155
2.0	5.061	4.159	3.537	3.032	2.642	2.334	1.450	1.040	0.808	0.658	0.554	0.477	0.418	0.370	0.298	0.246	0.208	0.178	0.154
2.5	5.273	4.259	3.546	3.042	2.639	2.317	1.432	1.034	0.806	0.659	0.554	0.477	0.417	0.369	0.297	0.246	0.208	0.178	0.154
3.0	5.187	4.179	3.462	2.936	2.541	2.224	1.386	1.013	0.799	0.655	0.553	0.476	0.416	0.369	0.297	0.246	0.207	0.178	0.154
3.5	5.851	5.386	4.251	3.337	2.628	2.290	1.342	0.992	0.790	0.652	0.551	0.475	0.416	0.368	0.296	0.245	0.207	0.177	0.154
4.0	12.862	8.571	5.167	3.762	3.063	2.502	1.340	0.985	0.786	0.650	0.551	0.474	0.415	0.368	0.296	0.245	0.206	0.177	0.153
4.5	5.850	5.385	4.250	3.336	2.627	2.289	1.341	0.991	0.789	0.650	0.550	0.474	0.414	0.367	0.295	0.244	0.206	0.176	0.153
5.0	5.185	4.177	3.459	2.933	2.538	2.222	1.383	1.011	0.796	0.652	0.550	0.473	0.414	0.366	0.295	0.243	0.205	0.176	0.152
5.5	5.269	4.255	3.542	3.038	2.635	2.313	1.428	1.029	0.802	0.654	0.550	0.473	0.413	0.365	0.294	0.242	0.204	0.175	0.151
6.0	5.056	4.154	3.531	3.027	2.636	2.328	1.444	1.034	0.802	0.653	0.548	0.472	0.412	0.364	0.293	0.242	0.203	0.174	0.151
6.5	5.267	4.253	3.540	3.036	2.633	2.311	1.426	1.027	0.800	0.652	0.547	0.471	0.411	0.363	0.292	0.241	0.203	0.173	0.150
7.0	5.181	4.173	3.455	2.929	2.534	2.217	1.379	1.006	0.791	0.648	0.546	0.469	0.409	0.362	0.290	0.239	0.202	0.172	0.149
7.5	5.844	5.378	4.243	3.329	2.620	2.282	1.334	0.984	0.782	0.643	0.543	0.467	0.408	0.360	0.289	0.238	0.201	0.171	0.148
8.0	12.853	8.562	5.158	3.753	3.054	2.493	1.331	0.976	0.777	0.641	0.542	0.465	0.406	0.359	0.287	0.237	0.199	0.170	0.147
8.5	5.840	5.375	4.240	3.326	2.617	2.279	1.331	0.981	0.778	0.640	0.540	0.464	0.404	0.357	0.286	0.235	0.198	0.169	0.146
9.0	5.174	4.166	3.448	2.922	2.527	2.210	1.372	0.999	0.784	0.641	0.539	0.462	0.402	0.355	0.284	0.234	0.196	0.168	0.145
9.5	5.257	4.243	3.529	3.026	2.622	2.301	1.415	1.016	0.789	0.641	0.537	0.460	0.400	0.353	0.282	0.232	0.195	0.166	0.144
10.0	5.043	4.140	3.518	3.013	2.622	2.314	1.430	1.020	0.788	0.638	0.534	0.457	0.399	0.351	0.280	0.230	0.193	0.165	0.142
10.5	5.252	4.237	3.524	3.020	2.617	2.295	1.410	1.011	0.783	0.636	0.532	0.455	0.395	0.348	0.278	0.228	0.191	0.163	0.141
11.0	5.164	4.155	3.438	2.912	2.516	2.200	1.361	0.988	0.773	0.630	0.528	0.451	0.392	0.346	0.275	0.226	0.189	0.161	0.139
11.5	5.824	5.359	4.224	3.310	2.601	2.262	1.314	0.964	0.762	0.623	0.523	0.448	0.389	0.342	0.273	0.223	0.187	0.159	0.138
12.0	12.831	8.540	5.136	3.731	3.032	2.470	1.308	0.953	0.754	0.618	0.520	0.444	0.385	0.339	0.269	0.221	0.185	0.157	0.136
12.5	5.825	5.359	4.222	3.307	2.598	2.258	1.306	0.955	0.753	0.615	0.515	0.440	0.382	0.335	0.266	0.218	0.182	0.155	0.134
13.0	5.166	4.156	3.436	2.908	2.510	2.192	1.344	0.970	0.756	0.613	0.511	0.436	0.377	0.331	0.263	0.215	0.180	0.153	0.132
13.5	5.247	4.230	3.515	3.009	2.603	2.279	1.383	0.984	0.757	0.610	0.506	0.431	0.372	0.327	0.259	0.211	0.177	0.150	0.130
14.0	5.030	4.125	3.499	2.992	2.598	2.288	1.392	0.982	0.751	0.602	0.500	0.425	0.367	0.322	0.254	0.208	0.173	0.148	0.128
14.5	5.236	4.218	3.501	2.994	2.587	2.262	1.367	0.968	0.741	0.596	0.493	0.418	0.361	0.316	0.249	0.203	0.170	0.145	0.125
15.0	5.143	4.131	3.409	2.879	2.479	2.158	1.311	0.938	0.725	0.584	0.484	0.410	0.354	0.310	0.244	0.199	0.166	0.142	0.123
15.5	5.799	5.328	4.187	3.267	2.553	2.210	1.255	0.906	0.706	0.570	0.474	0.401	0.346	0.302	0.239	0.194	0.163	0.139	0.120
16.0	12.797	8.499	5.088	3.676	2.971	2.403	1.238	0.885	0.689	0.557	0.463	0.391	0.337	0.294	0.232	0.189	0.159	0.135	0.117
16.5	5.779	5.304	4.158	3.234	2.516	2.171	1.222	0.874	0.677	0.544	0.450	0.380	0.327	0.286	0.226	0.184	0.154	0.132	0.114
17.0	5.103	4.080	3.348	2.808	2.401	2.084	1.241	0.873	0.665	0.530	0.436	0.368	0.316	0.276	0.218	0.179	0.150	0.128	0.111
17.5	5.154	4.119	3.387	2.865	2.461	2.139	1.254	0.865	0.649	0.513	0.420	0.354	0.304	0.266	0.210	0.172	0.145	0.124	0.108
18.0	4.884	3.951	3.300	2.795	2.407	2.102	1.230	0.836	0.621	0.489	0.400	0.337	0.291	0.254	0.202	0.166	0.140	0.121	0.105
18.5	4.961	3.894	3.185	2.695	2.306	1.997	1.155	0.784	0.584	0.461	0.378	0.319	0.275	0.242	0.193	0.159	0.135	0.116	0.102
19.0	4.444	3.454	2.808	2.348	2.013	1.752	1.023	0.705	0.532	0.424	0.351	0.299	0.259	0.228	0.184	0.153	0.130	0.112	0.099

TABLE VII. (*Continued.*)

Along axis z (mm)	Away from axis, ρ (mm)																		
	0.5	0.6	0.7	0.8	0.9	1.0	1.5	2.0	2.5	3.0	3.5	4.0	4.5	5.0	6.0	7.0	8.0	9.0	10.0
19.5	3.700	3.612	2.818	2.205	1.755	1.518	0.858	0.608	0.472	0.384	0.322	0.277	0.242	0.214	0.174	0.146	0.125	0.108	0.095
20.0	6.446	4.301	2.599	1.896	1.547	1.266	0.686	0.509	0.409	0.341	0.292	0.254	0.224	0.200	0.164	0.138	0.119	0.104	0.092
20.5	2.182	1.805	1.464	1.163	0.904	0.802	0.515	0.416	0.349	0.300	0.261	0.231	0.206	0.186	0.154	0.131	0.114	0.100	0.089
21.0	0.773	0.755	0.685	0.618	0.558	0.503	0.394	0.339	0.297	0.262	0.233	0.209	0.189	0.172	0.145	0.124	0.108	0.096	0.085
22.0	0.207	0.237	0.266	0.266	0.264	0.262	0.250	0.234	0.217	0.200	0.185	0.170	0.158	0.146	0.127	0.111	0.098	0.087	0.079
24.0	0.095	0.102	0.109	0.116	0.123	0.130	0.133	0.132	0.129	0.125	0.121	0.116	0.110	0.105	0.096	0.087	0.079	0.072	0.066
26.0	0.060	0.063	0.066	0.069	0.072	0.075	0.087	0.087	0.087	0.086	0.084	0.082	0.080	0.078	0.074	0.069	0.064	0.060	0.056
28.0	0.060	0.060	0.061	0.061	0.061	0.061	0.062	0.063	0.063	0.063	0.063	0.062	0.061	0.060	0.058	0.055	0.052	0.049	0.047
30.0	0.046	0.046	0.047	0.047	0.047	0.047	0.048	0.048	0.049	0.049	0.049	0.048	0.048	0.048	0.046	0.045	0.043	0.041	0.040
40.0	0.019	0.019	0.019	0.019	0.019	0.019	0.020	0.020	0.020	0.020	0.020	0.020	0.020	0.020	0.020	0.020	0.020	0.020	0.020
50.0	0.010	0.010	0.010	0.010	0.010	0.010	0.010	0.010	0.010	0.010	0.011	0.011	0.011	0.011	0.011	0.011	0.011	0.011	0.011
60.0	0.005	0.005	0.005	0.005	0.005	0.005	0.005	0.005	0.005	0.005	0.005	0.005	0.005	0.005	0.005	0.005	0.005	0.005	0.005

TABLE VIII. Absorbed dose rate, $\dot{D}$, in cGy h^{-1} at 2 mm along the transverse axis of the seed for a single ^{192}Ir seed and averaged over $\frac{2}{3}$ of the active source length at ρ=2 mm for 6,10,14,18, and 22 seed trains containing seeds of unit air kerma strength (1 U per seed). For comparison, the vendor-specified values are also shown.

	$\dot{D}$ (cGy h^{-1})	
Number of Seeds	This Recommendation	Vendor's Specification
1	24.12	
6	38.02	40.50
10	39.97	41.84
14	40.90	41.99
18	41.31	
22	41.58	

simulated values (0.604 cGy s^{-1} mCi cm) see Tables XIV and XV. These values differ by about 3%, which is not significant compared to the experimental uncertainties quoted in the publications. Second, the average of these two average values was calculated, see Table XVI. In this way, equal weight was given to the experimental and simulation results.

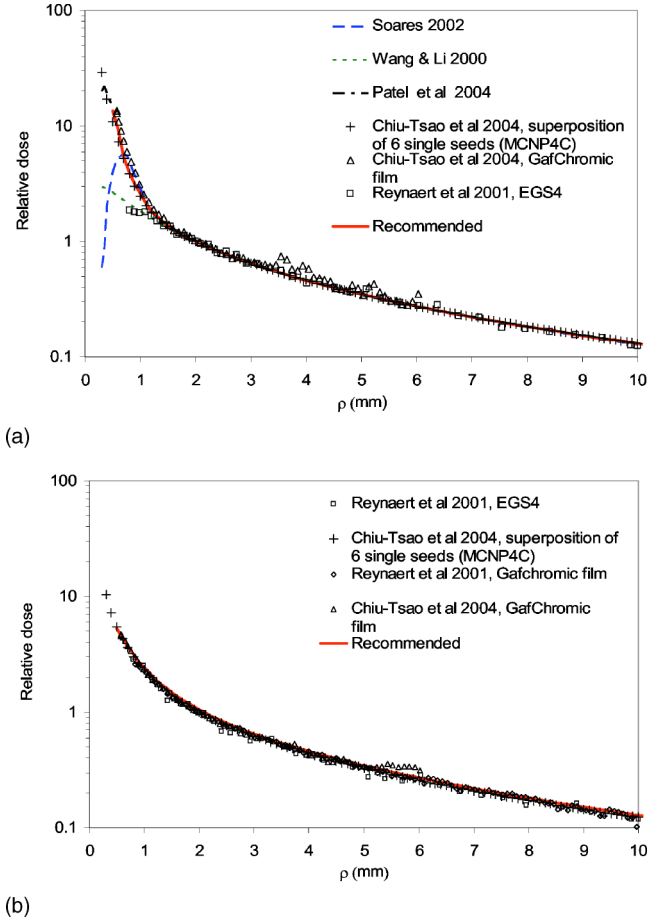

FIG. 7. (a) Comparison of relative depth-dose curves for an ^{192}Ir 6 seed train at the train center (located at an interseed gap). The curves represent the doses obtained by superposition using three separate sets of single seed reference dosimetry parameters reported by Soares (Ref. 75), Wang and Li (Ref. 27), and Patel *et al.* (Ref. 72). (b) Comparison of relative depth-dose curves for an ^{192}Ir 6 seed train at the seed center.

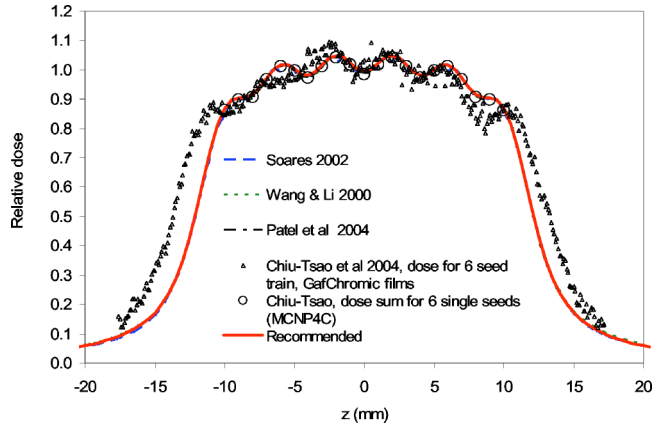

FIG. 8. Comparison of axial dose profiles at 2 mm depth for an ^{192}Ir 6-seed train normalized to averages of the central $\frac{2}{3}$ length of the seed train ($\pm$7.7 mm from the center). The curves represent the doses obtained by superposition using three separate sets of single-seed reference dosimetry parameters reported by Soares (Ref. 75), Wang and Li (Ref. 27), and Patel *et al.* (Ref. 72).

The resulting recommended value of the reference absorbed dose rate per unit activity per unit length equals 0.613 cGy s^{-1} mCi cm. As can be seen from Tables XIV and XV, all published values of this parameter are between +6% and −5% of the recommended value. As expected, no significant differences were found between the values published for the 27 and 20 mm sources.

As can be seen by comparing the EGSNRC results from Wang and Li (2001)[87] and Li *et al.* (2001)[88] in Table XV, the presence or absence of a catheter in a simulation or measurement may have a small effect (~3% according to these simulations) on the value of the reference absorbed dose rate per unit activity. A Monte Carlo analysis of the influence of a

TABLE IX. Comparison of published values of the reference absorbed does rate per unit contained activity for a single ^{90}Sr/^{90}Y seed.

Author	Type of Determination	Source Type	Dose Rate per Unit Contained Activity (Gy min^{-1} mCi^{-1})	% Difference from Reference Value (%)
Wang and Li 2000 (Ref. 27)	MC	5 F	1.09[a]	−0.8
Wang and Li 2002 (Ref. 28)	MC	3.5 F	1.11[a]	1.4
Wang and Li 2002 (Ref. 28)	MC	5 F	1.09[a]	−1.0
Asenjo *et al.* 2002 (Ref. 79)	MC	5 F	1.10[a]	0.3
		Average	1.10	
		SD	0.012	
		%SD	1.1%	

[a]The published values were multiplied by a factor of 2 to account for the contained activity specification convention used.

TABLE X. Comparison of the reference absorbed dose rate per unit contained activity at $\rho=2$ mm for (a) 30 mm (12 seed) $^{90}Sr/^{90}Y$ trains, (b) 40 mm (16 seed) $^{90}Sr/^{90}Y$ seed trains, and (c) 60 mm (24 seed) $^{90}Sr/^{90}Y$ seed trains.

(a)

Author	Type of Determination	Source Type	Dose Rate per Unit Contained Activity (Gy min^{-1} mCi^{-1})	% Difference from Reference Value (%)
Chibani and Li 2003 (Ref. 80)	MC	5 F	0.146	−4.9
Roa *et al.* 2004 (Ref. 81)	exp	5 F	0.144	−6.6
Roa *et al.* 2004	exp	3.5 F	0.166	7.6
Novoste (from Roa *et al.* 2004)	MC	5 F	0.168	9.1
Novoste (from Roa *et al.* 2004)	MC	3.5 F	0.174	13
Ye *et al.* 2003 (Ref. 71)	MC	5 F	0.140	−8.8
Ye *et al.* 2000 (Ref. 82)	MC	5 F	0.149[a]	−3.1
Novoste (from Ye *et al.* 2003)	MC	5 F	0.139	−9.6
Wang and Li 2000 (Ref. 27) superposition	MC	5 F	0.156	1.1
Wang and Li 2002 (Ref. 28) superposition	MC	3.5 F	0.158	2.6
Wang and Li 2002 superposition	MC	5 F	0.153	−0.5
		Average	0.154	
		SD	0.012	
		%SD	7.5%	

(b)

Author	Type of Determination	Source Type	Dose Rate per Unit Contained Activity (Gy min^{-1} mCi^{-1})	% Difference from Reference Value (%)
Roa *et al.* 2004	exp	3.5 F	0.111	−1.7
Novoste (from Roa *et al.* 2004)	MC	3.5 F	0.109	−3.8
NIST (unpublished)	exp[b]	3.5 F	0.110	−3.3
Wang and Li 2000 superposition	MC	5 F	0.117	3.0
Wang and Li 2002 superposition	MC	3.5 F	0.119	4.6
Wang and Li 2002 superposition	MC	5 F	0.115	1.3
		Average	0.113	
		SD	0.0040	
		%SD	3.5%	

(c)

Author	Type of Determination	Source Type	Dose Rate per Unit Contained Activity (Gy min^{-1} mCi^{-1})	% Difference from Reference Value (%)
Roa *et al.* 2004	exp	5 F	0.0696	−6.6
Novoste (from Roa *et al.* 2004)	MC	5 F	0.0698	−6.4
Wang and Li 2000 superposition	MC	5 F	0.0778	4.4
Wang and Li 2002 superposition	MC	3.5 F	0.0790	6.0
Wang and Li 2002 superposition	MC	5 F	0.0766	2.7
		Average	0.0746	
		SD	0.0045	
		%SD	6.1%	

[a]The published values were multiplied by a factor of 2 to account for the contained activity specification convention used.
[b]The estimated uncertainty in the NIST experimental determination of the reference absorbed dose rate per unit contained activity is dominated by the absorbed dose measurement uncertainty, given as $\pm 7.4\%$ (1σ) (Ref. 41).

centering catheter by Torres *et al.*[89] showed very similar results. However, a number of different clinical catheters (as well as a physics catheter for quality control measurements) have been used with this source, making it difficult to determine the appropriate correction factor for each value in the table. Furthermore, the resulting differences do not seem large in comparison to the variations arising from other differences between simulations and in comparison to the uncertainty quoted for the various measurement results. Therefore, no attempt has been made to correct for the presence or absence of a catheter.

The recommended values of the reference absorbed dose rate per unit contained activity have been derived from the above recommended value of the reference absorbed dose rate per unit activity per unit length by dividing by the active source length, see Table XV. The recommended values are 0.227 cGy s^{-1} mCi^{-1} for the 27 mm source and 0.307 cGy s^{-1} mCi^{-1} for the 20 mm source.

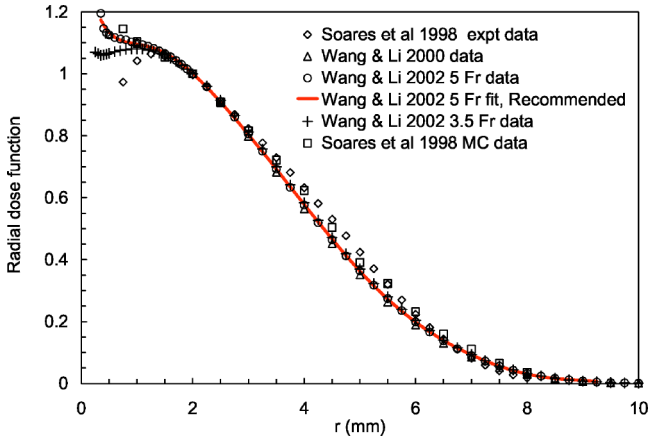

FIG. 9. Comparison of published radial dose functions for a single $^{90}Sr/^{90}Y$ seed. The red solid line shows the fit to the Wang and Li 5 F data that is recommended for both the 3.5 F and 5 F $^{90}Sr/^{90}Y$ seeds.

IV.C.3.b. Transverse dose function.

The arguments given in the preceding section to justify the use of a single value of the absorbed dose rate at the reference point per unit activity per unit length for both the 27 and 20 mm Guidant sources can be applied to any point on the source transverse axis where the dose can be assumed to be deposited by beta particles only. For this reason, one may expect the relative radial depth-dose distribution (i.e., normalized to unity at the reference point) of both sources to be the same. As the same geometry function is recommended for both sources, viz., $1/\rho$, one would then also expect the transverse dose functions of both sources to be the same at the clinically relevant distances.

Indeed, the results included in this comparison provide no evidence of significant differences between the transverse dose functions of the 27 and 20 mm sources for distances up to 6.5 mm. This may be seen in Fig. 13, which shows all transverse dose functions derived from the published dose distributions included in the present comparison. Because of this similarity, a single transverse dose function is recommended for both types of sources.

As shown in Fig. 13, there is good agreement between most simulation results. However, the two curves obtained with MCNP4B, while in good agreement with each other, deviate significantly from the other simulation results. The EGS4 results are also somewhat different from the other simulations. Appreciable discrepancies exist between the results obtained with GEANT 4 (version 4.1 with patch-01 and low-energy package G4EMLOW 1.1) and all other simulations, as was already noted by the authors.[89] It is to be noted that EGS4 and MCNP4B are older codes that have in the meantime been replaced by more recent versions (EGSNRC, MCNP4C, MCNPX), which are considered to better represent the state-of-the-art in Monte Carlo radiation transport simulation. Furthermore, the MCNP4B simulations were performed using the (default) MCNP electron energy indexing algorithm, which has been shown to lead to erroneous results.[90–92] In the MCNP4C and MCNPX simulations included in the comparison, the authors have used the so-called ITS electron energy indexing algorithm, which should give more accurate results.

There is fair agreement between the experimental and simulation results. The results from Piermattei *et al.*[86] disagree with all others at the shortest measurement distances and seem to include a background reading (visible at larger distances), which is not seen in any of the other results. Furthermore, in the region between about 3 and 4 mm the film measurements by Mourtada *et al.*[30] on the 27 mm source disagree with the other results by slightly more than the quoted uncertainty in the dose reading of $\sim$16% (2σ). Taking into account the measurement uncertainties (which are generally larger than the simulation uncertainties), there is fair agreement between the experimental and simulation results obtained with the more recent codes (i.e., all except those obtained with EGS4, GEANT4 or MCNP4B).

Given this agreement, it makes sense to base the recommended transverse dose function on the Monte Carlo results, since the spatial resolution is much better than in most of the measurements. Figure 14 contains the data points of the Monte Carlo results except for those obtained with either EGS4, GEANT4, or MCNP4B, which have been excluded for the reasons mentioned above.

TABLE XI. Reference values for the anisotropy function for a single $^{90}Sr/^{90}Y$ seed.

r	θ (degrees)																				
(mm)	0	1	2	3	5	7	10	12	15	20	25	30	35	40	45	50	55	60	70	80	90
0.5																	1.018	1.012	1.006	1.001	1.000
1											1.098	1.06	1.035	1.021	1.012	1.007	1.004	1.001	1.000	1.000	1.000
1.5	0.832	0.829	0.812	0.800	0.789	0.786	0.781	0.772	0.745	0.780	0.836	0.879	0.911	0.934	0.951	0.964	0.974	0.981	0.992	0.998	1.000
2	0.789	0.785	0.782	0.780	0.777	0.775	0.765	0.754	0.742	0.743	0.767	0.803	0.842	0.878	0.908	0.932	0.952	0.967	0.987	0.997	1.000
2.5	0.746	0.745	0.744	0.744	0.745	0.746	0.743	0.743	0.744	0.755	0.774	0.803	0.835	0.867	0.896	0.922	0.942	0.959	0.983	0.996	1.000
3	0.740	0.739	0.739	0.740	0.742	0.746	0.748	0.750	0.755	0.769	0.788	0.813	0.841	0.870	0.896	0.921	0.941	0.958	0.983	0.996	1.000
4	0.766	0.767	0.768	0.769	0.770	0.772	0.775	0.779	0.786	0.800	0.818	0.839	0.863	0.885	0.908	0.929	0.947	0.962	0.984	0.996	1.000
5	0.793	0.797	0.800	0.801	0.800	0.799	0.806	0.810	0.816	0.828	0.844	0.863	0.882	0.903	0.922	0.939	0.955	0.968	0.986	0.996	1.000
6	0.829	0.829	0.830	0.831	0.833	0.837	0.839	0.842	0.845	0.856	0.871	0.889	0.905	0.921	0.939	0.953	0.965	0.976	0.989	0.998	1.000
7	0.876	0.874	0.877	0.895	0.882	0.890	0.896	0.897	0.900	0.909	0.921	0.933	0.942	0.955	0.967	0.977	0.986	0.989	0.996	1.001	1.000
8	0.972	0.951	0.958	1.004	1.006	0.997	0.990	0.996	1.001	1.003	1.000	1.015	1.019	1.015	1.011	1.021	1.016	1.016	1.011	1.002	1.000

TABLE XII. Away-and-along table of dose rates for a single $^{90}Sr/^{90}Y$ seed normalized to unity at the reference point. Absolute values of the absorbed dose rate in Gy min^{-1} for a seed containing 1 mCi can be obtained by multiplication with 1.10.

	Away from axis, ρ (mm)											
Along axis, z (mm)	0.5	1	1.5	2	2.5	3	4	5	6	7	8	9
0	9.649×10^{0}	3.511×10^{0}	1.767×10^{0}	1.000×10^{0}	6.027×10^{-1}	3.780×10^{-1}	1.565×10^{-1}	6.347×10^{-2}	2.427×10^{-2}	8.481×10^{-3}	2.567×10^{-3}	1.426×10^{-3}
0.25	9.551×10^{0}	3.460×10^{0}	1.743×10^{0}	9.885×10^{-1}	5.969×10^{-1}	3.750×10^{-1}	1.555×10^{-1}	6.311×10^{-2}	2.415×10^{-2}	8.447×10^{-3}	2.471×10^{-3}	1.371×10^{-3}
0.5	3.780×10^{0}	3.298×10^{0}	1.660×10^{0}	9.477×10^{-1}	5.766×10^{-1}	3.659×10^{-1}	1.525×10^{-1}	6.206×10^{-2}	2.379×10^{-2}	8.321×10^{-3}	2.401×10^{-3}	1.445×10^{-3}
0.75	6.937×10^{0}	3.011×10^{0}	1.530×10^{0}	8.872×10^{-1}	5.458×10^{-1}	3.483×10^{-1}	1.470×10^{-1}	6.033×10^{-2}	2.319×10^{-2}	8.144×10^{-3}	2.384×10^{-3}	1.469×10^{-3}
1	7.302×10^{0}	2.581×10^{0}	1.360×10^{0}	8.068×10^{-1}	5.064×10^{-1}	3.275×10^{-1}	1.401×10^{-1}	5.772×10^{-2}	2.237×10^{-2}	7.818×10^{-3}	2.241×10^{-3}	1.465×10^{-3}
1.25	3.583×10^{0}	2.059×10^{0}	1.160×10^{0}	7.163×10^{-1}	4.603×10^{-1}	3.026×10^{-1}	1.318×10^{-1}	5.476×10^{-2}	2.133×10^{-2}	7.451×10^{-3}	2.285×10^{-3}	1.590×10^{-3}
1.5	2.685×10^{0}	1.549×10^{0}	9.588×10^{-1}	6.208×10^{-1}	4.115×10^{-1}	2.754×10^{-1}	1.226×10^{-1}	5.140×10^{-2}	2.015×10^{-2}	7.061×10^{-3}	2.176×10^{-3}	1.336×10^{-3}
1.75	1.701×10^{0}	1.124×10^{0}	7.756×10^{-1}	5.293×10^{-1}	3.619×10^{-1}	2.474×10^{-1}	1.124×10^{-1}	4.776×10^{-2}	1.887×10^{-2}	6.617×10^{-3}	1.967×10^{-3}	1.362×10^{-3}
2	1.150×10^{0}	8.424×10^{-1}	6.190×10^{-1}	4.445×10^{-1}	3.141×10^{-1}	2.192×10^{-1}	1.019×10^{-1}	4.383×10^{-2}	1.746×10^{-2}	6.192×10^{-3}	1.974×10^{-3}	1.354×10^{-3}
2.25	8.134×10^{-1}	6.393×10^{-1}	4.952×10^{-1}	3.700×10^{-1}	2.695×10^{-1}	1.920×10^{-1}	9.148×10^{-2}	3.987×10^{-2}	1.605×10^{-2}	5.613×10^{-3}	1.762×10^{-3}	1.231×10^{-3}
2.5	5.926×10^{-1}	4.938×10^{-1}	3.965×10^{-1}	3.067×10^{-1}	2.291×10^{-1}	1.664×10^{-1}	8.114×10^{-2}	3.590×10^{-2}	1.460×10^{-2}	5.083×10^{-3}	1.735×10^{-3}	1.189×10^{-3}
2.75	4.464×10^{-1}	3.854×10^{-1}	3.188×10^{-1}	2.532×10^{-1}	1.933×10^{-1}	1.428×10^{-1}	7.128×10^{-2}	3.206×10^{-2}	1.315×10^{-2}	4.540×10^{-3}	1.554×10^{-3}	1.528×10^{-3}
3	3.428×10^{-1}	3.043×10^{-1}	2.572×10^{-1}	2.086×10^{-1}	1.621×10^{-1}	1.216×10^{-1}	6.197×10^{-2}	2.834×10^{-2}	1.171×10^{-2}	4.030×10^{-3}	1.512×10^{-3}	1.238×10^{-3}
3.25	2.681×10^{-1}	2.420×10^{-1}	2.079×10^{-1}	1.714×10^{-1}	1.353×10^{-1}	1.027×10^{-1}	5.344×10^{-2}	2.480×10^{-2}	1.037×10^{-2}	3.634×10^{-3}	1.587×10^{-3}	1.259×10^{-3}
3.5	2.117×10^{-1}	1.934×10^{-1}	1.685×10^{-1}	1.404×10^{-1}	1.123×10^{-1}	8.622×10^{-2}	4.572×10^{-2}	2.155×10^{-2}	9.064×10^{-3}	3.117×10^{-3}	1.385×10^{-3}	1.336×10^{-3}
3.75	1.682×10^{-1}	1.549×10^{-1}	1.364×10^{-1}	1.148×10^{-1}	9.268×10^{-2}	7.185×10^{-2}	3.881×10^{-2}	1.860×10^{-2}	7.807×10^{-3}	2.817×10^{-3}	1.507×10^{-3}	1.455×10^{-3}
4	1.340×10^{-1}	1.243×10^{-1}	1.102×10^{-1}	9.350×10^{-2}	7.612×10^{-2}	5.950×10^{-2}	3.274×10^{-2}	1.589×10^{-2}	6.703×10^{-3}	2.316×10^{-3}	1.383×10^{-3}	1.561×10^{-3}
4.25	1.069×10^{-1}	9.970×10^{-2}	8.884×10^{-2}	7.586×10^{-2}	6.220×10^{-2}	4.901×10^{-2}	2.737×10^{-2}	1.350×10^{-2}	5.636×10^{-3}	2.147×10^{-3}	1.332×10^{-3}	1.639×10^{-3}
4.5	8.523×10^{-2}	7.981×10^{-2}	7.146×10^{-2}	6.134×10^{-2}	5.062×10^{-2}	4.019×10^{-2}	2.276×10^{-2}	1.131×10^{-2}	4.780×10^{-3}	1.909×10^{-3}	1.593×10^{-3}	0.000×10^{0}
4.75	6.788×10^{-2}	6.376×10^{-2}	5.729×10^{-2}	4.942×10^{-2}	4.102×10^{-2}	3.279×10^{-2}	1.886×10^{-2}	9.398×10^{-3}	3.891×10^{-3}	1.564×10^{-3}	1.488×10^{-3}	0.000×10^{0}
5	5.394×10^{-2}	5.078×10^{-2}	4.578×10^{-2}	3.964×10^{-2}	3.310×10^{-2}	2.664×10^{-2}	1.547×10^{-2}	7.735×10^{-3}	3.269×10^{-3}	1.556×10^{-3}	1.196×10^{-3}	0.000×10^{0}
5.25	4.280×10^{-2}	4.035×10^{-2}	3.644×10^{-2}	3.168×10^{-2}	2.659×10^{-2}	2.153×10^{-2}	1.269×10^{-2}	6.315×10^{-3}	2.598×10^{-3}	1.565×10^{-3}	1.265×10^{-3}	0.000×10^{0}
5.5	3.385×10^{-2}	3.197×10^{-2}	2.894×10^{-2}	2.524×10^{-2}	2.129×10^{-2}	1.738×10^{-2}	1.024×10^{-2}	5.067×10^{-3}	2.174×10^{-3}	1.306×10^{-3}	1.426×10^{-3}	0.000×10^{0}
5.75	2.671×10^{-2}	2.524×10^{-2}	2.289×10^{-2}	2.007×10^{-2}	1.703×10^{-2}	1.397×10^{-2}	8.201×10^{-3}	3.984×10^{-3}	1.784×10^{-3}	1.338×10^{-3}	1.712×10^{-3}	0.000×10^{0}
6	2.101×10^{-2}	1.992×10^{-2}	1.815×10^{-2}	1.599×10^{-2}	1.356×10^{-2}	1.110×10^{-2}	6.555×10^{-3}	3.200×10^{-3}	1.595×10^{-3}	1.366×10^{-3}	1.936×10^{-3}	0.000×10^{0}
6.25	1.652×10^{-2}	1.573×10^{-2}	1.436×10^{-2}	1.263×10^{-2}	1.071×10^{-2}	8.680×10^{-3}	5.149×10^{-3}	2.456×10^{-3}	1.607×10^{-3}	1.407×10^{-3}	0.000×10^{0}	0.000×10^{0}
6.5	1.297×10^{-2}	1.234×10^{-2}	1.122×10^{-2}	9.877×10^{-3}	8.323×10^{-3}	6.808×10^{-3}	4.009×10^{-3}	2.114×10^{-3}	1.546×10^{-3}	1.514×10^{-3}	0.000×10^{0}	0.000×10^{0}
6.75	1.008×10^{-2}	9.511×10^{-3}	8.684×10^{-3}	7.672×10^{-3}	6.504×10^{-3}	5.278×10^{-3}	3.119×10^{-3}	1.735×10^{-3}	1.490×10^{-3}	1.125×10^{-3}	0.000×10^{0}	0.000×10^{0}
7	7.726×10^{-3}	7.322×10^{-3}	6.687×10^{-3}	5.949×10^{-3}	4.957×10^{-3}	3.981×10^{-3}	2.354×10^{-3}	1.570×10^{-3}	1.436×10^{-3}	1.690×10^{-3}	0.000×10^{0}	0.000×10^{0}
7.25	5.931×10^{-3}	5.618×10^{-3}	5.136×10^{-3}	4.480×10^{-3}	3.727×10^{-3}	3.146×10^{-3}	1.863×10^{-3}	1.466×10^{-3}	1.391×10^{-3}	0.000×10^{0}	0.000×10^{0}	0.000×10^{0}
7.5	4.539×10^{-3}	4.219×10^{-3}	3.871×10^{-3}	3.356×10^{-3}	2.900×10^{-3}	2.309×10^{-3}	1.744×10^{-3}	1.470×10^{-3}	1.359×10^{-3}	0.000×10^{0}	0.000×10^{0}	0.000×10^{0}
7.75	3.305×10^{-3}	3.145×10^{-3}	2.902×10^{-3}	2.483×10^{-3}	2.230×10^{-3}	1.805×10^{-3}	1.572×10^{-3}	1.401×10^{-3}	1.454×10^{-3}	0.000×10^{0}	0.000×10^{0}	0.000×10^{0}
8	2.480×10^{-3}	2.373×10^{-3}	2.209×10^{-3}	2.010×10^{-3}	1.778×10^{-3}	1.545×10^{-3}	1.404×10^{-3}	1.357×10^{-3}	1.947×10^{-3}	0.000×10^{0}	0.000×10^{0}	0.000×10^{0}
8.25	2.027×10^{-3}	1.812×10^{-3}	1.788×10^{-3}	1.738×10^{-3}	1.515×10^{-3}	1.372×10^{-3}	1.389×10^{-3}	1.440×10^{-3}	0.000×10^{0}	0.000×10^{0}	0.000×10^{0}	0.000×10^{0}
8.5	1.611×10^{-3}	1.620×10^{-3}	1.357×10^{-3}	1.335×10^{-3}	1.447×10^{-3}	1.478×10^{-3}	1.447×10^{-3}	1.417×10^{-3}	0.000×10^{0}	0.000×10^{0}	0.000×10^{0}	0.000×10^{0}
8.75	1.591×10^{-3}	1.478×10^{-3}	1.598×10^{-3}	1.504×10^{-3}	1.501×10^{-3}	1.360×10^{-3}	1.606×10^{-3}	0.000×10^{0}	0.000×10^{0}	0.000×10^{0}	0.000×10^{0}	0.000×10^{0}
9	1.380×10^{-3}	1.214×10^{-3}	1.522×10^{-3}	1.385×10^{-3}	1.570×10^{-3}	1.428×10^{-3}	1.458×10^{-3}	0.000×10^{0}	0.000×10^{0}	0.000×10^{0}	0.000×10^{0}	0.000×10^{0}
9.25	1.470×10^{-3}	1.463×10^{-3}	1.441×10^{-3}	1.486×10^{-3}	1.424×10^{-3}	1.136×10^{-3}	0.000×10^{0}	0.000×10^{0}	0.000×10^{0}	0.000×10^{0}	0.000×10^{0}	0.000×10^{0}
9.5	1.337×10^{-3}	1.514×10^{-3}	1.481×10^{-3}	1.447×10^{-3}	1.297×10^{-3}	1.728×10^{-3}	0.000×10^{0}	0.000×10^{0}	0.000×10^{0}	0.000×10^{0}	0.000×10^{0}	0.000×10^{0}
9.75	1.513×10^{-3}	1.478×10^{-3}	1.674×10^{-3}	1.565×10^{-3}	0.000×10^{0}	0.000×10^{0}	0.000×10^{0}	0.000×10^{0}	0.000×10^{0}	0.000×10^{0}	0.000×10^{0}	0.000×10^{0}
10	0.000×10^{0}	0.000×10^{0}	0.000×10^{0}	0.000×10^{0}	0.000×10^{0}	0.000×10^{0}	0.000×10^{0}	0.000×10^{0}	0.000×10^{0}	0.000×10^{0}	0.000×10^{0}	0.000×10^{0}

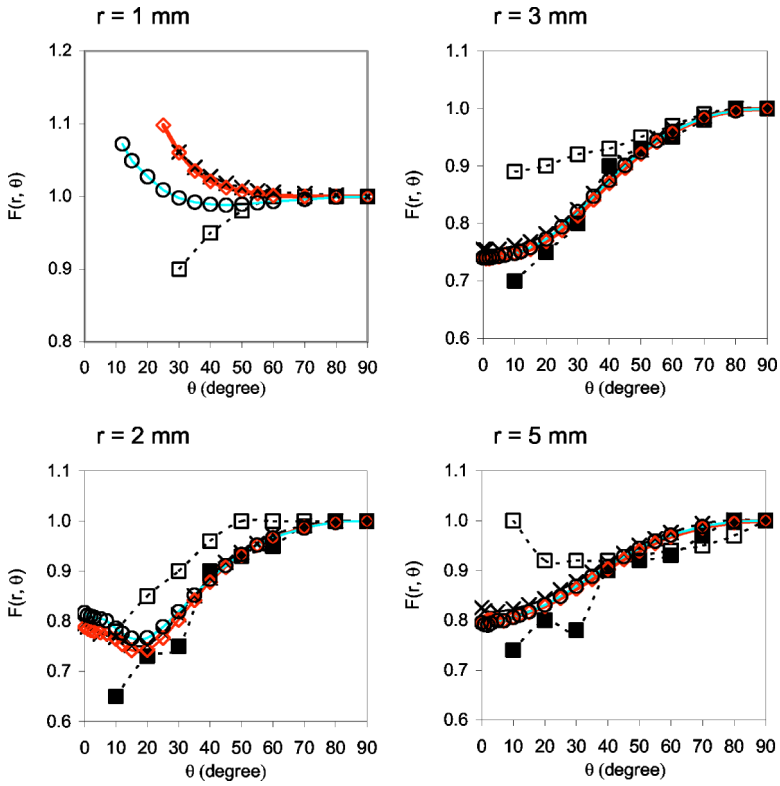

FIG. 10. Comparison of published 2D anisotropy functions for a single ^{90}Sr/^{90}Y seed source. The measured and calculated data reported by Soares *et al.* (Ref. 41) are shown by open and closed square symbols, respectively. The results reported by Wang and Li in 2000 (Ref. 27) are displayed by crosses. The data by Wang and Li in 2002 (Ref. 28) are indicated by diamonds and circles for the 5 F and 3.5 F sources, respectively. Recommended data are shown in red.

The recommended transverse dose function for both 20 and 27 mm Guidant ^{32}P sources is a fit to all Monte Carlo data points shown in Fig. 14 and is given by

$$g(\rho) = \sum_{i=0}^{4} \exp(a_i \rho^i). \quad (16)$$

The parameters of the fit are given in Table II. Note that ρ is expressed in millimeters. The fit is valid between ρ=0.5 and ρ=6.5 mm. Values of the recommended transverse dose function are given in Table III.

IV.C.3.c. Nonuniformity function.

Figure 15(a) compares the relative axial dose profiles derived from the available published dose distributions for the 20 mm Guidant ^{32}P source.[29,62,86,89,93] The data from Mourtada *et al.*[62] have been selected to derive the recommended nonuniformity function $F(\rho,z)$, since these data were available at a high spatial resolution and are in good agreement with the other published data. Values of the recommended nonuniformity function are given in Table XVII. Note that the red solid curve shown in Fig. 15(a) is equal to $F(\rho=2\text{ mm},z)$. It is noted that the red curve in Fig. 15(a) has been derived straight from the original, high-resolution Monte Carlo results provided to us by the authors. The values of $F(\rho,z)$ shown in Table XVII, on the other hand, have been derived from the dose rate table given in the article. This table was derived from fits through the high-resolution

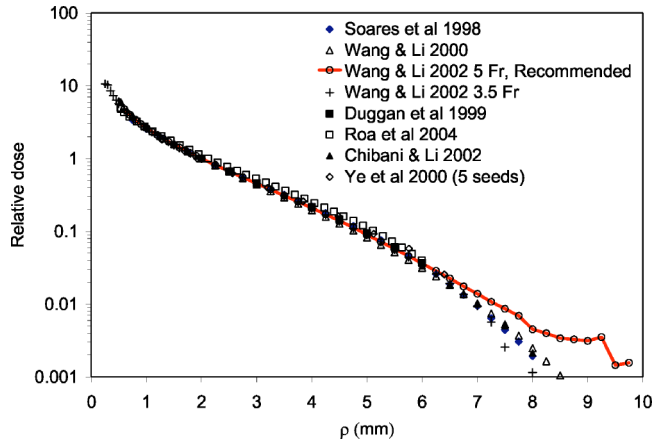

FIG. 11. Published relative depth-dose data for 30 mm (12 ^{90}Sr/^{90}Y seed) trains.

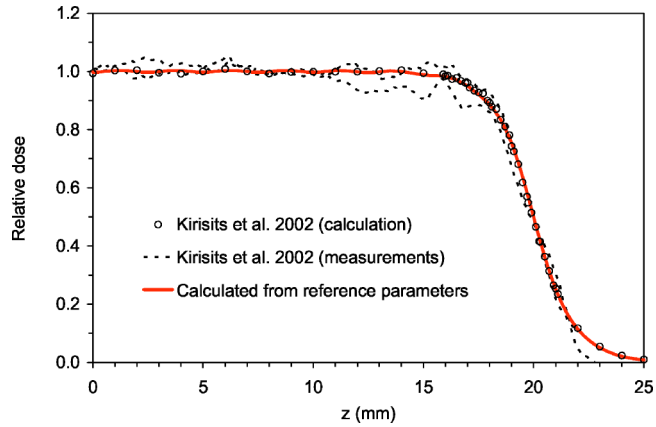

FIG. 12. Published axial profiles at 2 mm depth in water for 40 mm (16 ^{90}Sr/^{90}Y seed) sources compared to that calculated using the recommended parameters (shown by solid line in red).

TABLE XIII. Away-and-along table of dose rates for a 16 $^{90}Sr/^{90}Y$ seed (40 mm) train source calculated with the reference parameters and normalized to unity at the reference point. Absolute values of the absorbed dose rate in Gy min^{-1} for a 16 seed train containing a total of 1 mCi can be obtained by multiplication with 0.113.

Along axis, z (mm)	Away from axis, ρ (mm) 0.5	1	1.5	2	2.5	3	3.5	4	4.5	5	5.5	6	6.5	7	8
0	4.444×10^{0}	2.631×10^{0}	1.547×10^{0}	9.966×10^{-1}	6.663×10^{-1}	4.533×10^{-1}	3.093×10^{-1}	2.092×10^{-1}	1.394×10^{-1}	8.939×10^{-2}	5.731×10^{-2}	3.625×10^{-2}	2.252×10^{-2}	1.376×10^{-2}	8.674×10^{-3}
0.25	6.113×10^{0}	2.643×10^{0}	1.550×10^{0}	9.963×10^{-1}	6.668×10^{-1}	4.535×10^{-1}	3.091×10^{-1}	2.090×10^{-1}	1.384×10^{-1}	9.036×10^{-2}	5.728×10^{-2}	3.621×10^{-2}	2.239×10^{-2}	1.367×10^{-2}	8.803×10^{-3}
0.5	5.337×10^{0}	2.661×10^{0}	1.555×10	9.990×10^{-1}	6.671×10^{-1}	4.534×10^{-1}	3.092×10^{-1}	2.080×10^{-1}	1.384×10^{-1}	9.051×10^{-2}	5.838×10^{-2}	3.616×10^{-2}	2.242×10^{-2}	1.356×10^{-2}	7.527×10^{-3}
0.75	3.185×10^{0}	2.693×10^{0}	1.560×10^{0}	1.000×10^{0}	6.677×10^{-1}	4.548×10^{-1}	3.087×10^{-1}	2.082×10^{-1}	1.387×10^{-1}	9.051×10^{-2}	5.844×10^{-2}	3.732×10^{-2}	2.239×10^{-2}	1.382×10^{-2}	7.667×10^{-3}
1	6.444×10^{0}	2.711×10^{0}	1.569×10^{0}	1.003×10^{0}	6.680×10^{-1}	4.533×10^{-1}	3.085×10^{-1}	2.082×10^{-1}	1.384×10^{-1}	9.055×10^{-2}	5.828×10^{-2}	3.695×10^{-2}	2.236×10^{-2}	1.281×10^{-2}	7.847×10^{-3}
1.25	6.455×10^{0}	2.717×10^{0}	1.568×10^{0}	1.002×10^{0}	6.678×10^{-1}	4.531×10^{-1}	3.082×10^{-1}	2.082×10^{-1}	1.384×10^{-1}	9.059×10^{-2}	5.815×10^{-2}	3.697×10^{-2}	2.357×10^{-2}	1.283×10^{-2}	7.876×10^{-3}
1.5	6.444×10^{0}	2.711×10^{0}	1.569×10^{0}	1.003×10^{0}	6.680×10^{-1}	4.533×10^{-1}	3.085×10^{-1}	2.082×10^{-1}	1.384×10^{-1}	9.055×10^{-2}	5.828×10^{-2}	3.695×10^{-2}	2.236×10^{-2}	1.281×10^{-2}	7.847×10^{-3}
1.75	3.185×10^{0}	2.693×10^{0}	1.560×10^{0}	1.000×10^{0}	6.677×10^{-1}	4.548×10^{-1}	3.087×10^{-1}	2.082×10^{-1}	1.387×10^{-1}	9.051×10^{-2}	5.844×10^{-2}	3.732×10^{-2}	2.239×10^{-2}	1.382×10^{-2}	7.667×10^{-3}
2	5.337×10^{0}	2.661×10^{0}	1.555×10^{0}	9.990×10^{-1}	6.671×10^{-1}	4.534×10^{-1}	3.092×10^{-1}	2.080×10^{-1}	1.384×10^{-1}	9.051×10^{-2}	5.838×10^{-2}	3.616×10^{-2}	2.242×10^{-2}	1.356×10^{-2}	7.527×10^{-3}
4	6.444×10^{0}	2.711×10^{0}	1.569×10^{0}	1.003×10^{0}	6.680×10^{-1}	4.533×10^{-1}	3.085×10^{-1}	2.082×10^{-1}	1.384×10^{-1}	9.055×10^{-2}	5.828×10^{-2}	3.695×10^{-2}	2.236×10^{-2}	1.281×10^{-2}	7.847×10^{-3}
6	6.444×10^{0}	2.711×10^{0}	1.569×10^{0}	1.003×10^{0}	6.680×10^{-1}	4.533×10^{-1}	3.085×10^{-1}	2.082×10^{-1}	1.384×10^{-1}	9.055×10^{-2}	5.828×10^{-2}	3.695×10^{-2}	2.236×10^{-2}	1.281×10^{-2}	7.847×10^{-3}
8	5.337×10^{0}	2.661×10^{0}	1.555×10^{0}	9.990×10^{-1}	6.671×10^{-1}	4.534×10^{-1}	3.092×10^{-1}	2.080×10^{-1}	1.384×10^{-1}	9.051×10^{-2}	5.838×10^{-2}	3.616×10^{-2}	2.242×10^{-2}	1.356×10^{-2}	7.527×10^{-3}
10	4.444×10^{0}	2.631×10^{0}	1.547×10^{0}	9.966×10^{-1}	6.663×10^{-1}	4.533×10^{-1}	3.093×10^{-1}	2.092×10^{-1}	1.394×10^{-1}	8.939×10^{-2}	5.731×10^{-2}	3.625×10^{-2}	2.252×10^{-2}	1.376×10^{-2}	8.674×10^{-3}
12	5.336×10^{0}	2.660×10^{0}	1.554×10	9.981×10^{-1}	6.662×10^{-1}	4.528×10^{-1}	3.082×10^{-1}	2.080×10^{-1}	1.384×10^{-1}	9.051×10^{-2}	5.838×10^{-2}	3.616×10^{-2}	2.242×10^{-2}	1.356×10^{-2}	7.527×10^{-3}
14	6.440×10^{0}	2.707×10^{0}	1.564×10^{0}	9.993×10^{-1}	6.658×10^{-1}	4.514×10^{-1}	3.070×10^{-1}	2.071×10^{-1}	1.374×10^{-1}	8.969×10^{-2}	5.741×10^{-2}	3.613×10^{-2}	2.147×10^{-2}	1.281×10^{-2}	7.847×10^{-3}
16	6.417×10^{0}	2.685×10^{0}	1.545×10^{0}	9.827×10^{-1}	6.510×10^{-1}	4.395×10^{-1}	2.975×10^{-1}	1.998×10^{-1}	1.323×10^{-1}	8.601×10^{-2}	5.502×10^{-2}	3.456×10^{-2}	2.133×10^{-2}	1.189×10^{-2}	7.032×10^{-3}
18	5.162×10^{0}	2.502×10^{0}	1.418×10^{0}	8.851×10^{-1}	5.764×10^{-1}	3.838×10^{-1}	2.575×10^{-1}	1.709×10^{-1}	1.125×10^{-1}	7.269×10^{-2}	4.630×10^{-2}	2.900×10^{-2}	1.780×10^{-2}	1.063×10^{-2}	5.577×10^{-3}
20	2.222×10^{0}	1.316×10^{0}	7.733×10^{-1}	4.983×10^{-1}	3.332×10^{-1}	2.266×10^{-1}	1.547×10^{-1}	1.046×10^{-1}	6.968×10^{-2}	4.470×10^{-2}	2.865×10^{-2}	1.813×10^{-2}	1.126×10^{-2}	6.882×10^{-3}	4.337×10^{-3}
20.25	1.670×10^{0}	9.943×10^{-1}	6.377×10^{-1}	4.277×10^{-1}	2.933×10^{-1}	2.023×10^{-1}	1.392×10^{-1}	9.477×10^{-2}	6.257×10^{-2}	4.091×10^{-2}	2.625×10^{-2}	1.674×10^{-2}	1.028×10^{-2}	6.420×10^{-3}	4.353×10^{-3}
20.5	1.073×10^{0}	7.276×10^{-1}	5.155×10^{-1}	3.621×10^{-1}	2.547×10^{-1}	1.785×10^{-1}	1.243×10^{-1}	8.421×10^{-2}	5.643×10^{-2}	3.713×10^{-2}	2.409×10^{-2}	1.532×10^{-2}	9.558×10^{-3}	5.829×10^{-3}	2.965×10^{-3}
20.75	7.336×10^{-1}	5.488×10^{-1}	4.118×10^{-1}	3.026×10^{-1}	2.187×10^{-1}	1.563×10^{-1}	1.089×10^{-1}	7.488×10^{-2}	5.058×10^{-2}	3.343×10^{-2}	2.189×10^{-2}	1.396×10^{-2}	8.861×10^{-3}	5.772×10^{-3}	2.819×10^{-3}
21	5.239×10^{-1}	4.186×10^{-1}	3.297×10^{-1}	2.508×10^{-1}	1.852×10^{-1}	1.343×10^{-1}	9.528×10^{-2}	6.614×10^{-2}	4.497×10^{-2}	2.991×10^{-2}	1.960×10^{-2}	1.257×10^{-2}	8.065×10^{-3}	4.231×10^{-3}	2.761×10^{-3}
21.25	3.838×10^{-1}	3.235×10^{-1}	2.630×10^{-1}	2.061×10^{-1}	1.563×10^{-1}	1.152×10^{-1}	8.264×10^{-2}	5.798×10^{-2}	3.964×10^{-2}	2.659×10^{-2}	1.743×10^{-2}	1.133×10^{-2}	7.471×10^{-3}	3.913×10^{-3}	2.548×10^{-3}
21.5	2.903×10^{-1}	2.528×10^{-1}	2.111×10^{-1}	1.694×10^{-1}	1.309×10^{-1}	9.793×10^{-2}	7.127×10^{-2}	5.043×10^{-2}	3.466×10^{-2}	2.345×10^{-2}	1.550×10^{-2}	1.014×10^{-2}	5.729×10^{-3}	3.599×10^{-3}	2.351×10^{-3}
21.75	2.235×10^{-1}	1.996×10^{-1}	1.700×10^{-1}	1.390×10^{-1}	1.092×10^{-1}	8.285×10^{-2}	6.088×10^{-2}	4.340×10^{-2}	3.031×10^{-2}	2.049×10^{-2}	1.374×10^{-2}	9.334×10^{-3}	5.071×10^{-3}	3.145×10^{-3}	2.131×10^{-3}
22	1.750×10^{-1}	1.586×10^{-1}	1.371×10^{-1}	1.139×10^{-1}	9.069×10^{-2}	6.960×10^{-2}	5.163×10^{-2}	3.715×10^{-2}	2.595×10^{-2}	1.781×10^{-2}	1.208×10^{-2}	7.162×10^{-3}	4.616×10^{-3}	2.931×10^{-3}	1.950×10^{-3}
22.5	1.098×10^{-1}	1.015×10^{-1}	8.980×10^{-2}	7.601×10^{-2}	6.184×10^{-2}	4.827×10^{-2}	3.653×10^{-2}	2.686×10^{-2}	1.919×10^{-2}	1.241×10^{-2}	8.337×10^{-3}	5.549×10^{-3}	3.654×10^{-3}	2.489×10^{-3}	1.910×10^{-3}
23	6.981×10^{-2}	6.524×10^{-2}	5.834×10^{-2}	5.012×10^{-2}	4.134×10^{-2}	3.267×10^{-2}	2.539×10^{-2}	1.797×10^{-2}	1.283×10^{-2}	8.981×10^{-3}	6.230×10^{-3}	4.201×10^{-3}	2.802×10^{-3}	1.929×10^{-3}	8.524×10^{-4}
23.5	4.440×10^{-2}	4.177×10^{-2}	3.779×10^{-2}	3.269×10^{-2}	2.638×10^{-2}	2.118×10^{-2}	1.631×10^{-2}	1.221×10^{-2}	9.005×10^{-3}	6.404×10^{-3}	4.548×10^{-3}	3.114×10^{-3}	2.304×10^{-3}	9.218×10^{-4}	9.251×10^{-4}
24	2.718×10^{-2}	2.564×10^{-2}	2.319×10^{-2}	2.014×10^{-2}	1.699×10^{-2}	1.375×10^{-2}	1.095×10^{-2}	8.407×10^{-3}	6.160×10^{-3}	4.548×10^{-3}	3.260×10^{-3}	2.389×10^{-3}	1.033×10^{-3}	9.226×10^{-4}	8.151×10^{-4}
24.5	1.694×10^{-2}	1.594×10^{-2}	1.455×10^{-2}	1.286×10^{-2}	1.093×10^{-2}	9.044×10^{-3}	7.245×10^{-3}	5.653×10^{-3}	4.212×10^{-3}	3.198×10^{-3}	2.456×10^{-3}	1.051×10^{-3}	9.400×10^{-4}	7.888×10^{-4}	7.691×10^{-4}
25	1.068×10^{-2}	1.015×10^{-2}	9.406×10^{-3}	8.329×10^{-3}	7.201×10^{-3}	5.919×10^{-3}	4.879×10^{-3}	3.982×10^{-3}	3.144×10^{-3}	1.447×10^{-3}	1.080×10^{-3}	9.475×10^{-4}	9.190×10^{-4}	8.291×10^{-4}	8.803×10^{-4}

TABLE XIV. Comparison of published experimental values of the reference absorbed dose rate per unit contained activity for the 20 and 27 mm Guidant ^{32}P sources.

Author	Type of Determination	Catheter Included	Active Source Length (mm)	Reference Absorbed Dose Rate per Unit Activity (cGy s^{-1} mCi^{-1})	Reference Absorbed Dose Rate per Unit Activity per Unit Source Length (cGy s^{-1} mCi^{-1} cm)
Mourtada *et al.* 2000 (Ref. 30)	MD-55-2 and HD-810 radiochromic films	Yes	27	0.229[a]	0.618
	Plastic scintillator	No	27	0.229	0.618
Bohm *et al.* 2001 (Ref. 85)	MD-55-2 film	No	27	0.218[b]	0.589
Mourtada *et al.* 2003 (Ref. 29)	Extrapolation chamber	No	20	0.321[c]	0.642
	HD-810 film	No	20	0.312[c]	0.625
	MD-55-2 film	No	20	0.308[c]	0.617
Piermattei *et al.* 2003 (Ref. 86)	HS-14 film	Yes	20	0.324	0.648
Average of experimental values					0.622
Standard deviation					0.019

[a]Average of both film measurements, converted from A150 to water by author.
[b]Converted from polystyrene to water by author.
[c]Scaled from polystyrene to water by means of Eq. (12), using a scaling factor of 0.938 and assuming a density of 1.055 g cm^{-3} for polystyrene.

Monte Carlo data in order to reduce the influence of statistical noise.[62] It is also noted that the values of the recommended nonuniformity function have been mirrored, and therefore are symmetric, about the source transverse axis as they were calculated for the distal half of the source length only. Mirroring seems justified because of the symmetry of the source design (see Sec. II B 3), as is also discussed in the original work[62] and is confirmed by Fig. 15(a).

The construction of the 27 mm Guidant ^{32}P source is essentially the same as that of the 20 mm source, except for the active source length and the fact that the 27 mm source has only one (distal) marker whereas the 20 mm source has markers at both the proximal and distal ends, see Sec. II B 3. In principle, the presence of a marker may affect the shape of

TABLE XV. Comparison of published simulated values of the reference absorbed dose rate per unit contained activity for the 20 and 27 mm Guidant ^{32}P sources.

Author	Type of Determination	Catheter Included	Active Source Length (mm)	Reference Absorbed Dose Rate per Unit Activity (cGy s^{-1} mCi^{-1})	Reference Absorbed Dose Rate per Unit Activity per Unit Source Length (cGy s^{-1} mCi^{-1} cm)
Mourtada *et al.* 2000 (Ref. 30)	MCNP4B	Yes	27	0.229	0.618
Bohm *et al.* 2001 (Ref. 85)	MCNP4B	Yes	27	0.232	0.626
Wang & Li 2001 (Ref. 87)	EGSnrc	Yes	27	0.225	0.608
	EGS4	Yes	27	0.222	0.599
Li *et al.* 2001 (Ref. 88)	EGSnrc	No	27	0.219[a]	0.590
Mourtada *et al.* 2003 (Ref. 29)	CYLTRAN	Yes	20	0.301[b]	0.603
	MCNPX	Yes	20	0.303[b]	0.606
	MCNP4C	Yes	20	0.306[b]	0.612
	EGSnrc	Yes	20	0.299[b]	0.599
	EGS4	Yes	20	0.296[b]	0.592
	PENELOPE	Yes	20	0.298[b]	0.596
Torres *et al.* 2004 (Ref. 89)	GEANT4	No	27	0.231	0.624
	PENELOPE	No	27	0.215	0.581
	GEANT4	No	20	0.311	0.622
	PENELOPE	No	20	0.291	0.582
Mourtada *et al.* 2004 (Ref. 62)	MCNPX 2.4.0	Yes	20	0.300	0.600
Average of simulated values					0.604
Standard deviation					0.014

[a]The same EGSnrc result for a 27 mm source without catheter is also given in Wang & Li (2001) (Ref. 87). The value has only been included once in the present comparison.
[b]Results of simulations in water as provided by author (values not given in reference).

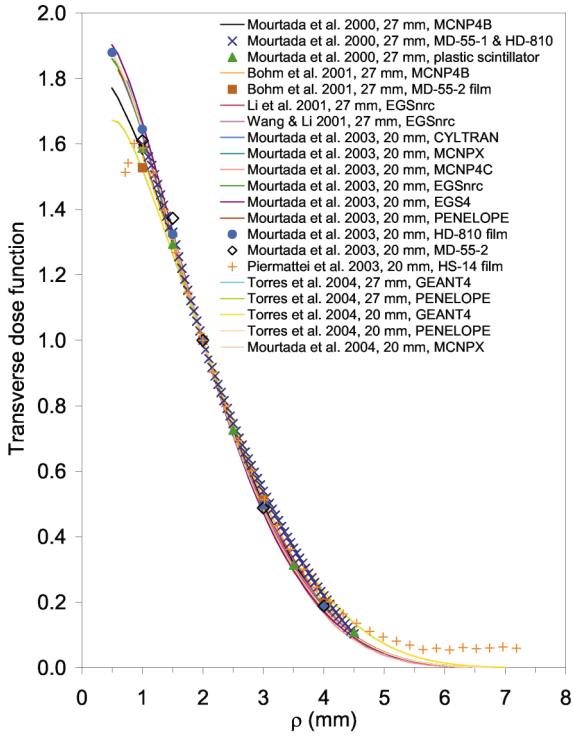

FIG. 13. Comparison of transverse dose functions for 20 and 27 mm ^{32}P wire sources. The measured data are shown using symbols. The solid lines indicate simulated values.

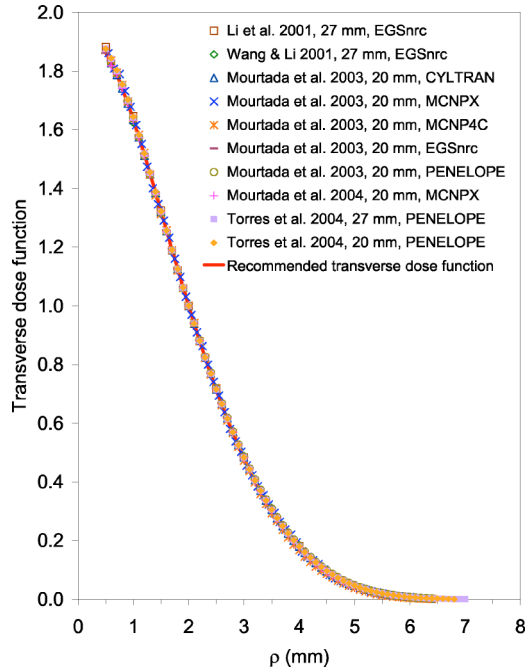

FIG. 14. Comparison between transverse dose functions for the 20 and 27 mm ^{32}P wire sources obtained using the most recent versions of various Monte Carlo codes. All data points available from these studies are shown. The red solid line represents the recommended transverse dose function, which is a fit to all of these data points.

the dose fall-off near the end of the source. As can be seen in Fig. 15(b), however, at $\rho=2$ mm the axial dose profiles appear to be very similar to the nonuniformity function $F(\rho=2\text{ mm}, z)$ recommended for the 20 mm source at both the proximal and distal ends of the source. The same was found at smaller radial distances, down to $\rho=0.5$ mm, where the dose profile is believed to be most sensitive to the presence of a marker. Excellent agreement was also found at $\rho=4$ mm, as expected. Therefore, the recommended nonuniformity function of the 27 mm source is the same as that for the 20 mm source, except that a central region with a length of 7 mm has been added, see Table XVII. In this central region, it is assumed that $F(\rho,z)=1$.

It is noted that, because of this additional central region, the nonuniformity function of the 27 mm source is not exactly normalized to unity over the central two-thirds of the active source length. However, the resulting error is considered insignificant ($\sim$0.07%) in view of the simplicity and consistency obtained by using the same longitudinal fall-off data for both the 20 and 27 mm sources.

IV.C.3.d. Comparison of dose distributions. Table XVIII contains normalized dose distributions for the 20 and 27 mm Guidant ^{32}P sources, calculated using the recommended dose calculation parameters. The relative depth-dose distribution calculated with the recommended dose calculation parameters (which is the same for the 20 and 27 mm sources) is compared with published measurements and simulations in Fig. 16.

V. DISCUSSION AND CONCLUSIONS

For the ^{192}Ir source we have made a recommendation of using the radial dose function from AAPM TG-43,[51] and a 2D anisotropy function from Patel *et al.*[72] The reason is as follows. The closest radial distance of approach from the seed center to any tissue is 0.5 mm, due to the nylon ribbon

TABLE XVI. Recommended values of the reference absorbed dose rate per unit contained activity for the 20 and 27 mm Guidant ^{32}P sources.

Value	Reference Dose Rate per Unit Activity per Unit Source Length (cGy s^{-1} mCi^{-1} cm)	Reference Dose Rate per Unit Activity (cGy s^{-1} mCi^{-1})	
		27 mm source	20 mm source
Average of experimental values	0.622		
Average of simulated values	0.604		
Recommended value	**0.613**[a]	**0.227**	**0.307**

[a]Calculated as the mean of the average of the experimental values and the average of the simulated values.

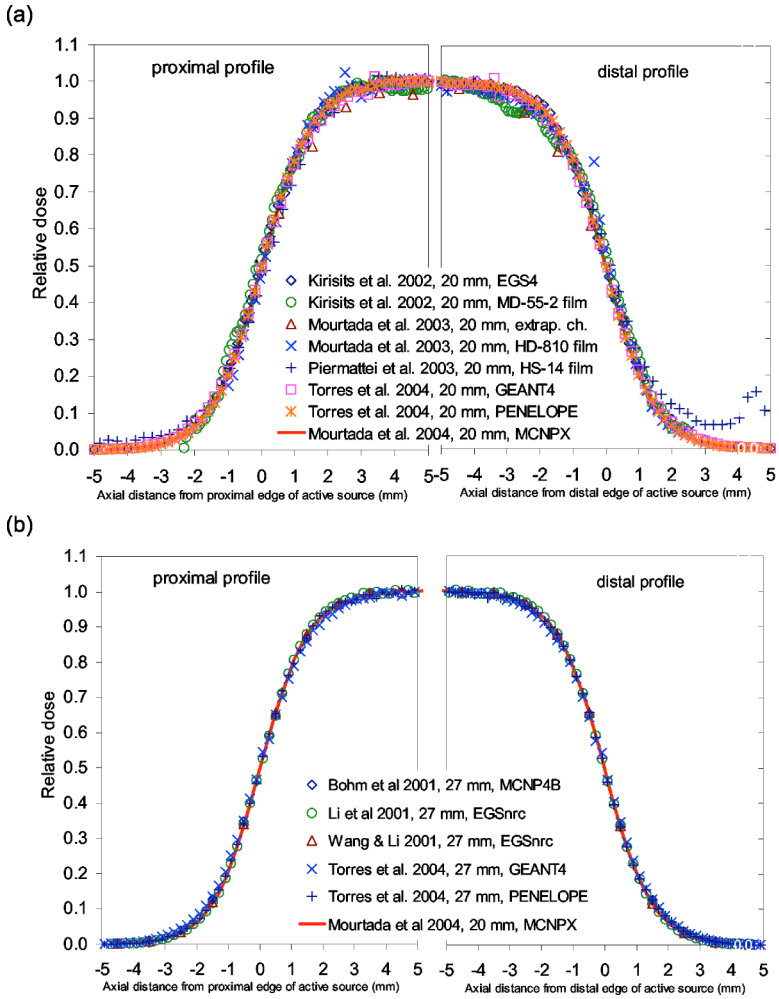

FIG. 15. Comparison of axial dose profiles for the (a) 20 mm and (b) 27 mm ^{32}P sources to the recommended nonuniformity function (shown in red) at $\rho=2.0$ mm. Left: Proximal profile. Right: Distal profile.

wall thickness and catheter wall thickness, even if the ^{192}Ir seed ribbon is eccentrically positioned in the catheter lumen. The contribution from beta particles and conversion electrons causes only a 4% greater value of the radial dose function than predicted by the TG-43 polynomial fit at 0.5 mm along the transverse axis of the seed. On the other hand, as shown in Fig. 6, the anisotropy function values reported by Wang and Li[27] were much lower than those reported by Patel *et al.*[72] for short distances and shallow polar angles. For $\theta=10°$, the differences are up to 85%, 75%, 50%, and 20% at 2, 2.5, 3, and 4 mm, respectively. This major underestimate of doses near the gap between neighboring ^{192}Ir seeds is due to the lack of consideration (by Wang and Li) of the contributions from the beta particles and conversion electrons that are emitted from the unencapsulated ends of the ^{192}Ir seeds. Therefore, we recommend the use of the Patel *et al.* anisotropy function (Table IV).

For ^{90}Sr/^{90}Y sources we recommend the use of the TG-43/60 formalism for single seed sources and the dose superposition method to arrive at the dose distributions for trains of sources. The recommended values of reference absorbed dose rate per unit contained activity for single seeds, and trains of 12, 16, and 24 seeds were obtained from averages of available measurements and calculations as shown in Tables IX and X. The convention of using the activity of only the parent radionuclide in quoting contained activity for these sources is necessary to properly use these data. The recommended values for the radial dose distribution for a single seed were obtained from a fit of the data of Wang and Li,[28] which was the Monte Carlo study with the highest density of points and which best represented the average of available data (see Fig. 9). The recommended values for the single source anisotropy function were also taken from Wang and Li,[28] for the same reasons as for the radial dose function. Differences between the 5 F and 3.5 Fr seed data were not perceptible enough to warrant separate data for each seed model.

For ^{32}P line sources, we recommend the use of a modified version of the TG-43/60 dose calculation formalism defined in cylindrical coordinates. Instead of the radial dose function and anisotropy function, this formalism makes use of the transverse dose function and the nonuniformity function defined in Sec. II D 2. Furthermore, it employs a geometry function based on the infinite-line source approximation.

The recommended values of the reference absorbed dose rate per unit source strength for the 20 and 27 mm ^{32}P sources are based on a comparison of published values of the same quantity, divided by the active source length. As argued in Sec. IV C 3, this allowed us to recommend consensus values for both sources that are consistent with one another.

TABLE XVII. Condensed recommended nonuniformity function for the 20 and 27 mm Guidant ^{32}P sources. For the 27 mm source, $F(\rho,z)=1$ for $0<z<3.5$ mm. Furthermore, $F(\rho,-z)=F(\rho,z)$ for both sources.

z (mm)		ρ (mm)									
27 mm Source	20 mm Source	0.6	1.0	1.5	2.0	2.5	3.0	3.5	4.0	4.5	5.0
±3.5	±0.0	9.982×10^{-1}	1.000×10^{0}	1.001×10^{0}	1.002×10^{0}	1.002×10^{0}	9.993×10^{-1}	9.992×10^{-1}	9.992×10^{-1}	1.000×10^{0}	1.001×10^{0}
±4.0	±0.5	9.982×10^{-1}	1.000×10^{0}	1.001×10^{0}	1.002×10^{0}	1.002×10^{0}	9.977×10^{-1}	9.992×10^{-1}	9.996×10^{-1}	1.000×10^{0}	1.001×10^{0}
±4.5	±1.0	9.988×10^{-1}	1.000×10^{0}	1.001×10^{0}	1.002×10^{0}	1.002×10^{0}	9.972×10^{-1}	1.001×10^{0}	1.000×10^{0}	1.001×10^{0}	1.002×10^{0}
±5.0	±1.5	9.988×10^{-1}	1.000×10^{0}	1.001×10^{0}	1.002×10^{0}	1.002×10^{0}	9.999×10^{-1}	1.003×10^{0}	1.001×10^{0}	1.001×10^{0}	1.003×10^{0}
±5.5	±2.0	9.999×10^{-1}	1.000×10^{0}	1.001×10^{0}	1.002×10^{0}	1.002×10^{0}	1.002×10^{0}	1.004×10^{0}	1.002×10^{0}	1.002×10^{0}	1.004×10^{0}
±6.0	±2.5	1.000×10^{0}	1.001×10^{0}	1.001×10^{0}	1.002×10^{0}	1.002×10^{0}	1.002×10^{0}	1.004×10^{0}	1.003×10^{0}	1.003×10^{0}	1.004×10^{0}
±6.5	±3.0	1.001×10^{0}	1.001×10^{0}	1.001×10^{0}	1.002×10^{0}	1.002×10^{0}	1.002×10^{0}	1.003×10^{0}	1.004×10^{0}	1.003×10^{0}	1.003×10^{0}
±7.0	±3.5	1.002×10^{0}	1.001×10^{0}	1.001×10^{0}	1.002×10^{0}	1.002×10^{0}	1.003×10^{0}	1.003×10^{0}	1.005×10^{0}	1.003×10^{0}	1.001×10^{0}
±7.5	±4.0	1.003×10^{0}	1.001×10^{0}	1.001×10^{0}	1.001×10^{0}	1.001×10^{0}	1.005×10^{0}	1.003×10^{0}	1.005×10^{0}	1.002×10^{0}	1.000×10^{0}
±8.0	±4.5	1.003×10^{0}	1.001×10^{0}	1.001×10^{0}	1.001×10^{0}	1.001×10^{0}	1.005×10^{0}	1.003×10^{0}	1.004×10^{0}	1.001×10^{0}	9.990×10^{-1}
±8.5	±5.0	1.002×10^{0}	1.001×10^{0}	1.000×10^{0}	1.000×10^{0}	1.000×10^{0}	1.004×10^{0}	1.001×10^{0}	1.001×10^{0}	1.000×10^{0}	9.987×10^{-1}
±9.0	±5.5	1.001×10^{0}	9.998×10^{-1}	9.990×10^{-1}	9.985×10^{-1}	9.985×10^{-1}	1.001×10^{0}	9.981×10^{-1}	9.981×10^{-1}	9.994×10^{-1}	9.985×10^{-1}
±9.5	±6.0	9.988×10^{-1}	9.982×10^{-1}	9.969×10^{-1}	9.959×10^{-1}	9.950×10^{-1}	9.955×10^{-1}	9.931×10^{-1}	9.932×10^{-1}	9.963×10^{-1}	9.965×10^{-1}
±10.0	±6.5	9.955×10^{-1}	9.954×10^{-1}	9.931×10^{-1}	9.909×10^{-1}	9.886×10^{-1}	9.872×10^{-1}	9.846×10^{-1}	9.846×10^{-1}	9.891×10^{-1}	9.892×10^{-1}
±10.5	±7.0	9.905×10^{-1}	9.907×10^{-1}	9.865×10^{-1}	9.812×10^{-1}	9.769×10^{-1}	9.733×10^{-1}	9.691×10^{-1}	9.692×10^{-1}	9.733×10^{-1}	9.730×10^{-1}
±11.0	±7.5	9.840×10^{-1}	9.827×10^{-1}	9.741×10^{-1}	9.632×10^{-1}	9.554×10^{-1}	9.484×10^{-1}	9.415×10^{-1}	9.410×10^{-1}	9.447×10^{-1}	9.425×10^{-1}
±11.5	±8.0	9.757×10^{-1}	9.686×10^{-1}	9.506×10^{-1}	9.312×10^{-1}	9.175×10^{-1}	9.059×10^{-1}	8.960×10^{-1}	8.948×10^{-1}	8.972×10^{-1}	8.932×10^{-1}
±12.0	±8.5	9.625×10^{-1}	9.403×10^{-1}	9.053×10^{-1}	8.755×10^{-1}	8.547×10^{-1}	8.396×10^{-1}	8.280×10^{-1}	8.260×10^{-1}	8.274×10^{-1}	8.223×10^{-1}
±12.5	±9.0	9.307×10^{-1}	8.764×10^{-1}	8.214×10^{-1}	7.852×10^{-1}	7.609×10^{-1}	7.466×10^{-1}	7.355×10^{-1}	7.325×10^{-1}	7.346×10^{-1}	7.296×10^{-1}
±13.0	±9.5	8.169×10^{-1}	7.342×10^{-1}	6.822×10^{-1}	6.545×10^{-1}	6.369×10^{-1}	6.295×10^{-1}	6.218×10^{-1}	6.187×10^{-1}	6.217×10^{-1}	6.186×10^{-1}
±13.5	±10.0	4.925×10^{-1}	4.927×10^{-1}	4.940×10^{-1}	4.948×10^{-1}	4.936×10^{-1}	4.973×10^{-1}	4.950×10^{-1}	4.925×10^{-1}	4.973×10^{-1}	4.963×10^{-1}
±14.0	±10.5	1.661×10^{-1}	2.504×10^{-1}	3.050×10^{-1}	3.351×10^{-1}	3.514×10^{-1}	3.642×10^{-1}	3.675×10^{-1}	3.675×10^{-1}	3.730×10^{-1}	3.729×10^{-1}
±14.5	±11.0	5.774×10^{-2}	1.101×10^{-1}	1.660×10^{-1}	2.051×10^{-1}	2.293×10^{-1}	2.452×10^{-1}	2.526×10^{-1}	2.557×10^{-1}	2.607×10^{-1}	2.595×10^{-1}
±15.0	±11.5	2.651×10^{-2}	5.083×10^{-2}	8.573×10^{-2}	1.163×10^{-1}	1.382×10^{-1}	1.521×10^{-1}	1.604×10^{-1}	1.657×10^{-1}	1.691×10^{-1}	1.656×10^{-1}
±15.5	±12.0	1.442×10^{-2}	2.639×10^{-2}	4.462×10^{-2}	6.248×10^{-2}	7.790×10^{-2}	8.861×10^{-2}	9.515×10^{-2}	9.977×10^{-2}	1.016×10^{-1}	9.638×10^{-2}
±16.0	±12.5	7.922×10^{-3}	1.447×10^{-2}	2.358×10^{-2}	3.232×10^{-2}	4.157×10^{-2}	4.954×10^{-2}	5.353×10^{-2}	5.481×10^{-2}	5.561×10^{-2}	5.122×10^{-2}
±16.5	±13.0	4.079×10^{-3}	7.647×10^{-3}	1.194×10^{-2}	1.613×10^{-2}	2.095×10^{-2}	2.521×10^{-2}	2.781×10^{-2}	2.668×10^{-2}	2.654×10^{-2}	2.473×10^{-2}
±17.0	±13.5	1.931×10^{-3}	3.617×10^{-3}	5.130×10^{-3}	7.632×10^{-3}	9.694×10^{-3}	9.621×10^{-3}	1.178×10^{-2}	1.233×10^{-2}	1.067×10^{-2}	1.020×10^{-2}
±17.5	±14.0	8.565×10^{-4}	1.594×10^{-3}	1.598×10^{-3}	3.231×10^{-3}	3.674×10^{-3}	4.644×10^{-3}	4.912×10^{-3}	5.469×10^{-3}	4.358×10^{-3}	3.672×10^{-2}

Similarly, we recommend a single transverse dose function for both the 20 and the 27 mm ^{32}P source. The recommended transverse dose function is a fit to the data points of a selected subset of the Monte Carlo data published for both sources. This function agrees within experimental uncertainty with the large majority of the published measurements.

The recommended nonuniformity function for the 20 mm ^{32}P source is a mirror-symmetric data set published by a single author, which has been selected because of its high spatial resolution and good agreement with other published data. The nonuniformity function for the 27 mm source is the same, except for the addition of a central, 7 mm long, uniform region.

The reader may have noticed that different approaches have been used for obtaining the consensus data. For example, in some cases a recommended dose calculation parameter may consist of (a fit of) values published in a single paper, whereas in other cases an average of multiple data sets may have been calculated. This is because the use of a single method would not have allowed us to obtain the best possible consensus data set in all cases.

One of the difficulties encountered in this meta-analysis is that not all authors provided clear and/or complete uncertainty data with their results. When calculating an average of multiple data sets, for example, one would like to introduce weighting factors to account for the different relative uncertainties in different data sets. Regretfully, the available uncertainty data did not permit such a rigorous and straightforward approach: Whereas some measurements were published with a complete uncertainty analysis, other papers provided only limited information; whereas the statistical uncertainty in Monte Carlo results was usually specified and/or could be considered negligibly small, often no attention was paid to possible systematic errors.

Hence, rather than following a single and straightforward approach to calculate the consensus data sets, we carefully evaluated the published data, taking into account any information available on the associated uncertainty. Based on this evaluation we determined which approach would provide the best possible consensus data for each individual case. The rationale for following a given approach is explained where necessary. In some cases we were able to derive an indica-

TABLE XVIII. Away-and-along table of dose rates for the 20 and 27 mm Guidant ^{32}P sources, normalized to an average value of 1 over the central $\frac{2}{3}$ of the active source length at ρ=2 mm (see also the comment in Sec. IV C 3 with respect to the normalization for the case of the 27 mm source). Absolute dose rates in cGy s^{-1} for sources containing 1 mCi of ^{32}P can be obtained by multiplying with 0.307 and 0.227 for 20 and 27 mm sources, respectively.

z (mm)		ρ (mm)									
27 mm source	20 mm source	0.6	1.0	1.5	2.0	2.5	3.0	3.5	4.0	4.5	5.0
±3.5	±0.0	6.081×10^{0}	3.269×10^{0}	1.763×10^{0}	1.002×10^{0}	5.716×10^{-1}	3.196×10^{-1}	1.729×10^{-1}	8.855×10^{-2}	4.197×10^{-2}	1.787×10^{-2}
±4.0	±0.5	6.081×10^{0}	3.269×10^{0}	1.763×10^{0}	1.002×10^{0}	5.716×10^{-1}	3.191×10^{-1}	1.729×10^{-1}	8.858×10^{-2}	4.197×10^{-2}	1.788×10^{-2}
±4.5	±1.0	6.084×10^{0}	3.269×10^{0}	1.764×10^{0}	1.002×10^{0}	5.716×10^{-1}	3.189×10^{-1}	1.733×10^{-1}	8.861×10^{-2}	4.200×10^{-2}	1.790×10^{-2}
±5.0	±1.5	6.084×10^{0}	3.269×10^{0}	1.764×10^{0}	1.002×10^{0}	5.716×10^{-1}	3.198×10^{-1}	1.736×10^{-1}	8.868×10^{-2}	4.200×10^{-2}	1.791×10^{-2}
±5.5	±2.0	6.091×10^{0}	3.269×10^{0}	1.764×10^{0}	1.002×10^{0}	5.716×10^{-1}	3.203×10^{-1}	1.737×10^{-1}	8.878×10^{-2}	4.204×10^{-2}	1.793×10^{-2}
±6.0	±2.5	6.094×10^{0}	3.269×10^{0}	1.764×10^{0}	1.002×10^{0}	5.716×10^{-1}	3.204×10^{-1}	1.737×10^{-1}	8.888×10^{-2}	4.207×10^{-2}	1.793×10^{-2}
±6.5	±3.0	6.097×10^{0}	3.269×10^{0}	1.765×10^{0}	1.002×10^{0}	5.716×10^{-1}	3.204×10^{-1}	1.736×10^{-1}	8.901×10^{-2}	4.207×10^{-2}	1.791×10^{-2}
±7.0	±3.5	6.104×10^{0}	3.270×10^{0}	1.765×10^{0}	1.002×10^{0}	5.716×10^{-1}	3.208×10^{-1}	1.736×10^{-1}	8.908×10^{-2}	4.207×10^{-2}	1.789×10^{-2}
±7.5	±4.0	6.107×10^{0}	3.270×10^{0}	1.764×10^{0}	1.001×10^{0}	5.713×10^{-1}	3.213×10^{-1}	1.736×10^{-1}	8.905×10^{-2}	4.204×10^{-2}	1.786×10^{-2}
±8.0	±4.5	6.107×10^{0}	3.270×10^{0}	1.764×10^{0}	1.001×10^{0}	5.709×10^{-1}	3.215×10^{-1}	1.735×10^{-1}	8.895×10^{-2}	4.200×10^{-2}	1.784×10^{-2}
±8.5	±5.0	6.104×10^{0}	3.269×10^{0}	1.763×10^{0}	1.000×10^{0}	5.706×10^{-1}	3.212×10^{-1}	1.732×10^{-1}	8.875×10^{-2}	4.197×10^{-2}	1.784×10^{-2}
±9.0	±5.5	6.097×10^{0}	3.266×10^{0}	1.760×10^{0}	9.985×10^{-1}	5.696×10^{-1}	3.201×10^{-1}	1.727×10^{-1}	8.845×10^{-2}	4.194×10^{-2}	1.783×10^{-2}
±9.5	±6.0	6.084×10^{0}	3.261×10^{0}	1.757×10^{0}	9.959×10^{-1}	5.676×10^{-1}	3.184×10^{-1}	1.718×10^{-1}	8.801×10^{-2}	4.181×10^{-2}	1.780×10^{-2}
±10.0	±6.5	6.064×10^{0}	3.252×10^{0}	1.750×10^{0}	9.909×10^{-1}	5.640×10^{-1}	3.157×10^{-1}	1.704×10^{-1}	8.725×10^{-2}	4.151×10^{-2}	1.767×10^{-2}
±10.5	±7.0	6.034×10^{0}	3.237×10^{0}	1.738×10^{0}	9.812×10^{-1}	5.573×10^{-1}	3.113×10^{-1}	1.677×10^{-1}	8.588×10^{-2}	4.084×10^{-2}	1.738×10^{-2}
±11.0	±7.5	5.994×10^{0}	3.210×10^{0}	1.716×10^{0}	9.632×10^{-1}	5.450×10^{-1}	3.033×10^{-1}	1.629×10^{-1}	8.339×10^{-2}	3.964×10^{-2}	1.684×10^{-2}
±11.5	±8.0	5.943×10^{0}	3.164×10^{0}	1.675×10^{0}	9.312×10^{-1}	5.234×10^{-1}	2.897×10^{-1}	1.551×10^{-1}	7.929×10^{-2}	3.765×10^{-2}	1.595×10^{-2}
±12.0	±8.5	5.863×10^{0}	3.072×10^{0}	1.595×10^{0}	8.755×10^{-1}	4.876×10^{-1}	2.685×10^{-1}	1.433×10^{-1}	7.320×10^{-2}	3.472×10^{-2}	1.469×10^{-2}
±12.5	±9.0	5.669×10^{0}	2.863×10^{0}	1.447×10^{0}	7.852×10^{-1}	4.341×10^{-1}	2.388×10^{-1}	1.273×10^{-1}	6.491×10^{-2}	3.083×10^{-2}	1.303×10^{-2}
±13.0	±9.5	4.976×10^{0}	2.399×10^{0}	1.202×10^{0}	6.545×10^{-1}	3.634×10^{-1}	2.013×10^{-1}	1.076×10^{-1}	5.483×10^{-2}	2.609×10^{-2}	1.105×10^{-2}
±13.5	±10.0	3.000×10^{0}	1.610×10^{0}	8.704×10^{-1}	4.948×10^{-1}	2.816×10^{-1}	1.591×10^{-1}	8.566×10^{-2}	4.364×10^{-2}	2.087×10^{-2}	8.865×10^{-3}
±14.0	±10.5	1.012×10^{0}	8.180×10^{-1}	5.375×10^{-1}	3.351×10^{-1}	2.004×10^{-1}	1.165×10^{-1}	6.359×10^{-2}	3.257×10^{-2}	1.565×10^{-2}	6.661×10^{-3}
±14.5	±11.0	3.517×10^{-1}	3.598×10^{-1}	2.926×10^{-1}	2.051×10^{-1}	1.308×10^{-1}	7.842×10^{-2}	4.371×10^{-2}	2.266×10^{-2}	1.094×10^{-2}	4.635×10^{-3}
±15.0	±11.5	1.615×10^{-1}	1.661×10^{-1}	1.511×10^{-1}	1.163×10^{-1}	7.882×10^{-2}	4.864×10^{-2}	2.776×10^{-2}	1.469×10^{-2}	7.097×10^{-3}	2.958×10^{-3}
±15.5	±12.0	8.781×10^{-2}	8.620×10^{-2}	7.862×10^{-2}	6.248×10^{-2}	4.444×10^{-2}	2.834×10^{-2}	1.646×10^{-2}	8.841×10^{-3}	4.264×10^{-3}	1.721×10^{-3}
±16.0	±12.5	4.826×10^{-2}	4.729×10^{-2}	4.155×10^{-2}	3.232×10^{-2}	2.371×10^{-2}	1.584×10^{-2}	9.263×10^{-3}	4.857×10^{-3}	2.333×10^{-3}	9.148×10^{-4}
±16.5	±13.0	2.485×10^{-2}	2.498×10^{-2}	2.105×10^{-2}	1.613×10^{-2}	1.195×10^{-2}	8.064×10^{-3}	4.812×10^{-3}	2.364×10^{-3}	1.113×10^{-3}	4.417×10^{-4}
±17.0	±13.5	1.176×10^{-2}	1.182×10^{-2}	9.039×10^{-3}	7.632×10^{-3}	5.530×10^{-3}	3.077×10^{-3}	2.039×10^{-3}	1.093×10^{-3}	4.477×10^{-4}	1.822×10^{-4}
±17.5	±14.0	5.217×10^{-3}	5.206×10^{-3}	2.815×10^{-3}	3.231×10^{-3}	2.096×10^{-3}	1.485×10^{-3}	8.499×10^{-4}	4.847×10^{-4}	1.829×10^{-4}	6.559×10^{-4}

tion of the uncertainty in the consensus data from statistical analysis of the available data. An example hereof is the standard deviations calculated from the published values of the source strengths.

Ideally, treatment planning for brachytherapy should use a full 3D description of the dose profiles around the source or sources used for the treatment and the location of these sources relative to the anatomic structures of interest in the treatment. In the special case of intravascular brachytherapy, the treatment geometry is very simple and such detailed 3D descriptions of target structures and dose distributions are not always necessary or available. True 3D imaging modalities (e.g., combining angiography and IVUS) are not available in most centers. Therefore, a multilevel approach, as has been proposed for external beam therapy reporting[94,95] and recently adopted for intravascular brachytherapy treatment planning by ESTRO[96] is appropriate. The recommended values of the various factors and functions presented in this report can be used in dose calculations at each of these levels. The ESTRO recommendations are summarized below.

Basic treatment planning (level 1) uses angiographic data only and is based on the intervention length plus safety margins and the reference lumen diameter. Dose is prescribed to a specific point related to the source axis or the vessel lumen diameter. Dose reporting is limited to points at the vessel lumen surface and at a reference depth into the vessel wall at the representative central plane, including minimum and maximum variations in the case of noncentered devices. The calculation of these doses is possible using the reference absorbed dose rate and a description of the radial dose profile in the central plane of the sources used. In order to encompass the entire target length, the choice of an adequate active source length is based on a longitudinal dose profile. For simplification of the treatment planning process, the respective devices are characterized with a reference isodose length (RIL), which is defined as the length enclosed by the 90% points of the axial dose profile at the reference depth. Thus, the dosimetric data for basic treatment planning are reduced to values for the reference absorbed dose rate, the radial dose profile at the central plane, and the RIL. These data are re-

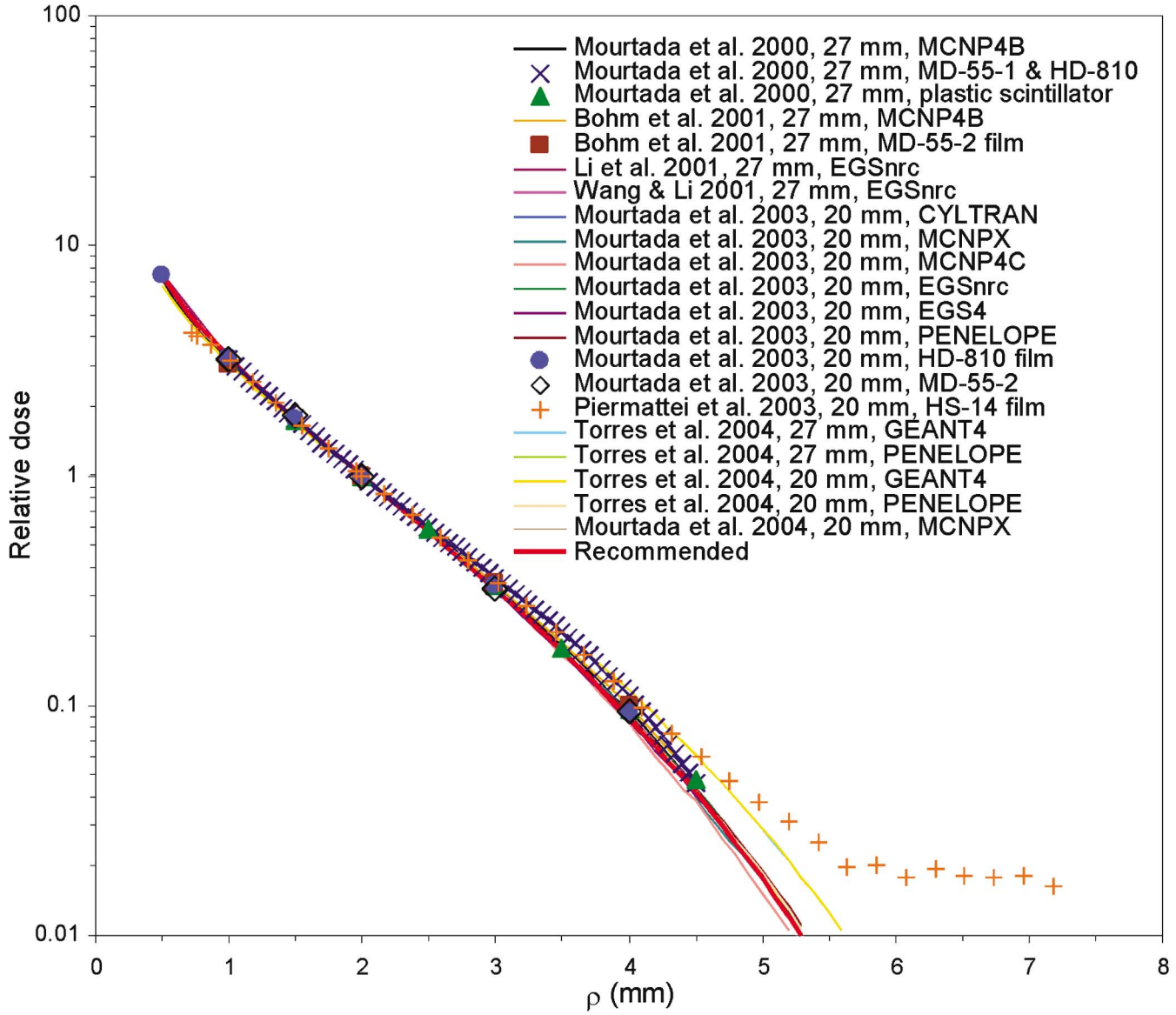

FIG. 16. Comparison between the relative depth-dose distributions calculated with the recommended dose calculation parameters (equal for 20 and 27 mm sources, shown in red) and published measurements and simulations.

lated to an entire, rectilinear source arrangement, including each seed in the case of a source train or including each dwell position in the case of a stepped source. All of these data can be derived from the AAPM recommended values for the dose calculation parameters presented in this report.

Advanced treatment planning (level 2) additionally uses IVUS-based information for dose calculations with respect to anatomical and pathological structures in the vessel wall not limited to the central plane. In addition to the dose calculations performed for level 1 planning, 2D dose calculations are performed in the central plane and in at least two well-defined peripheral planes. These calculations are based on 2D dose information for the entire source arrangement, which is assumed to be rectilinear and includes the contributions from all seeds and/or dwell positions. The AAPM recommended values for the dose calculation parameters presented in this report can be used for these calculations.

In developmental treatment planning (level 3) the calculation of dose volume histograms for vessel wall structures is included in the treatment planning process or at least in retrospective analysis of the actual treatment. In level 3 planning, the calculation is based on a full 3D dose distribution, and the reference dosimetry data necessary for such calculations are presented in this report. If the 3D curvature of the source is known (e.g., using imaging modalities combining angiography and IVUS), the 3D dose distribution should be based on the superposition of the dose distributions of the individual seeds in the case of a train source, or of a series of small wire segments in the case of a wire source, taking into account the 3D position and orientation of each seed or segment.

From the many papers on absorbed dose measurements for intravascular brachytherapy published in the last decade, part of which are included in the present study, it can be

concluded that much valuable experience has been gained in the dosimetry at submillimeter distances from brachytherapy sources. Many of these advances will no doubt benefit future applications of brachytherapy at millimeter and submillimeter distances. The very high dose rate gradients and highly divergent nature of the fields in the close vicinity to small sources pose daunting challenges to accurate measurements, as was repeatedly demonstrated during the recent efforts in the standardization of the sources.[97] Typical dose rate gradients are on the order of 100% per millimeters, which means that a positioning error of 0.1 mm introduces a 10% error in dose measurement. Additional uncertainties are introduced by the physical properties of the sources themselves. ^{90}Sr/^{90}Y source trains delivered in the treatment catheter are never truly colinear (as they are modeled) due to the necessity of free movement within the catheter. The colinearity of the seeds in the train varies each time the sources are delivered to the catheter. For ^{192}Ir seeds the lack of encapsulation on the seed ends allows the low-energy beta particles from this isotope to escape into the air space in the ribbon catheter, and these contribute to absorbed dose at shallow depths (less than 1 mm) in the gaps between the seeds. In addition, the nominal 1 mm spacing between the seeds in these ribbons could sometimes vary, causing multiseed ribbons to be longer than expected (see Fig. 8).

The special measurement problems posed by intravascular brachytherapy have led to developments and improvements in several measurement systems. For example, radiochromic film dosimetry has been improved to meet these challenges, and a new generation of small volume scintillator systems has been developed for *in vitro* dosimetry of these sources.[98,42] Very precise contained activity measurement techniques for the beta particle sources were developed,[99] which, when combined with Monte Carlo results, allow the prediction of reference absorbed dose rates. This provides an alternative means to determine the reference absorbed dose rate with high accuracy.

In addition to measurements, a variety of Monte Carlo codes has been used to determine the dose distribution about intravascular sources. Some interesting observations can be made from the Monte Carlo studies discussed in this article. It has been demonstrated that, for a given source design, very good agreement can be obtained between the dose distributions predicted by different codes, although these may use different multiple-scattering algorithms, cross-section libraries, etc., Fig. 14 provides an example of the very close agreement that can be obtained. Whereas this convergence may support an optimistic view on the current state-of-the-art of Monte Carlo radiation transport simulation, it is important to note that such good agreement can be obtained only if the source emission spectrum, the source geometry, and the materials are implemented very similarly in the different simulations, as was indeed the case in the studies presented in Fig. 14. Since inaccurate modeling of the source may lead to systematic errors in the calculated dose distributions, it is important that source manufacturers provide accurate and complete information regarding the source design. Although it has been shown that good agreement between different simulations and between simulations and experiments can be achieved, this is certainly not trivial. Some examples of significant discrepancies that may occur can be found in the discussion of the Monte Carlo results in Sec. IV C 3. Especially electron transport simulations may suffer from, e.g., boundary-crossing artifacts, step-size artifacts, and/or other problems. Furthermore, it is generally crucial to set proper values for a variety of radiation transport parameters in order to get good results. Therefore, it remains of great importance that the user of a Monte Carlo code acquires a thorough understanding of its algorithms and their limitations.

The experiences gained as described in the previous paragraphs will also find utilization in other fields requiring dosimetry of small radiation sources, such as traditional brachytherapy with low-energy photon sources. The same challenging field characteristics are also present here, and the advances made in measurement and calculation technology can be applied to absorbed dose determinations with these sources as well. These advances hopefully will lead to improved standards based on absorbed dose rather than air kerma for these sources, as well as for new sources, which do not lend themselves to air kerma strength measurement, such as x-ray probe systems[100] or plaque sources for the treatment of age-related macular degeneration.[101]

[a]Author to whom correspondence should be addressed. Electronic mail: soutung@optonline.net

[1]P. Tripuraneni, "The future of CART in the era of drug eluting stents: 'It's not over until it's over,"' Brachytherapy **2**, 74–76 (2003).
[2]P. M. Devlin, "The future of coronary artery radiation therapy—The CART before the (unbridled) horse," Brachytherapy **2**, 73–74 (2003).
[3]M. C. Morice *et al.* and RAVEL Study Group, "A randomized comparison of a sirolimus-eluting stent with a standard stent for coronary revascularization," N. Engl. J. Med. **346**, 1773–1780 (2002).
[4]J. W. Moses *et al.* and SIRIUS Investigators, "Sirolimus-eluting stents versus standard stents in patients with stenosis in a native coronary artery," N. Engl. J. Med. **349**, 1315–1323 (2003).
[5]G. W. Stone *et al.* and TAXUS-IV Investigators, "A polymer-based, paclitaxel-eluting stent in patients with coronary artery disease," N. Engl. J. Med. **350**, 221–231 (2004).
[6]R. Torguson, M. Sabate, R. Deible, K. Smith, W. W. Chu, K. M. Kent, A. D. Pichard, W. O. Suddath, L. F. Satler, and R. Waksman, "Intravascular brachytherapy versus drug-eluting stents for the treatment of patients with drug-eluting stent restenosis," Am. J. Cardiol. **98**, 1340–1344 (2006).
[7]R. Waksman, B. Bhargava, L. White, R. C. Chan, R. Mehran, A. J. Lansky, G. S. Mintz, L. F. Satler, A. D. Pichard, M. B. Leon, and K. K. Kent, "Intracoronary beta radiation therapy inhibits recurrence of in-stent restenosis," Circulation **101**, 1895–1898 (2000).
[8]A. E. Raizner, S. N. Oesterle, R. Waksman, P. W. Serruys, A. Colombo, Y. L. Lim, A. C. Yeung, W. J. Van Der Giessen, L. Vandertie, J. K. Chiu, L. R. White, P. J. Fitzgerald, G. L. Kaluza, and N. M. Ali, "Inhibition of restenosis with beta-emitting radiotherapy: Report of the proliferation reduction with vascular energy trial (PREVENT)," Circulation **102**, 951–958 (2000).
[9]M. B. Leon, P. S. Teirstein, J. W. Moses, P. Tripuraneni, A. J. Lansky, S. Jani, S. C. Wong, D. Fish, S. Ellis, D. R. Holmes, D. Kereiakes, R. E. Kuntz, "Localized intracoronary gamma-radiation therapy to inhibit the recurrence of restenosis after stenting," N. Engl. J. Med. **344**, 250–256 (2001).
[10]J. A. Condado, R. Waksman, J. F. Saucedo, B. Bhargava, A. J. Lansky, C. Calderas, O. Gurdiel, J. Gonzalez, M. Fadoul, B. Parra, L. Iturria, and B. Amezaga, "Five-year clinical and angiographic follow-up after intracoronary iridium-192 radiation therapy," Cardiovasc. Radiat. Med. **3**, 74–81 (2002).
[11]R. Nath, H. Amols, C. Coffey, D. Duggan, S. Jani, Z. Li, M. Schell, C. Soares, J. Whiting, P. Cole, I. Crocker, and R. Schwartz, "Intravascular

brachytherapy physics: Report of the AAPM Radiation Therapy Committee Task Group No. 60," Med. Phys. **26**, 119–152 (1999).
[12]M. Price, H. Giap, and P. S. Teirstein, "Intracoronary radiation therapy for multi-drug resistant in-stent restenosis: Initial clinical experience," Catheterization and Cardiovasc. Intervent. **69**, 132–134 (2007).
[13]P. Ortolani, A. Marzocchi, M. Aquilina, W. Gaiba, S. Neri, C. Marrozzini, T. Palmerini, N. Taglieri, and A. Branzi, "^{32}P Brachytherapy in the treatment of complex Cypher in-stent restenosis," J. Interv. Cardiol. **18**, 205–211 (2005).
[14]P. S. Teirstein *et al.*, "Catheter-based radiotherapy to inhibit restenosis after coronary stenting," N. Engl. J. Med. **336** 1697–1703 (1997).
[15]R. Waksman *et al.*, "Intracoronary gamma radiation therapy after angioplasty inhibits recurrence in patients with in-stent restenosis," Circulation **101**, 2165–2171 (2000).
[16]J. J. Popma, M. Suntharalingam, A. J. Lansky, R. R. Heuser, B. Speiser, P. S. Teirstein, V. Massullo, T. Bass, R. Henderson, S. Silber, P. von Rottkay, R. Bonan, K. K. L. Ho, Al. Osattin, and R. E. Kuntz, "Randomized trial of ^{90}Sr/^{90}Y β-radiation versus placebo control for treatment of in-stent restenosis," Circulation **106**, 1090–1096 (2002).
[17]S. B. King, III, D. O. Williams, P. Chougele, J. L. Klein, R. Waksman, R. Hilstead, J. Macdonald, K. Anderberg, and I. R. Crocker, "Endovascular β-radiation to reduce restenosis after balloon angioplasty: Results of the beta energy restenosis trial (BERT)," Circulation **97**, 2025–2030 (1998).
[18]P. W. Serruys, G. Sianos, W. van der Giessen, H. J. R. M. Bonnier, P. Urban, W. Wijns, E. Benit, M. Vandormal, R. Dörr, C. Disco, M. Debbas, and S. Silber, "Intracoronary β-radiation to reduce restenosis after balloon angioplasty and stenting," Eur. Heart J. **23**, 1351–1359 (2002).
[19]R. Waksman, A. Raizner, A. Yeung, A. Lansky, and L. Vandertie, "Use of localised intracoronary β radiation in treatment of in-stent restenosis: The INHIBIT randomised controlled trial," Lancet **359**, 551–557 (2002).
[20]L. Anderson, R. Nath, K. Weaver, D. Nori, T. L. Phillips, Y. H. Son, S. Chiu-Tsao, A. S. Meigooni, J. A. Meli, and V. Smith, *Interstitial Brachytherapy, Physical, Biological and Clinical Considerations* (Raven, New York, 1990).
[21]N. S. Patel, S. Chiu-Tsao, Y. Ho, T. Duckworth, J. A. Shih, H. S. Tsao, H. Quon, and L. B. Harrison, "High beta and electron dose from ^{192}Ir: implications for "gamma" intravascular brachytherapy," Int. J. Radiat. Oncol., Biol., Phys. **54**, 972–980 (2002).
[22]NCRP Report No. 58, *A handbook of radioactivity measurements procedures. National Council of Radiation Protection and Measurements* (National Council on Radiation Protection and Measurements, Bethesda, 1985).
[23]N. B. Grove and M. J. Martin, "Log-f tables for beta decay," Nucl. Data Tables **10** 205–317 (1971).
[24]S. Jani, V. Massullo, P. Tripuraneni, and P. Teirstein, "The Ir-192 radioactive seed ribbon," in *Handbook of Vascular Brachytherapy*, 2nd ed., edited by R. Waksman and P. Serruys (Martin Dunitz Ltd., United Kingdom, 2000), pp. 52–56.
[25]R. Waksman, E. Cheneau, A. Ajani, R. L. White, E. Pinnow, R. Torguson, R. Dieble, L. F. Satler, A. D. Pichard, K. M. Kent, P. S. Tierstein, and J. Lindsay, "Intracoronary radiation therapy inproves the clinical and angiographic outcomes of diffuse in-stent restenotic lesions," Circulation **107**, 1744–1749 (2003).
[26]National Nuclear Data Center, Brookhaven National Laboratory, www.nndc.bnl.gov (2007 January 10).
[27]R. Wang and X. A. Li, "A Monte Carlo calculation of dosimetric parameters of ^{90}Sr/^{90}Y and ^{192}Ir SS sources for intravascular brachytherapy," Med. Phys. **27**, 2528–2535 (2000).
[28]R. Wang and X. A. Li, "Dosimetric comparison of two ^{90}Sr/^{90}Y sources for intravascular brachytherapy: An EGSnrc Monte Carlo calculation," Phys. Med. Biol. **47**, 4259–4269 (2002).
[29]F. A. Mourtada, C. G. Soares, S. M. Seltzer, P. M. Bergstrom, Jr., J. M. Fernandez-Varea, J. Asenjo, and S. H. Lott, "Dosimetry characterization for a ^{32}P source wire used for intravascular brachytherapy with automated stepping," Med. Phys. **30**, 959–971 (2003).
[30]F. A. Mourtada, C. G. Soares, S. M. Seltzer, and S. H. Lott, "Dosimetry characterization of ^{32}P catheter-based vascular brachytherapy source wire," Med. Phys. **27**, 1770–1776 (2000).
[31]J. A. Halbleib, R. P. Kensek, T. A. Mehlhorn, G. D. Valdez, S. M. Seltzer, and M. J. Berger, Report SAND91-1634, *ITS Version 3.0: Integrated TIGER Series of Coupled Electron/Photon Monte Carlo Transport Codes* (Sandia National Laboratories, Albuquerque, NM, 1992).
[32]W. R. Nelson, H. Hirayama, and D. W. Rogers, Report SLAC-265, *The EGS4 Code System* (Stanford Linear Accelerator Center, Stanford University, Stanford, CA, 1985).
[33]I. Kawrakow and D. W. O. Rogers, NRCC Report PIRS-701, *The EGSnrc Code System: Monte Carlo Simulation of Electron and Photon Transport* (National Research Council of Canada, Ottawa, 2000).
[34]J. F. Briesmeister, ed., Report LA-12625-M, *MCNP™-A General Monte Carlo N-Particle Transport Code: Version 4B* (Los Alamos National Laboratory, Los Alamos, NM, 1997).
[35]J. F. Briesmeister, ed., Report LA-13709-M, *MCNP™-A General Monte Carlo N-Particle Transport Code: Version 4C* (Los Alamos National Laboratory, Los Alamos, NM, 2000).
[36]L. S. Waters, Report LA-CP-02–408, *MCNPX-User's Manual Version 2.4.0* (Los Alamos National Laboratory, 2002).
[37]F. Salvat, J. M. Fernández-Varea, and J. Sempau, *PENELOPE, A Code System for Monte Carlo Simulation of Electron and Photon Transport*, Workshop Proceedings, Issy-les-Moulineaux, France 7–10 July 2003 (OECD/NEA, Paris, France, 2003).
[38]S. Agostinelli *et al.*, "GEANT4—a simulation toolkit," Nucl. Instrum. Methods Phys. Res. A **506**, 250–303 (2003).
[39]J. F. Williamson, "Comparison of measured and calculated dose rates in water near I-125 and Ir-192 seeds," Med. Phys. **18**, 776–786 (1991).
[40]P. Papagiannis, A. Angeloloulos, E. Pantelis, L. Sakelliou, D. Baltas, P. Karaiskos, P. Sandilos, and L. Vlachos, "Dosimetry comparison of ^{192}Ir sources," Med. Phys. **29**, 2239–2246 (2002).
[41]C. G. Soares, D. Halpern, and C. K. Wang, "Calibration and characterization of beta-particle sources for intravascular brachytherapy," Med. Phys. **25**, 339–346 (1998).
[42]M. Bambynek, D. Flühs, U. Quast, D. Wegener, and C. G. Soares, "A high-precision, high-resolution and fast dosimetry system for beta sources applied in cardiovascular brachytherapy," Med. Phys. **27**, 662–667 (2000).
[43]D. R. Schaart, A. J. J. Bos, A. J. M. Winkelman, and M. C. Clarijs, "The radial depth-dose distribution of a ^{188}W/^{188}Re beta line source measured with novel, ultra-thin TLDs in a PMMA phantom: Comparison with Monte Carlo simulations," Phys. Med. Biol. **47**, 3605–3627 (2002).
[44]H.-J. Selbach and C. G. Soares, "New developments on primary standards for brachytherapy at NIST (US) and PTB (Germany)," in *Standards and Codes of Practice in Medical Radiation Dosimetry, Proceedings of an International Symposium, Vienna, 25–28 November 2002*, Vol. 2, pp. 101–110 (International Atomic Energy Agency, Vienna, 2003).
[45]J. van der Marel and E. van Dijk, "Developments of a Dutch primary standard for beta emitting brachytherapy sources," in *Standards and Codes of Practice in Medical Radiation Dosimetry, Proceedings of an International Symposium, Vienna, 25–28 November 2002*, Vol. 2, pp. 93–100 (International Atomic Energy Agency, Vienna, 2003).
[46]A. Niroomand-Rad, C. R. Blackwell, B. M. Coursey, K. P. Gall, J. M. Galvin, W. L. McLaughlin, A. S. Meigooni, R. Nath, J. E. Rodgers, and C. G. Soares, "Radiochromic film dosimetry: Report of the AAPM Radiation Therapy Committee Task Group No. 55," Med. Phys. **25**, 2093–2115 (1998).
[47]C. G. Soares, "Radiochromic film dosimetry," Radiat. Meas. **41**, S100–S116 (2006).
[48]M. J. Butson, P. K. N. Yu, T. Cheung, and P. Metcalfe, "Radiochromic film for medical radiation dosimetry," Mater. Sci. Eng. **R41**, 61–120 (2003).
[49]IAEA TECDOC-1274, *Calibration of photon and beta ray sources used in brachytherapy. Guidelines on standardized procedures at Secondary Standards Dosimetry Laboratories (SSDLs) and hospitals*. (International Atomic Energy Agency, Vienna, 2002).
[50]J. F. Dempsey, D. A. Low, S. Mutic, J. Markman, A. S. Kirov, G. H. Nussbaum, and J. F. Williamson, "Validation of a precision radiochromic film dosimetry system for quantitative two-dimensional imaging of acute exposure dose distributions,." Med. Phys. **27**, 2462–2475 (2000).
[51]R. Nath, L. L. Anderson, G. Luxton, K. A. Weaver, J. F. Williamson, and A. S. Meigooni, "Dosimetry of interstitial brachytherapy sources: Recommendations of the AAPM Radiation Therapy Committee Task Group No. 43," Med. Phys. **22**, 209–234 (1995).
[52]M. J. Rivard, B. M. Coursey, L. A. DeWerd, W. F. Hanson, M. S. Huq, G. S. Ibbott, M. G. Mitch, R. Nath, and J. F. Williamson, "Update of AAPM Task Group No. 43 Report: A revised AAPM protocol for brachytherapy dose calculations," Med. Phys. **31**, 633–647 (2004).
[53]D. R. Schaart, M. C. Clarijs, and A. J. J. Bos, "On the applicability of the AAPM TG-60/TG-43 dose calculation formalism to intravascular line

sources: Proposal for an adapted formalism," Med. Phys. **28**, 638–653 (2001).
[54]N. S. Patel, S. T. Chiu-Tsao, H. S. Tsao, and L. B. Harrison, "A new treatment planning formalism for catheter-based b sources used in intravascular brachytherapy," Cardiovasc. Radiat. Med. **2**, 157–164 (2001).
[55]R. Wang and X. A. Li, "Monte Carlo dose calculations of beta-emitting sources for intravascular brachytherapy: A comparison between EGS4, EGSnrc, and MCNP," Med. Phys. **28**, 134–141 (2001).
[56]N. S. Patel, S. T. Chiu-Tsao, P. Fan, H. S. Tsao, S. F. Liprie, and L. B. Harrison, "The use of cylindrical coordinates for treatment planning parameters of an elongated ^{192}Ir source," Int. J. Radiat. Oncol., Biol., Phys. **51**, 1093–1102 (2001).
[57]M. J. Rivard, "Refinements to the geometry factor used in the AAPM Task Group No. 43 necessary for brachytherapy dosimetry calculations," Med. Phys. **26**, 2445–2450 (1999).
[58]P. Karaiskos, L. Sakelliou, P. Sandilos, and L. Vlachas, "Limitations of the point and line source approximations for the determination of geometry factors around brachytherapy sources," Med. Phys. **27**, 124–128 (2000).
[59]E. Kouwenhoven, R. van der Laarse, and D. R. Schaart, "Variation in the interpretation of the AAPM TG-43 geometry factor leads to unclearness in brachytherapy dosimetry," Med. Phys. **28**, 1965–1966 (2001).
[60]J. A. Meli, "Let's abandon geometry factors other than that of a point source in brachytherapy dosimetry," Med. Phys. **29**, 1917–1918 (2002).
[61]M. J. Rivard, B. M. Coursey, L. A. DeWerd, W. F. Hanson, M. S. Huq, G. S. Ibbott, R. Nath, and J. F. Williamson, "Comment on: Let's abandon geometry factors other than that of a point source in brachytherapy dosimetry," Med. Phys. **29**, 1919–1920 (2002).
[62]F. A. Mourtada, C. G. Soares, and J. L. Horton, "A segmented ^{32}P source Monte Carlo model to derive AAPM TG-60 dosimetric parameters used for intravascular brachytherapy," Med. Phys. **31**, 602–608 (2004).
[63]W. G. Cross, "Variation of beta dose attenuation in different media," Phys. Med. Biol. **13**, 611–618 (1968).
[64]International Commission on Radiation Units and Measurements, ICRU Report 56, *Dosimetry of External Beta Rays for Radiation Protection* (International Commission on Radiation Units and Measurements, Bethesda, MD, 1997).
[65]D. R. Schaart, "The scaling method applied to beta particle line sources with a finite diameter," Med. Phys. **29**, 2682–2686 (2002).
[66]AAPM Report No. 21. *Recommendations of AAPM Task Group 32: Specification of Brachytherapy Source Strength* (American Institute of Physics, New York, 1987).
[67]T. P. Loftus, "Standardization of ^{192}Ir gamma ray sources in terms of exposure," J. Res. Natl. Bur. Stand. **85**, 19–25 (1980).
[68]R. Wang and R. S. Sloboda, "Influence of source geometry and materials on the transverse axis dosimetry of ^{192}Ir brachytherapy sources," Phys. Med. Biol. **43**, 37–48 (1998).
[69]J. C. Anctil, B. G. Clark, and C. J. Arsenault, "Experimental determination of dosimetry functions of Ir-192 sources," Med. Phys. **25**, 2279–2287 (1998).
[70]Z. Chen and R. Nath, "Dose rate constant and energy spectrum of interstitial brachytherapy sources," Med. Phys. **28**, 86–96 (2001).
[71]S. J. Ye, E. I. Parsai, and J. J. Feldmeier "Dosimetric characteristics of a linear array of β or γ-emitting seeds in intravascular irradiation: Monte Carlo studies for the AAPM TG-43/60 formalism," Med. Phys. **30**, 403–414 (2003).
[72]N. S. Patel, S. Chiu-Tsao, J. A. Shih, Y. Ho, H. S. Tsao, and L. B. Harrison, "Treatment Planning dosimetric parameters for ^{192}Ir seed at short distances: Effects of air channels and neighboring seeds," Med. Phys. **31**, 1521–1528 (2004).
[73]D. Baltas, P. Karaiskos, P. Papagiannis, L. Sakelliou, E. Loeffler, and N. Zamboglou, "Beta versus gamma dosimetry close to Ir-192 brachytherapy sources," Med. Phys. **28**, 1875–1882 (2001).
[74]N. C. Yang and R. C. Chan, "Beta particle and conversion electron contributions on Ir-192 dosimetry in intravascular Brachytherapy," Med. Phys. **28**, 1182 (2001).
[75]C. G. Soares, "Dosimetric issues in vascular brachytherapy (TG43/60)," in *Intravascular Brachytherapy/Fluoroscopically Guided Interventions*, S. Balter, R. C. Chan, and T. B. Shope, Jr., eds. Medical Physics Monograph No. 28, AAPM 2002 summer School Proceedings (Medical Physics Publishing, Madison, WI, 2002), pp. 321–372.
[76]R. Capote, E. Mainegra, and E. López, "Anisotropy function for ^{192}Ir low-dose-rate brachytherapy sources: An EGS4 Monte Carlo study," Phys. Med. Biol. **46**, 1487–1499 (2001).
[77]N. Reynaert, M. Van Eijkeren, Y. Taeymans, and H. Thierens, "Dosimetry of ^{192}Ir sources used for endovascular brachytherapy," Phys. Med. Biol. **46**, 499–516 (2001).
[78]S. Chiu-Tsao, T. L. Duckworth, N. S. Patel, J. Pisch, and L. B. Harrison, "Verification of Ir-192 near-source dosimetry using GAFCHROMIC film," Med. Phys. **31**, 201–207 (2004).
[79]J. Asenjo, J. M. Fernandez-Varea, and A. Sanchez-Reyes, "Characterization of a high-dose-rate ^{90}Sr/^{90}Y source for intravascular brachytherapy by using the Monte Carlo code PENELOPE," Phys. Med. Biol. **47**, 697–711 (2002).
[80]O. Chibani and X. A. Li, "IVBTMC, a Monte Carlo dose calculation tool for intravascular brachytherapy," Med. Phys. **30**, 44–51 (2003).
[81]D. E. Roa, H. Song, N. Yue, F. d'Errico, and R. Nath, "Dosimetric characteristics of the Novoste Beta-Cath ^{90}Sr/^{90}Y source trains at submillimeter distances," Med. Phys. **31**, 1269–1276 (2004).
[82]S. J. Ye, X. A. Li, J. R. Zimmer, J. J. Chu, and C. K. Choi, "Dosimetric perturbations of linear array of beta-emitter seeds and metallic stent in intravascular brachytherapy," Med. Phys. **27**, 374–380 (2000).
[83]D. M. Duggan, C. W. Coffey, J. L. Lobdell, and M. C. Schell, "Radiochromic film dosimetry of a high dose rate beta particle sources for intravascular brachytherapy," Med. Phys. **26**, 2461–2464 (1999).
[84]C. Kirisits, D. Georg, P. Wexberg, B. Pokrajac, and R. Pötter, "Determination and application of the reference isodose length (RIL) for commercial endovascular brachytherapy devices," Radiother. Oncol. **64**, 309–315 (2002).
[85]T. D. Bohm, F. A. Mourtada, and R. K. Das, "Dose rate table for a ^{32}P intravascular brachytherapy source from Monte Carlo calculations," Med. Phys. **28**, 1770–1775 (2001).
[86]A. Piermattei, A. Fidanzio, F. Perrone, L. Azario, L. Grimaldi, P. Viola, and R. Capote, "Experimental dosimetry of a ^{32}P catheter-based endovascular brachytherapy source," Phys. Med. Biol. **48**, 2283–2296 (2003).
[87]R. Wang and X. A. Li, "Monte Carlo characterization of a ^{32}P source for intravascular brachytherapy," Med. Phys. **28**, 1776–1785 (2001).
[88]X. A. Li, M. Suntharalingam, and C. Yu, "Dosimetry of source stepping for intravascular brachytherapy," Cardiovasc. Rad. Med. **2**, 165–172 (2001).
[89]J. Torres, M. J. Buades, J. F. Almansa, R. Guerrero, and A. M. Lallena, "Dosimetry characterization of ^{32}P intravascular brachytherapy source wires using PENELOPE and GEANT4," Med. Phys. **31**, 296–304 (2004).
[90]R. Jeraj, P. J. Keall, and P. M. Ostwald, "Comparisons between MCNP, EGS4 and experiment for clinical electron beams," Phys. Med. Biol. **44**, 705–717 (1999).
[91]N. Reynaert, H. Palmans, H. Thierens, and R. Jeraj, "Parameter dependence of the MCNP electron transport in determining dose distributions," Med. Phys. **29**, 2446–2454 (2002).
[92]D. R. Schaart, J. T. M. Jansen, J. Zoetelief, and P. F. A. de Leege, "A comparison of MCNP4C electron transport with ITS 3.0 and experiment at incident energies between 100 keV and 20 MeV: Influence of voxel size, substeps and energy indexing algorithm," Phys. Med. Biol. **47**, 1459–1484 (2002).
[93]C. Kirisits, "Determination and application of the reference isodose length (RIL) for commercial endovascular brachytherapy devices," Radiother. Oncol. **64**, 309–315 (2002).
[94]ICRU Report No. 50, *Prescribing, recording and reporting photon beam therapy* (International Commission on Radiation Units and Measurements, Bethesda, 1993).
[95]ICRU Report No. 62, *Prescribing, recording and reporting photon beam therapy (Supplement to ICRU Report 50)*. (International Commission on Radiation Units and Measurements, Bethesda, 1999).
[96]R. Pötter *et al.*, "Recommendations of the EVA GEC ESTRO Working Group: prescribing, recording, and reporting in endovascular brachytherapy. Quality assurance, equipment, personnel and education," Radiother. Oncol. **59**, 339–360 (2001).
[97]C. G. Soares, "Consistency standards for source strength of beta-particle sources," Vasc. Radiother. Monitor **3**, 59–63 (2001).
[98]D. Flühs, M. Heintz, F. Indenkämpen, C. Wieczorek, H. Kolanoski, and U. Quast, "Direct reading measurement of absorbed dose with plastic scintillators—The general concept and applications to ophthalmic dosimetry," Med. Phys. **23**, 427–434 (1996).
[99]R. Collé, "Chemical digestion and radionuclidic assay of TiNi-encapsulated ^{32}P intravascular brachytherapy sources," Int. J. Appl. Radiat. Isot. **50**, 811–833 (1999).

[100]M. Dinsmore, K. J. Harte, A. P. Sliski, D. O. Smith, P. M. Nomikos, M. J. Dalterio, A. J. Boom, W. F. Leonard, P. E. Oettinger, and J. C. Yanch, "A new miniature x-ray source for interstitial radiosurgery: device description," Med. Phys. **23**, 45–52 (1996).

[101]R. Hearn, C. G. Soares, J. Bergman, K. Millage, M. Napolitino, and J. Rodgers, "Radiological characterization of a ^{103}Pd ocular brachytherapy source," Med. Phys. **31**, 1914 (2004) (abstract).